1973

The Determination Of Radio Meteor Mass Distributions

Jeffrey Graham Collins

CANADA

NATIONAL LIBRARY OF CANADA

CANADIAN THESES ON MICROFILM

BIBLIOTHÈQUE NATIONALE DU CANADA

THÈSES CANADIENNES SUR MICROFILM

NL-101(1/66)

THE DETERMINATION OF RADIO METEOR MASS DISTRIBUTIONS

by

Jeffrey Graham Collins

Department of Physics

Submitted in partial fulfillment

of the requirements for the degree of

Doctor of Philosophy

Faculty of Graduate Studies

The University of Western Ontario

London, Canada

April, 1973

ABSTRACT

It has always been assumed that the meteoroid mass distribution index can be obtained from an observation of the meteor echo amplitude distribution provided that the radar or scatter equipment used is of sufficient sensitivity. A theoretical analysis of the scattering of electromagnetic waves by columns of ionisation indicates that the change in the reflection mechanism between echoes of the underdense and overdense type occurs over a much larger range than had been anticipated. Consequently, most previous estimates of the meteoroid mass distribution index are in error.

Radio meteor echoes were observed on forward-scatter circuits operating at 49.97 MHz and 40.356 MHz. Data for the Arietid shower in June, 3 days of sporadic activity and the δ-Aquarid shower in July and the Perseid shower in August 1971 were obtained. Utilising the theory developed, the meteoroid mass distribution indices were found to be in good agreement with those obtained from data supplied by other authors.

A further consequence of the theory is that with certain simplifying assumptions, a rough estimate of the limiting magnitude of the equipment can be made. This value is independent of the equipment parameters usually employed and relies on a knowledge of the true meteoroid mass distribution index.

The sporadic meteor observations of mid July 1971 displayed a strong diurnal variation in amplitude distribution index. This is believed to be due to atmospheric absorption, an estimate of which was made from a consideration of the variation.

ACKNOWLEDGEMENTS

The author would like to extend to his supervisor, Dr. J. Jones, his sincere thanks for the empathy, advice and guidance given to him during the course of this work. The author would also like to thank Dr. Jones for suggesting the problem, and also the members of his advisory committee, Dr. R. Lowe and Dr. G.F. Lyon, for their advice and suggestions concerning this thesis.

He would like to thank the many members of the Centre for Radio Science for their help and encouragement. In particular, he would like to thank Mr. J. Young, Mr. J. Haycock and Mr. S. Craig for their technical expertise and Dr. A.R. Webster for allowing the author to draw freely from his work. Gratitude is also due to Dr. J.K.E. Tunaley for many helpful discussions.

These acknowledgements would be incomplete if they did not contain thanks to my wife for her continued patience, understanding and encouragement.

TABLE OF CONTENTS

TABLE OF CONTENTS (Cont'd)

TABLE OF CONTENTS (Cont'd)

TABLE OF CONTENTS (cont'd)

LIST OF SYMBOLS

A, A_1, A_2	attenuated radio echo amplitude.
A_o	unattenuated radio echo amplitude.
A_n	complex expression for the parallel polarisation reflection coefficient.
a	semimajor axis of the orbit of a body.
a_n	incident radio wave amplitude.
B	magnetic induction.
B_n	complex expression for the transverse polarisation reflection coefficient.
b_n	reflected (or scattered) radio wave amplitude.
c	velocity of light.
D	diffusion coefficient.
D_e	electric displacement vector.
Dec	abbreviation for "declination".
E	electric field vector.
e	eccentricity of the orbit of a body.
e_e	electronic charge.
F	radius of the first Fresnel zone.
f	radio frequency in MHz.
G	antenna gain.
G_R, G_T	receiving, transmitting antenna gain.
$g_{/\!/}$, $g_{\perp}$	reflection coefficient for parallel, transverse polarisation of the electric vector.

LIST OF SYMBOLS (cont'd)

H	magnetic field vector.
$H_n^{(1)}$	Hankel function of the first kind.
H_s	scale height.
h	height of meteor ionisation.
I, I_1, I_2	Luminous intensities of stars or meteors.
$\int$	integral along the echo line.
i	inclination of the plane of the orbit of a body to the plane of the ecliptic.
i.p.s.	abbreviation for "inches per second".
J	current density vector.
J_n	Bessel function of the first kind.
j	$\sqrt{-1}$.
k	the wave number.
L	polarisation ratio $g_{\perp}/g_{//}$.
L.T.M.P.	abbreviation for "local time at the mid-point" (of the forward-scatter system).
M, M_1, M_2	magnitudes of stars or meteors on the comparison stellar magnitude, or, radio magnitude scale.
$\hat{M}$	magnetisation vector.
M_{av}	average radio magnitude.
M_o	limiting radio magnitude.
m	meteoroid mass.

LIST OF SYMBOLS (cont'd)

m_e	electron mass.
N, N_1, N_2	number of meteors exceeding a certain echo amplitude.
N_e	electron volume density.
n	order of the functions.
P	polarisation vector.
P_n	coefficients appearing in the parallel polarisation solution of the reflection of radio waves from a meteor train.
P_R, P_T	received, transmitted radio power.
p_{at}	atmospheric pressure.
ρ	r/r_d.
q	perihelion distance of a body in orbit about the sun.
R	range.
R.A.	abbreviation for "right ascension".
R_R, R_T	range from receiver, transmitter to meteor train.
R_x	receiver.
r	radial extent of ionisation ($\epsilon(r) \geq 0.9999$).
r_d	radius of column of ionisation ($\exp(-1)$).
r_o	initial radius of column of ionisation.
s	meteoroid mass distribution index.
s'	meteor echo amplitude distribution index.
T_n	coefficients appearing in the transverse polarisation solution of the reflection of radio waves from a meteor train.

T_x	transmitter.
t	time.
v	meteoroid velocity.
v_h	heliocentric meteoroid velocity.
v_o	geocentric meteoroid velocity.
v_e	electron velocity.
Y_n	Bessel function of the second kind.
Z	$\bar{\alpha}'/\alpha_o$.
α	electron line density.
α_o	value of α at the most sensitive point along the echo line.
α_T	transitional electron line density.
β	involved in relationship between s and s'.
γ	vernal equinox.
δ	orientation of the meteor train in the tangent plane.
ϵ	dielectric constant.
θ	angle involved in cylindrical coordinate system.
$\emptyset$	$\sqrt{\ln(\alpha_T/\alpha_o)}$.
$\hat{\theta}$	angle of elevation of the forward-scatter antenna beam.
λ	radio wavelength.

LIST OF SYMBOLS (cont'd)

$\varkappa$	$\Omega + \omega$
ν	angle between the amplitude vector of the incident wave and the line of sight to the observer.
ρ	charge density.
ρ_{air}	air density.
σ	standard deviation.
τ	decay time of a meteor echo.
τ_n	Neumann factor.
τ_R	registration time.
Γ	damping constant.
ϕ	half the forward-scatter angle.
χ^2	Chi-square.
ω	argument of perihelion.
ω_p, ω_e	plasma frequency and incident radio wave frequency in radians per second.
Ω	ascending node.
$\mho$	descending node.

LIST OF FIGURES

LIST OF FIGURES (cont'd)

LIST OF FIGURES (cont'd)

LIST OF FIGURES (cont'd)

Chapter 1

INTRODUCTION

1.1 Early investigation

Meteoroids can be divided into two basic categories namely shower and sporadic. Those belonging to the sporadic population are distributed over a large volume of space whereas shower meteoroids exist in homogeneous groups moving in well defined orbits around the Sun. There is strong evidence that the sporadic meteoroids also belong to the solar system. Shower meteoroids move in approximately parallel paths and when incident on the Earth's atmosphere, they appear to an observer to radiate from a fixed position on the celestial sphere known as the radiant of the shower. A shower is usually named after the constellation in which the radiant appears. If more than one radiant happens to occur within a given constellation, the name is prefixed in each case by the Greek letter designation of the nearest prominent star.

An excellent historical survey concerning the early study of meteor phenomena is provided by McKinley (1961). In the first chapter of his book he deals with

the ancient records, nineteenth century observations and the modern day visual and photographic techniques. This section will however be concerned only with the development of the radio technique for the observation of meteor trains.

Radio investigation of ionospheric phenomena began around 1930 when a number of investigators reported on some unusual night time echoes from the E-region. Shafer and Goodall (1932) and Skellet (1933) demonstrated that these echoes were due to meteoroids entering the Earth's atmosphere. Notable works on the physical theory of meteors were attempted by Lindemann and Dobson (1923), Sparrow (1926) and Öpik (1933). It is now generally agreed that on entering the atmosphere the meteoroid collides with individual air molecules the greater proportion of which transfer energy to its surface. Provided heat losses due to thermal radiation are small, the surface temperature of the meteoroid eventually becomes high enough for significant evaporation of meteoric material. The ablated atoms collide with air molecules and become ionised and a train of free electrons and positive ions is left behind the meteoroid. The ablated atoms have thermal velocities relative to the meteoroid but meteoric velocities relative to the surrounding air molecules. Thus due

to its energy, a meteoroid atom may collide with several air molecules before it is brought into thermal equilibrium with the surrounding atmosphere and hence the column of ionisation will possess a finite width at the time of formation. It is this column which is investigated by means of radar.

In the early years of radar, the increase in ionospheric ionisation produced by meteoroids was largely only of interest from the point of view of increasing the efficiency of radio communications. It was not realised at the time that radar could be an important tool in the investigation of meteor phenomena. During World War II, the development of radar advanced due largely to the stimulus of the war, but of course, little or no meteor investigation could be attempted during these years. After the war, the large radar networks were left intact for a while and much significant research was completed (see Hey, Parsons and Stewart 1947, and Hey and Stewart 1947).

The majority of radar observations made during the early years was by the back-scatter technique. That is, the transmitter and receiver were situated in the same location or quite close to each other. The region of sky under investigation was determined by the orientation of the transmitting and receiving antennas. A further development of radar primarily aimed at the

improvement of long range radio communications was the introduction of oblique or forward-scattering. Here transmitter and receiver are separated by a large distance, perhaps in the region of fifteen hundred kilometers and the area of sky under investigation is approximately midway between them. One of the initial ideas was that communications could be improved by utilising the bursts of ionisation produced by meteoroids entering the atmosphere. Information could be transmitted when the ionisation rose above a certain threshold level. The concept of forward-scattering was not a new one, but was not fully explored experimentally until about 1950 (see Forsyth et al 1957, Hines 1955 and Forsyth, Hines and Vogan 1955).

Today, both back-scatter and forward-scatter radar techniques are of primary importance in meteor investigation. An advantage that radar systems possess over nearly all other techniques is one of sensitivity. Even a modest back-scatter circuit can detect meteors far fainter than is possible by conventional photographic means. Further advantages include the fact that it can be used under all weather conditions, and at any time of the day or night.

1.2 The observation of meteor trains by radar

The formation of the train when a meteoroid

enters the atmosphere was explained in Section 1.1. Maximum ionisation occurs at approximately 100 km above the surface of the Earth. A small fast meteoroid will burn out higher than this whilst a slow, large one will burn out lower and may even reach the surface of the Earth as a meteorite.

In order to obtain a detectable echo from a faint meteor train, two basic conditions must be fulfilled. First, the reflection must be specular. Secondly, the amount of ionisation produced by the meteoroid must exceed the mimimum detectable ionisation at the specular point which depends, among other things, on the position of the train in the antenna beam, and on the mass of the meteoroid.

The scattering phenomenon may be divided into two regimes depending on whether the number of electrons produced per meter of path length is greater or less than a certain critical value given as 2.4×10^{14} m^{-1} (Kaiser and Closs, 1952). For those trains with electron line densities less than this figure, the radio wave penetrates the column freely and each electron acts as an individual scatterer. This is known as the underdense case. For those trains with electron line densities in excess of 2.4×10^{14} m^{-1}, the radio wave does not penetrate the column but is effectively reflected from a boundary surface inside which the density of

electrons is sufficient to cause total reflection. This is known as the overdense case. The transition electron line density of 2.4×10^{14} m^{-1} was derived for the back-scatter case, but the argument is the same for both oblique and back-scattering.

After the creation of a meteor train, the echo amplitude is determined by summing the individual amplitude vectors from the electrons throughout the ionised cylinder. There are destructive interference effects between the electrons in any given cross section of the cylinder. This destructive interference will be far greater in the case of back-scatter than forward-scatter due to the scattering angle. (The scattering angle is the angle subtended by rays drawn from the transmitter and receiver to the meteor train).

Hines and Forsyth (1957) showed that the conversion of the back-scatter theory to forward-scatter necessitated the inclusion of the factor cos ϕ where 2ϕ is the scattering angle. In effect, the wavelength of the incident radio wave λ, becomes λ sec ϕ. The back-scatter echo amplitude is of the form (Kaiser, 1953)

$$A = A_o \exp(-\text{constant}/\lambda^2) \qquad (1.1)$$

where A is the echo amplitude and A_o the unattenuated amplitude. If λ becomes λ sec ϕ and if ϕ is large ($\sim 80^o$), $A \simeq A_o$. That is to say, the echo will be unattenuated. Values of ϕ of the order of 80^o are

obtained by the use of forward-scatter geometry.

The visual magnitude of a meteor is obtained by comparing the brightest part of the meteor train with the luminous intensity of the stars in its vicinity. The stellar magnitude may be expressed by the relation,

$$M_1 - M_2 = 2.5(\text{Log}_{10} I_2 - \text{Log}_{10} I_1) \text{-------(1.2)}$$

where M_1 and M_2 are the magnitudes of the stars having luminous intensities I_1 and I_2. An arbitrary zero magnitude was selected corresponding reasonably closely to the magnitude of the star Vega in the constellation Lyra. Thus from equation (1.2) the magnitude M of a star having luminous intensity I is given by

$$M = \text{constant} - 2.5 \text{ Log}_{10} I$$

The visual magnitude scale is defined so that a change of one magnitude represents a factor of 2.5 in luminosity (Swihart, 1968). The definition of the radio magnitude scale is such that the visual and radio magnitude scales correspond as closely as possible. In view of this, the radio magnitude is defined as

$$M = 40 - 2.5 \text{ Log}_{10} \alpha_{max} \text{----------(1.3)}$$

where α_{max} is the maximum value of the electron line density α (in M.K.S. units). There is a velocity dependence of ionisation which slightly modifies the form

of equation (1.3). However this equation is commonly accepted as the defining equation of the radio magnitude scale.

1.3 Purpose of the Experiment

The purpose of the experiment was to obtain meaningful values of the meteoroid mass distribution index for both shower and sporadic meteoroids by observation of faint radio meteors.

The mass distribution of meteoroids as deduced from radar investigation of faint meteors is observed to be of the form

$$N = \text{constant} \times m^{1-s} \qquad \text{---------- (1.4)}$$

where N is the number of meteoroids having mass greater than M, and s is the mass distribution index (Kaiser, 1953). Meteoroid mass cannot be observed directly. The amplitude of the meteor echo is the observed parameter. We can define the meteor echo amplitude distribution index by

$$\frac{d \log_{10} N}{d \log_{10} A} = 1 - s' \qquad \text{---------- (1.5)}$$

where N is the number of meteor echoes exceeding amplitude A and s' is the amplitude distribution index.

When the observation of faint radio meteors is used to determine the meteoroid mass distribution

index it is usual to make the assumption that the maximum electron line density produced by the meteoroid is proportional to the initial mass (Herlofson, 1948). The amplitude of the meteor echo received will be some function of this electron line density.

The amplitude of an echo produced by a meteor train of a particular electron line density will be different for forward and back-scattering. This is due to the inclusion of the $\sec\phi$ term for forward-scatter.

The power received from a sufficiently underdense meteor train is proportion to α^2, whilst that received from a sufficiently overdense train is proprotional to $\alpha^{\frac{1}{2}}$ (Kaiser, 1960). Therefore, the amplitudes of meteor echoes should be proportional to α and $\alpha^{\frac{1}{2}}$ for the underdense and overdense cases repectively. Equation (1.5) illustrates that it is possible to obtain a value of s' by measurement of the slope of a graph of $\log_{10}N$ versus $\log_{10}A$. If the meteoroids under investigation produce trains which are sufficiently underdense than the value of s' measured will be equal to s, at least for the case of forward-scattering. This can be seen to be true because in this case $A \propto \alpha \propto m$.

The transition between the underdense and over-

dense regimes of $\log_{10}$ N versus $\log_{10}$ A is illustrated in Figure 1.1. The magnitude range of the transition region has never been accurately determined. One estimate due to Kaiser and Closs (1952) was approximately 2^M. Brysk and Buchanan (1965) concluded that underdense type echoes would occur if $\alpha \leq 10^{13}$ m^{-1} whilst overdense echoes would occur for $\alpha \geq 10^{16}$ m^{-1} and thus their estimate of the size of the transition region was approximately 7.5^M. This estimate agrees well with calculations made in this work. It can be appreciated that if s is determined by measurement of the slope of the underdense asymptote assuming a transition region smaller than approximately 7.5^M, then values of s so determined may be in error.

The transition region has been investigated for four distinct cases in this work and a method has been developed to determine the mass distribution index utilising the curvature of the region. A theoretical investigation was prompted by the fact that in 1968, forward-scatter studies of sporadic meteors at a frequency of 49 MHz yielded an anomalously high value of mass distribution index (Collins, 1969). This value of s was 3.15 ± 0.04 which should be compared with the usually accepted value of approximately 2.0. The limiting magnitude of the equipment was calculated to

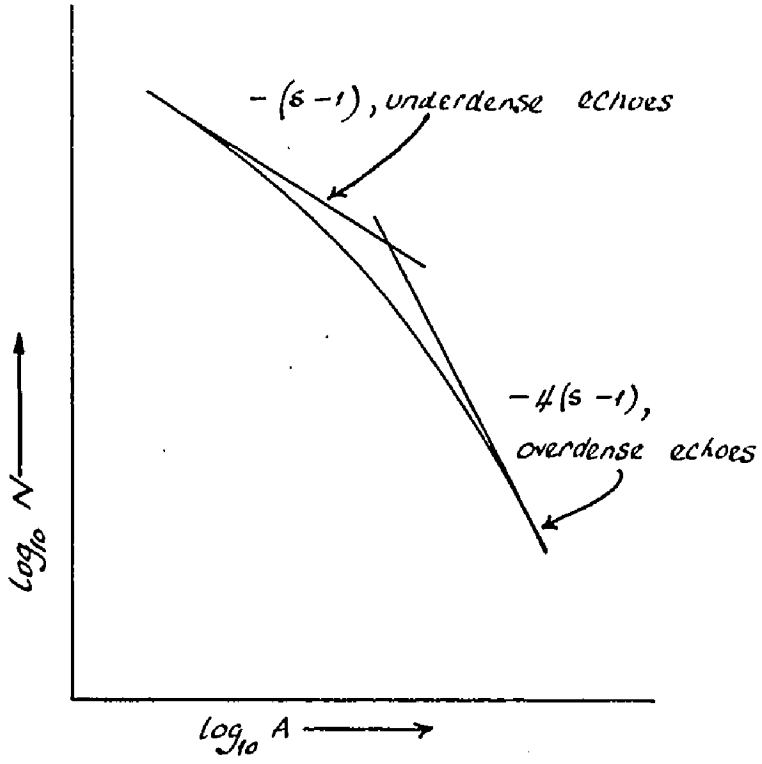

The transition between underdense and overdense asymptotes for a graph of $\log_{10} N$ plotted versus $\log_{10} A$

Figure 1.1

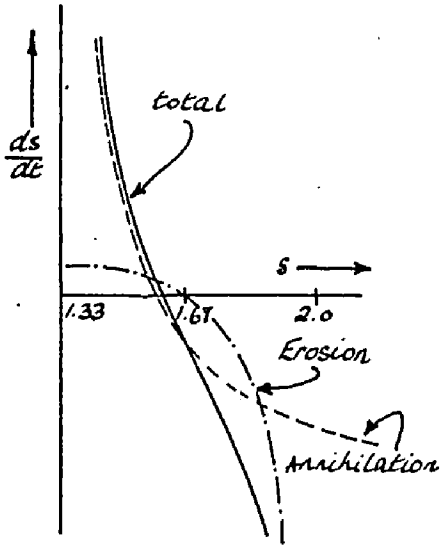

Rate of change of mass distribution index s as a function of s (Jones, 1968)

Figure 1.2

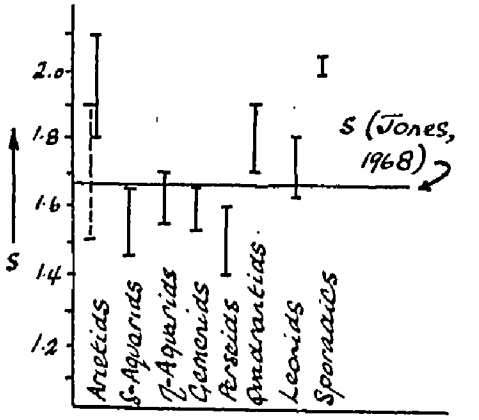

The s values deduced for shower and sporadic meteoroids from the observations of underdense meteor trains (Jones, 1968)

Figure 1.3

be approximately + 6.6^{M}. This was thought to be of such sensitivity that any value of slope measured from the underdense region of the curve similar to Figure 1.1, would in fact be the slope of the asymptote to this region and would therefore yield an accurate value of the mass distribution index. Investigation apparently showed this was not the case. Curvature of the graph indicated that an asymptotic limit had not been reached and hence a theoretical investigation of the transition region was warranted.

1.4 The significance of the meteoroid mass distribution index

A close correlation between the orbit of a meteoroid shower and that of a comet has been established for a number of cases (Lovell, 1954). It is generally believed that some showers may originate from the disruption of comets when subjected to thermal forces caused by the sun's radiation (Whipple, 1963). Sporadic meteoroids move in random orbits and it has been postulated that the population of sporadic and shower meteoroids are closely related (Jacchia, 1963). Planetary perturbations may cause some shower particles to separate from the main stream and this may account for the origin of sporadic meteoroids (Plavec, 1956). Dohnanyi (1970) examined this theory. He points out

that inelastic collisions can destroy some particles and create a spectrum of fragments, the result being an evolution of the mass distribution of the meteoric population. Dohnanyi states that if the observed distribution of meteoroid masses is to be maintained in a steady state a source must exist. He states that otherwise, the present population of sporadic meteoroids will be unstable since the number of particles destroyed by collisions in a given mass range per unit time is greater than the rate at which fragments in this same mass range are created by the disruption of larger particles. Dohnanyi finds that shower meteoroids qualify for such a source provided that the mass distribution of sporadic meteoroids is 2.17.

The condition for stability of the meteoroid mass distribution as defined by Jones (1968) concerns the variation of the mass distribution index with time. Figure 1.2 shows ds/dt plotted versus s according to Jones. The effects of erosion and annihilation are considered and the figure shows that a stable value of s is very close to 1.7.

The theoretical model employed by Jones neglected debris, the result of collisions. He arrived at the conclusion that the mass distribution of all showers should be essentially the same, the value of s

obtained being 1.67. Using data obtained by several authors (see Jones, 1968 for a list) he found agreement within experimental error for the δ-Aquarid, η-Aquarid, Geminid, Perseid and Leonid showers with his theoretically calculated value (see Figure 1.3).

Jones maintained that the small variation in s was due to the Poynting-Robertson effect and to the effects of the solar wind and radiation pressure. Dohnanyi (1970) proposed however, that the Poynting-Robertson effect is neglibible in the range of photographic meteors and that the collisional processes dominate in the evolution of meteoroid masses. He does however state that radiation pressure would provide a small particle cut-off in the mass distribution.

The foregoing illustrates the importance of obtaining a reliable value of the mass distribution index for both the shower and sporadic meteoroids. In the following sections a method is illustrated by which it is felt that reliable values of this index may be obtained.

Chapter 2

A DESCRIPTION OF THE APPARATUS

2.1 The scatter circuits

Two forward-scatter circuits were employed in the experiment operating at 40.356 MHz and 49.97 MHz. The transmitters were situated in Winnipeg, Manitoba (Long. 97.1° W, Lat. 49.9° N). The resulting signals were received at Delaware Radio Observatory (Long. 81.4° W, Lat. 42.9° N) approximately 20 km southwest of London, Ontario. The forward-scatter path length was calculated to be approximately 1530 km and the scattering angle 158°.

The transmitted power for both scatter circuits was 30 watts continuous wave. Five element Yagi antennas were used to transmit and receive the signals. The positioning of the antennas should have been such that they illuminated a region midway between Winnipeg and London (see Appendix 1). The antenna gain (over a flat ground) was 50 over an isotropic radiator.

Two crystal controlled Ferranti V.H.F. receivers were employed as receiving apparatus. The output from each receiver was converted to an amplitude modulated 500 Hz signal which was then fed onto a tape recorder. The maximum receiver sensitivity was 0.0794 μv into 50 Ω or 1.26×10^{-16} watts.

The maximum theoretical sensitivity, or limiting magnitude of the equipment can be calculated using equation (1.3) and an equation obtained by Hines and Forsyth (1951) (or McKinley, 1961) which states

$$P_R = 5 \times 10^{-32} \frac{P_T G_T G_R \lambda^3 \alpha^2 \sin^2 \nu}{R_T R_R (R_T + R_R)(1 - \sin^2 \phi \cos^2 \delta)} \text{ ----------(2.1)}$$

where P_R is the power received in watts

P_T the power transmitted in watts

G_T and G_R the antenna gain for transmission and reception, respectively.

R_T and R_R the range from the meteor train to the transmitter and receiver respectively.

δ the orientation of the meteor train in the tangent plane

and ν the angle between the electric vector of the incident wave and the line of sight to the observer.

A typical forward-scatter arrangement is shown in Figure 2.1. The limiting magnitude calculated for the Winnipeg/London scatter circuits was $+7.7^{\underline{M}}$ and $+7.3^{\underline{M}}$ for 40 and 49 MHz respectively.

The tape recorder used was a Phillips Model EL3534 A. This recorder was particularly well suited to long duration recording as it possessed a low tape speed of 15/16 inches per second (i.p.s.). As the tape recorder was a two track

Table 1

	Db below 1 volt	Volts $\times 10^6$	Power in watts $\times 10^6$	Theoretical Magnitude	
				49 Mhz	40 Mhz
1	142	0.079	1.26	7.3	7.7
2	138	0.126	3.18	6.8	7.2
3	134	0.2	8.0	6.3	6.7
4	130	0.316	22.0	5.8	6.2
5	126	0.5	50.0	5.3	5.7
6	122	0.794	126.0	4.8	5.2

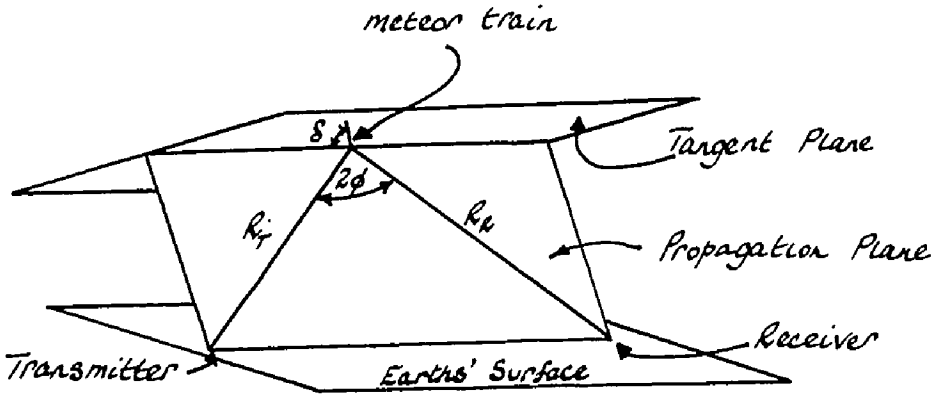

Forward-Scatter Geometry

Figure 2.1

model, it was possible to record both the 40 MHz and the 49 MHz data simultaneously on one tape.

Two types of tape were used during the experiment. Initially 1 mil. tape was employed exclusively, but later on it was found to be more convenient to use 1/2 mil. even though it was delicate. The advantage of the 1/2 mil. tape was one of duration of recording. One reel of 1/2 mil. tape played at a tape speed of 15/16 ips lasted for 24 hours.

Fifteen minute time signals were put on the record by means of a motor operated switch. The switch was normally closed and when open it disconnected one of the signal lines to the tape recorder. Thus a knowledge of the time of the first time signal allowed the times of succeeding signals to be easily calculated. With the meteor echoes stored on magnetic tape, playback could be performed at any convenient time. The recorded signal was fed into a Clevite Brush mark 260 chart recorder through a detector. A record which lent itself to reasonably straight forward analysis was thus obtained.

The tapes were played back at twice the recorded speed in order to minimize play-back time. It was found that there was no amplitude attenuation of the echoes due to the chart recorder at this speed, as the rise time of a typical meteor echo corresponded to a frequency which was below the maximum frequency response of the chart recorder. Amplitude attenuation of the echoes did tend to become

significant at higher tape speeds however.

2.2 Calibration Procedure

A calibration of the equipment was performed at the beginning and end of each record. If the tape had to be turned over midway through a record, a further calibration was performed. It was found unnecessary to calibrate more often as except in the event of power or heating failure the gain and linearity of the receivers remained constant.

The calibration procedure was a standard one. A signal of the required frequency from a Schlumberger signal generator (Model FS1/FSM500/FS30) was fed through the pre-amplifier to the antenna input of the appropriate receiver. Maximum signal input was 122db below 1 volt corresponding to a simulated antenna signal of 0.794 μv. The minimum signal was 142db below 1 volt (0.0794 μv). The calibration levels chosen and the correspondence between these levels and input power is shown in Table 1.

The limiting magnitude of the equipment was calculated for level 1. As each of the levels chosen are 4db apart, this can be seen to correspond to a separation of $0.5^{\frac{M}{4}}$. The magnitude of each level is thus readily calculable.

To establish a maximum/minimum level for ease of playback, the following procedure was adopted. Before stepping the signal from levels 1 to 6, the maximum signal was fed on to the tape, then switched off and on again repeatedly.

Upon playback the maximum signal could be made to correspond to the maximum deflection and the minimum signal (due only to receiver noise) to zero deflection. This simple procedure allowed the recording to be centred on the chart paper.

2.3 Analysis Procedure

Analysis consisted of counting the number of meteor echoes with amplitudes greater than certain discrete levels corresponding to the predetermined values of power delivered to the input terminals of the receiver. It was felt that the best method of counting the echoes was to obtain a graphical record and then submit this record to analysis.

A mask was made to fit over the chart. Lines corresponding to calibration marks were drawn on the mask and echoes exceeding the calibration levels were then easily noted and recorded. If the calibration levels changed from record to record, the lines could easily be removed from the mask and new ones substituted.

Special charts were prepared for permanently recording the echoes. These charts were divided into sections entitled "decay", "overdense", and "drifting". A "decay" echo is one which is of the underdense type, typified by a fast rise time and an exponential decay. An "overdense" echo is characterised by a fast rise time but then displaying a flat top or a fluctuating signal followed by an exponential

decay. A "drifting" echo is one which appears to have drifted into the antenna beam; that is to say it does not fulfill the conditions of specular reflection, and thus has a very slow rise time. Such drifting meteor trains were excluded from further analysis. Examples of these echoes are shown in Figure 2.2.(1) is a small amplitude overdense echo showing great amplitude fluctuation or fading. (2) is an echo with a comparatively slow rise time which may indicate that it drifted into the antenna beam. (3),(4),(5) and (6) are underdense echoes of various amplitudes whilst (7) and (8) are echoes which show a fast rise time and a slow decay presumably of the transition type, that is exhibiting characteristics similar to both underdense and overdense echoes.

Care had to be taken during analysis to avoid counting noise interference. Due to their exceedingly short duration, noise spikes were severely attenuated by the chart recorder. True meteor echoes and noise signals could be differentiated by means of two tests. First, noise spikes did not exhibit exponential decay such as is found in Figure 2.2 (3),(4),(5) and (6). Secondly, noise spikes were heard as "ticking" sounds when played back through the tape recorder speakers whereas true meteor echoes behaved as a pure amplitude modulated 500 Hz signal. Occasionally, the chart was impossible to analyse due to the presence of continued noise often due to large electrical storms in the area. Also,

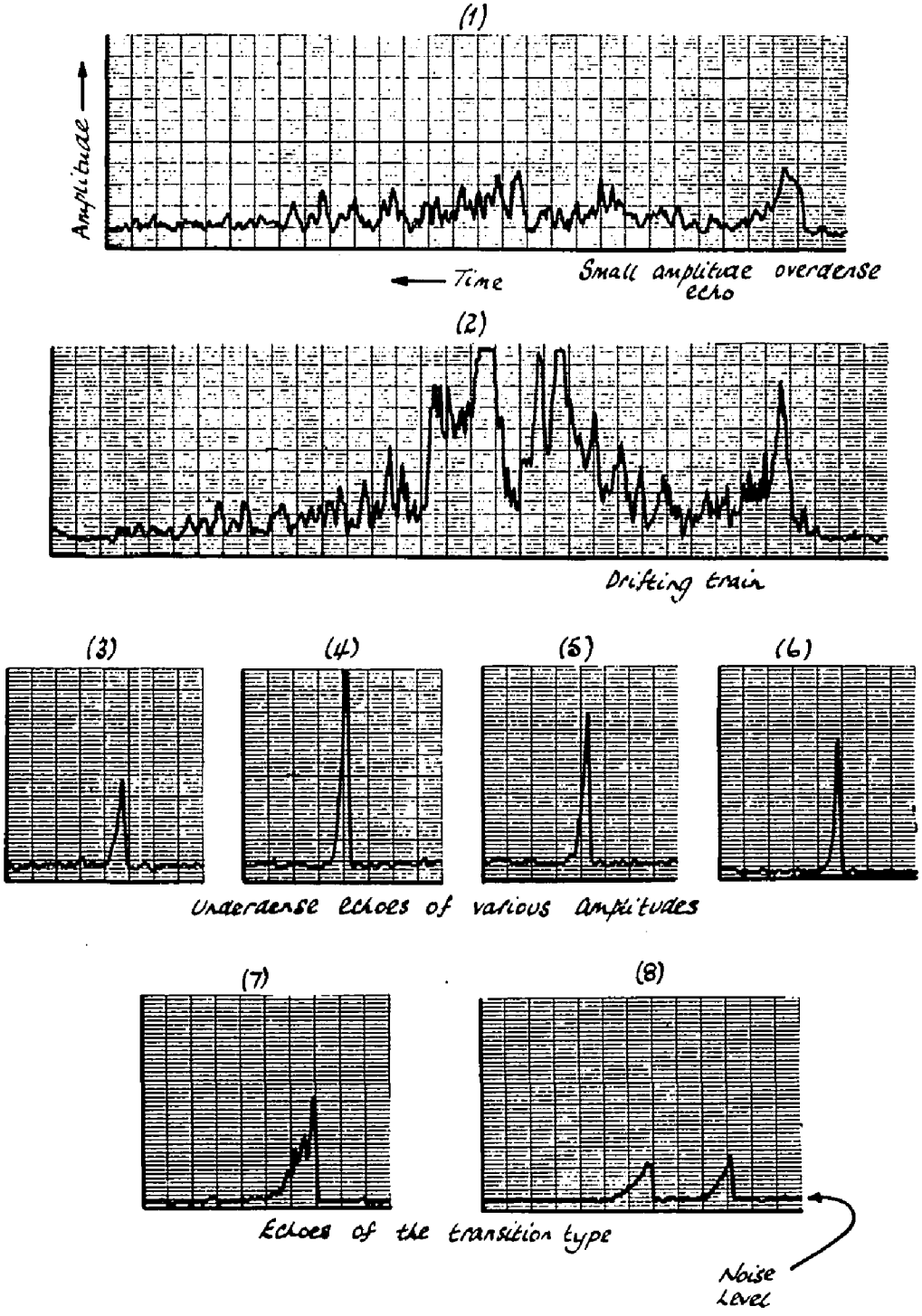

Examples of various meteor echoes

Figure 2.2

sometimes during the day, the noise level would increase due perhaps to sporadic E. The samples of chart upon which these phenomena occurred were omitted from the analysis. Corrections to the hourly rate were appropriately made. Further corrections to the meteor rate due to time signal interruptions etc. were found to be unnecessary.

Chapter 3

THEORETICAL CONSIDERATIONS

3.1 The Meteor Train

(a) Formation

As the meteoroid plunges into the atmosphere there is ablation of meteoric material which, due to its high energy relative to the surrounding air, becomes involved in several collisions with air molecules before being brought into thermal equilibrium. The radial extent of the ionisation produced is known as the initial radius of the meteor train. This initial radius grows smaller due to the reduction in the mean free path of the air molecules as the meteoroid reaches lower levels. Furthermore the upper parts of the train will have diffused radially by the time the meteoroid finally burns out. The column of ionisation will therefore take on a shape as shown in Figure 3.1.

As the meteoroid approaches the point where its path is perpendicular to a line from the observing station (the reflection point) the amplitude of the received echo rises. It attains one half of its final value when the meteoroid passes the reflection point. As it continues along its path, the echo amplitude continues to rise and then exhibits a

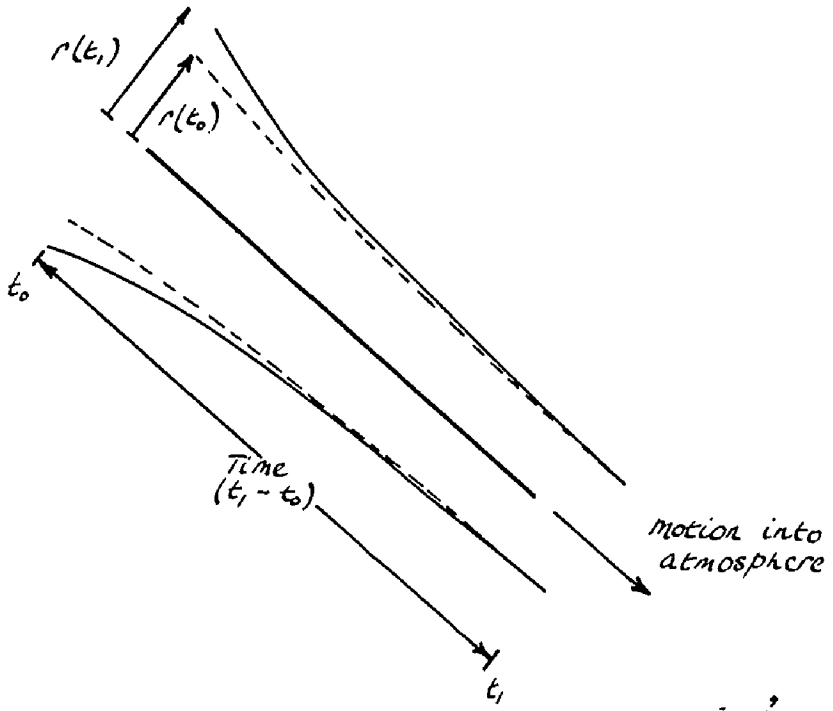

The column of ionisation as a meteoroid enters the Earth's atmosphere. $r(t_0)$ is the radius of the column of ionisation at formation whereas $r(t_1)$ is the radius of the column after it has diffused during $(t_1 - t_0)$. The radial extent of the diffusion is exaggerated.

Figure 3.1

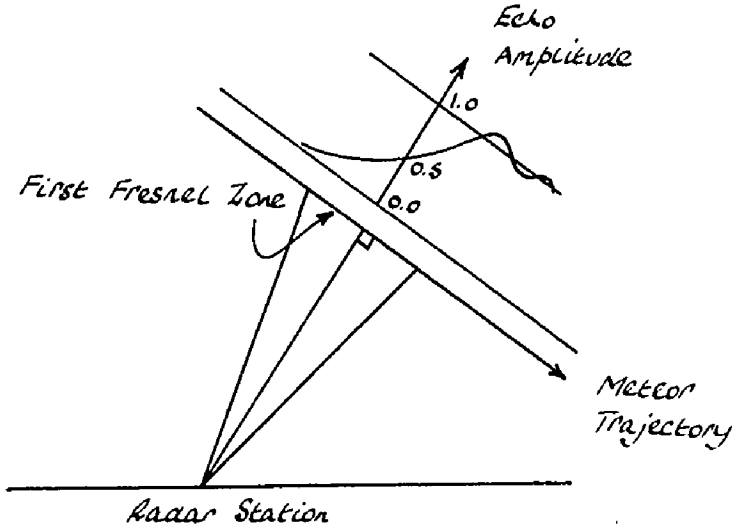

Meteor Echo Amplitude as a Function of time

Figure 3.2

damped oscillation about its final amplitude (Figure 3.2). The reflection of radio waves from a meteor train is analogous to Fresnel diffraction at a straight edge, the oscillations representing the passage of the head or body of the meteoroid through successive Fresnel zones (see for example Wood, 1934). The amplitude of the echo is obtained by integrating the individual contributions from all the electrons in the train. Lovell and Clegg (1948) showed that practically all the effective contribution to the echo comes from the first Fresnel zone.

Bearing this in mind, it is shown in Appendix 2 that it is not unreasonable to assume that the column of ionisation is formed instantly and is cylindrical in shape.

(b) Dissipation

The processes which concern the dissipation of the column of ionisation are diffusion, recombination and attachment.

Diffusion

Huxley (1952) gave a mathematical treatment of the diffusion of a cylindrical distribution of electrons and positive ions in the absence of a magnetic field. He deduced that if the initial column can be approximated to a line distribution (a cylindrical column with

negligible initial radius) then

$$N_e = \frac{\alpha}{4\pi Dt} \exp\left[-\frac{r^2}{4Dt}\right]$$

where N_e is the electron volume density, D the diffusion coefficient and r the radius of the column at time t. Thus the radial density distribution is Gaussian and since at radius $r^2 = r_d^2 = 4Dt$ the electron density is $\frac{1}{e}$ of the axial density, this quantity may be taken to be a characteristic measure of the radius of the column at time t.

McKinley (1961) indicated a more general solution of the diffusion equation the standard form of which is

$$\frac{\partial N_e}{\partial t} = \frac{D}{r} \frac{\partial}{\partial r}\left[r \frac{\partial N_e}{\partial r}\right]$$

One particular solution is

$$N_e = \frac{1}{A(t + k)} \exp\left[-\frac{r^2}{B(t + k)}\right]$$

where A, B and k are constants. McKinley goes on to show that the volume density may be expressed as

$$N_e = \frac{\alpha}{\pi(4Dt + r_o^2)} \exp\left[-\frac{r^2}{4Dt + r_o^2}\right] = N_o \exp\left[-\frac{r^2}{r_d^2}\right] \quad --(3.1)$$

where r_o is the initial radius of the column of ionisation. The Earth's magnetic field will modify the form of the diffusion equations somewhat but Kaiser et al (1969) have shown that this effect is negligibly small

at heights 100 km and below.

Recombination

Free electrons in the meteor train will eventually tend to recombine with the positive ions forming neutral molecules. Kaiser and Greenhow (1953) and Kaiser (1953) deduced that the effects of recombination may be neglected in comparison with ambipolar diffusion effects for both underdense and overdense trains.

Attachment

Electrons may also attach themselves to neutral molecules to create negative ions. This process is known as attachment. Kaiser (1953) maintains that attachment will have little or no effect on echoes received from underdense trains at the commonly used wavelengths in meteor radars (4-30 metres). The effect on overdense trains will be to limit the duration of very long echoes.

3.2 The Reflection of Radio Waves from the Meteor Train (Approximate Solutions)

Blackett and Lovell (1941) derived the radio reflection coefficient for a cylindrical column of ionisation with diameter small compared to the wavelength. Lovell and Clegg (1948) applied this theory to the case of the ionised train produced by the passage of a meteoroid through the atmosphere. In spite of the

limitations of the theory (namely that the diameter of the column of ionisation had to be small compared to the wavelength and that the electron density had to be sufficiently low to enable the incident wave to penetrate the column without significant modification) it gave an adequate explanation of many of the observed phenomena.

The Lovell-Clegg theory does break down however when the electron line density approaches a certain critical value, the transitional electron line density.

The power P_R delivered to the terminals of a receiver by a meteor train of electron line density α at range R is given by

$$P_R = \frac{P_T G^2 \lambda^3}{32\pi^2 R^3} \left[\frac{e_e^2}{m_e c^2}\right]^2 \alpha^2 \qquad \text{----------(3.2)}$$

where G is the antenna gain in the direction of the reflection point referred to an isotropic radiator and e_e and m_e are the electronic charge and mass respectively. Equation (3.2) is the Lovell-Clegg formula and will hold so long as the initial simplifying assumptions hold.

The meteor train may also be treated as a column of dielectric constant $\epsilon(r)$ where

$$\epsilon(r) = 1 - \frac{4\pi N_e e_e^2}{k^2 m_e c^2} \qquad \text{----------(3.3)}$$

where k is the wavenumber. N_e must be small for the Lovell-Clegg formula to be true and hence $\epsilon(r) \simeq 1$. In most cases, this need not initially be true; the dielectric constant may initially be negative and may only approach unity when the column has diffused for some time. This would of course render the Lovell-Clegg theory invalid.

A more comprehensive treatment of the problem of the reflection of radio waves from meteor trains was given by Kaiser and Closs (1952). Their treatment involved the use of the dielectric constant given by equation (3.3). This theory, based on an essentially quasi-electrostatic approach and considered no term greater than the dipole term, dealt strictly with back-scatter radar observations and predicted that there is a critical electron line density on either side of which the two distinct types of echo occur. The predicted value of this electron line density is 2.4×10^{14} m^{-1}. The type of radio echo obtained from a meteor train will largely depend on whether the electron line density is less than, approximately equal to or greater than this transitional value.

In summary, for the underdense meteor train, the radiation penetrates the whole train and the Lovell-Clegg formula is expected to hold. When the electron

line density exceeds the transition value the incident wave is no longer able to penetrate the column and reflection is similar to that from a metallic cylinder. Here of course the Lovell-Clegg formula will break down.

3.3 The Reflection of Radio Waves from the Meteor Train (Exact Solution)

As the meteoroid enters the Earth's atmosphere, the rate of ablation according to classical theory (summarized by Herlofson, 1948) is expected to be smooth. This theory has been modified (Jones and Kaiser, 1966, Lebedinec and Portnyagin, 1967) but they conclude that smooth trains are still expected for sufficiently faint meteors. Jones (1969) in an investigation of radio-meteor ionisation profiles concluded that small scale ($\simeq$ 1km) irregularities have a root mean square deviation of less than 30% of the mean electron line density. Jones and Read (1972) in an examination of the effects of the wind shear gradient on the scatter of decay times of underdense radio-meteor echoes, remark that any component of dispersion due to ionisation irregularities along the train must be substantially less than the dispersion due to the wind shear gradient. The foregoing therefore implies that the rate of ablation of meteoric material can be

considered smooth over a region equal to the length of the first Fresnel zone. Therefore the radio echo from a meteor train can be considered to originate from a relatively constant electron line density and thus, no compensation for irregularly ionised trains need be introduced in any theoretical analysis of the reflection process.

The exact solution of the problem of radio reflections from an ionised cylinder can be reduced to a formal electrodynamic problem (Keitel, 1955 and Lebedinec and Sosnova, 1967). The scattering of a plane wave normally incident on a meteor train possessing a Gaussian radial distribution of ionisation can be investigated for various electron line densities and scattering angles. The following theory was adapted for four cases, 180^{o} and 160^{o} forward-scattering (where the angle refers to the forward-scatter angle 2ϕ), orthogonal and back-scattering, with electron line densities in the range 10^{12} - 10^{17} m^{-1}.

The effect of electrons within a column on a passing radio wave is taken into account by determining the reduced dielectric constant for any portion of the train, from the equation of motion of the electrons.

Consider the system (in cylindrical coordinates) shown in Figure 3.3. Let the axis of the column of

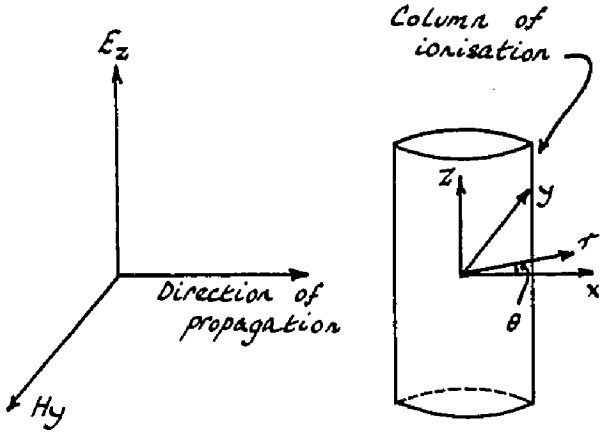

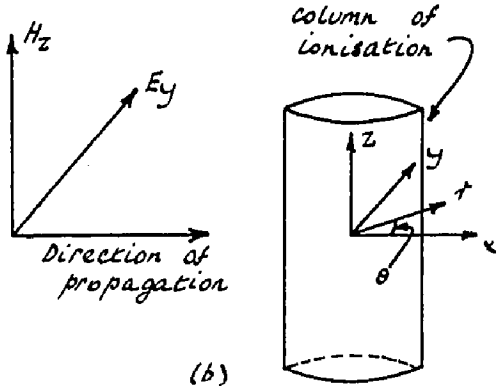

Geometry of plane waves normally incident on a column of ionisation.
(a) parallel electric polarisation (b) transverse electric polarisation

Figure 3.3

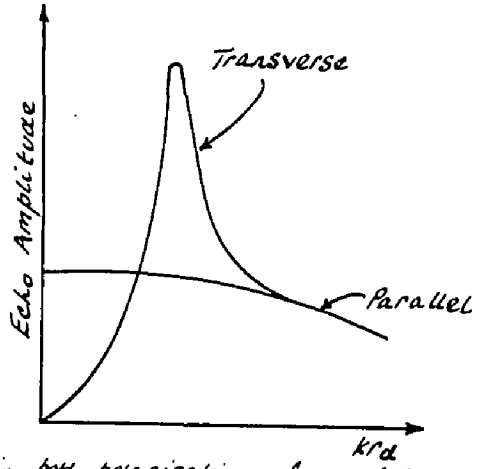

Echo amplitude in both polarisations for a column which expands without any other effect except diffusion (Herlofson, 1951)

Figure 3.4

ionisation coincide with the z axis as shown. The (plane) waves are normally incident on the column from the negative x direction ($\theta = 180^{o}$). Such a wave may be resolved into two plane waves with polarisations shown in Figure 3.3(a) and 3.3(b) each of which may be treated separately.

The wave matching technique used by Herlofson (1951) provides equations which describe the electromagnetic fields scattered by such a column of ionisation. For a unit amplitude plane wave with parallel polarisation (Figure 3.3(a)) the electric field within the column of ionisation is

$$E_z = \sum_{o}^{\infty} P_n(r) \cos(n\theta) \qquad \text{----------(3.4)}$$

where the function $P_n(r)$ satisfies the equation

$$\frac{d^2P_n(r)}{dr^2} + \frac{1}{r}\left[\frac{d\,P_n(r)}{dr}\right] + \left[k^2\epsilon(r) - \frac{n^2}{r^2}\right]P_n = 0 \qquad \text{----(3.5)}$$

and n = 0, 1, 2 etc.

Expansions similar to equation (3.4) are used for the electric field of the incident wave in terms of Bessel functions of argument kr and of scattered waves in terms of Hankel functions of the first kind, of argument kr. To satisfy the boundary conditions at the matching radius, the reflection coefficient ($g_{//}$) is

given by

$$g_{//} = \sum_{0}^{n} A_n \cos(n\theta) \text{ ----------(3.6)}$$

where

$$A_n = -\tau_n \left[\frac{J_n(kr)P_n'(r) - kJ_n'(kr)P_n(r)}{H_n^{(1)}(kr)P_n'(r) - kH_n^{(1)'}(kr)P_n(r)} \right] \text{---(3.7)}$$

τ_n is the Neumann factor where

$\tau_n = 1$ if $n = 0$

$\tau_n = 2$ if $n \neq 0$

Also, $J_n(kr)$ is a Bessel function of the first kind, $H_n^{(1)}(kr) = J_n(kr) + jY_n(kr)$ a Hankel function of the first kind and $J_n'(kr)$ and $H_n^{(1)'}(kr)$ are the first derivatives of the respective functions.

The radius r is the radius at which the incident and scattered waves are matched to fields within the column. The matching radius is chosen as either the outer limit of the ionisation or as the radius at which the ionisation density is essentially zero, rendering the dielectric constant given by equation (3.3) very nearly equal to unity.

For a unit amplitude plane wave with transverse polarisation, (Figure 3.3(b)) the magnetic field within the column of ionisation has a z-component only. The

magnetic field is given by

$$H_z = \sum_{o}^{n} T_n(r) \cos(n\theta) \text{ ----------(3.8)}$$

where $T_n(r)$ satisfies the differential equation

$$\frac{d^2T_n(r)}{dr^2} + \left[\frac{1}{r} - \frac{1}{\epsilon(r)} \frac{d\epsilon(r)}{dr}\right] \frac{dT_n(r)}{dr} + \left[k^2\epsilon(r) - \frac{n^2}{r^2}\right] \times T_n(r) = 0 \text{ ----------(3.9)}$$

The reflection coefficient is similarly given by

$$g_{\perp} = \sum_{o}^{n} B_n \cos(n\theta) \text{ ----------(3.10)}$$

where

$$B_n = \tau_n \left[\frac{k\, J_n'(kr)\, T_n(r) - J_n(kr)\, T_n'(r)}{k\, H_n^{(1)\prime}(kr) T_n(r) - H_n^{(1)}(kr) T_n'(r)}\right] \text{-------(3.11)}$$

The development of equations (3.5), (3.7), (3.9) and (3.11) is presented in Appendix 5.

A study of the reflection of radio waves from meteor trains apparently involves the calculation of two reflection coefficients, one for transverse electric polarisation and the other for parallel polarisation of the electric vector. In the following discussion it will be shown that this is not necessary and that the calculation of one coefficient is

sufficient.

Herlofson (1951) investigated both parallel and transverse polarisation reflection for several idealised models of a meteor train and his results for back-scattering are summarised in Figure 3.4.

Herlofson states that when the electron density is so great that the dielectric constant (as predicted by equation (3.3)) has a large negative value, the echo from a column will be much weaker in the transverse than the parallel case. In parallel scattering the electrons slide up and down along the cylinder and the motion is not hindered by a great electron density. In transverse scattering, the electrons move across the column and space charges which tend to restore the equilibrium are set up along the boundaries. When the electron density becomes sufficiently great the electrostatic forces will substantially prevent displacement of the charges and the cylinder will not respond to the incident wave in the same manner.

As the column expands, the dielectric constant becomes less negative and reflection from transverse polarisation increases; upon expanding further, the amplitude of the reflection due to transverse polarisation passes through a maximum or resonance value. After this value has been reached, the amplitude of the echo falls. Eventually the transverse polarisation reflection coefficient ($g_{\perp}$) will equal that of the parallel polarisation reflection coefficient ($g_{//}$). This

can be seen by considering equations (3.5) and (3.9). In equation (3.9) as r increases $\epsilon(r) \to 1$ and therefore $\epsilon(r)' \to 0$ whereupon equation (3.9) will be identical to equation (3.5).

Generally, the reflection of the incident wave seems to involve the effects of both transverse and parallel polarisation. Apparently, only under exceptional circumstances will either equation (3.5) or (3.9) individually satisfy the conditions involving reflection from a meteor train.

In their theoretical back-scatter investigation, Lebedinec and Sosnova (1967) show that over a fairly wide range of values of electron line density and kr_d, $g_\perp$ tends to be larger than $g_{//}$ attaining a maximum value of $g_\perp/g_{//} \simeq 100$ at $\alpha \simeq 2.3 \times 10^{14}$ m^{-1} at resonance (where the ratio $g_\perp/g_{//} = L$ is known as the polarisation ratio) (see Figure 3.5). In a similar theoretical investigation, Keitel (1955) calculated the exact solution of the reflection equations by numerical integration of equations (3.5) and (3.9). The reflection coefficients calculated by Keitel are shown in Figure 3.6 for back-scattering.

The lowest value of electron line density employed by Keitel was $10^{13} m^{-1}$. The nearest value to this employed by Lebedinec and Sosnova was $2 \times 10^{13} m^{-1}$. The reflection coefficients for parallel polarisation calculated by Keitel for $10^{13} m^{-1}$ and Lebedinec and Sosnova for $2 \times 10^{13} m^{-1}$ appear

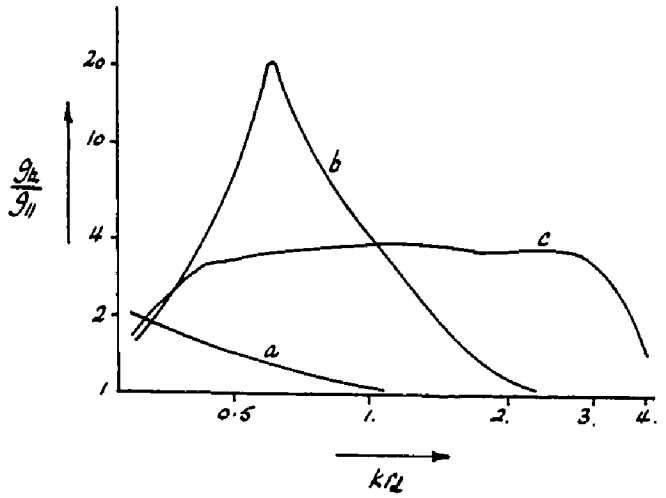

Ratio of reflection coefficients according to Ketebaiec and Sosnova (1967). a, b and c correspond to 2×10^{13}, 2×10^{14} and 10^{15} electrons per meter respectively, for back scattering.

Figure 3.5

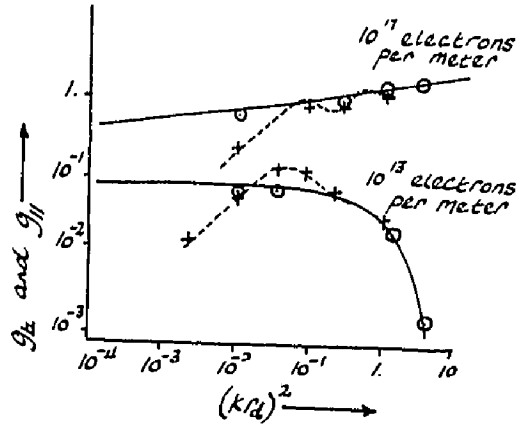

Parallel Polarisation

⊙ Calculated (Keitel, 1955), —— Approximate (Kaiser and Closs, 1952)

Transverse Polarisation

\+ Calculated (Keitel, 1965), ---- Approximate (Kaiser and Closs, 1952)

Comparison of exact scattering coefficients for back-scattering and approximate reflection coefficients found by Kaiser and Closs (1952) for the Gaussian column (Keitel, 1965)

Figure 3.6

consistent.

We turn now to the examination of experimental evidence. Billam and Browne, (1955) investigated polarisation effects associated with meteor trains by the use of mutually perpendicular antennas. They reported that they observed polarisation effects as predicted by the Kaiser and Closs (1952) theory. That is, for an underdense meteor echo, they observed a sharp increase in L to a maximum shortly after the beginning of the echo, followed by a decay to a constant value which the theory predicts to be unity. A histogram of the values of L for the measured short duration echoes due to Billam and Browne (1955), is given in Figure 3.7.

Billam and Browne also stated that no long duration overdense echoes were observed which showed the kind of polarisation effect predicted for short duration echoes. Most of the long duration echoes exhibited a constant L (unity). They concluded that the maximum L for short duration echoes is approximately double the value of 2.0 predicted by Kaiser and Closs.

Van Valdenburg (1954) also studied polarisation effects of short duration echoes. He estimated that of the echoes which were measured, 80% had a maximum L of less than 4. Closs, Clegg and Kaiser (1953) also performed an experiment utilising transverse and parallel polarisation, and concluded that the most probable value of L was 1.7.

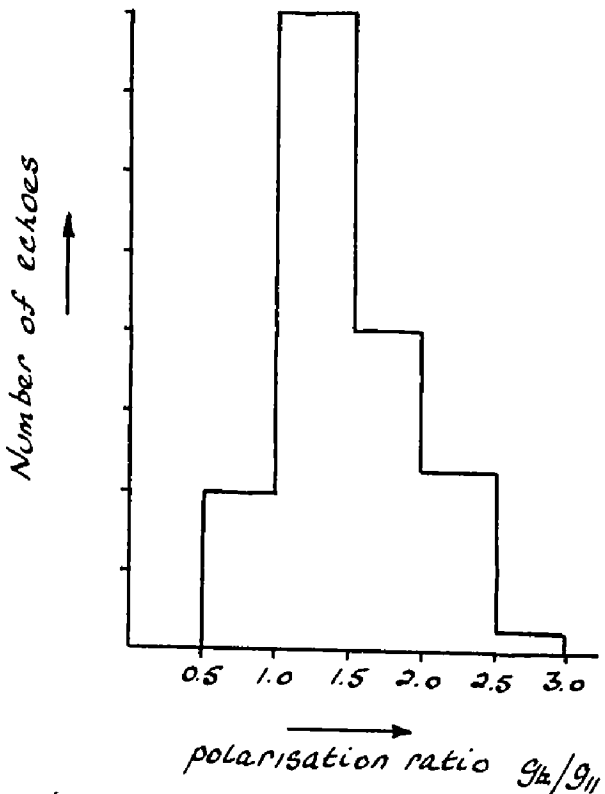

Distribution of values of constant polarisation ratio ($g_\perp / g_{||}$) for short duration echoes after Billam and Browne (1955)

Figure 3.7

Table 2		
Authors	λ	kr_d
Billam and Browne (1955)	5.4	1.16
Closs, Clegg and Kaiser (1953)	4.0	1.57
Van Valdenburg (1954)	13.1	0.18

It appears then, that large values of L have not been experimentally observed; summarising the experimental evidence, it would seem that the majority of underdense echoes exhibit a maximum L certainly below 4.0 and apparently averaging about 2.0, quickly falling to unity.

The reasons that large values of L are not observed may be as follows. The initial radius of a meteor train (r_o) is of the order of 1m. (Baggaley, 1970, and Greenhow and Hall, 1960). In Figure 3.5 one notes that the value of L is plotted against kr_d (which therefore reduces to k if t = 0). The wavelength employed by Billam and Browne was 5.4m, Closs Clegg and Kaiser 4.0m and Van Valdenburg 13.1m. The various values of kr_d calculated using these wavelengths is displayed in Table 2.

Lebedinec and Sosnova show that the maximum value of L should occur when $kr_d \simeq 0.6$ (as illustrated in Figure 3.5) and therefore owing to the λ dependence, the condition of the column of ionisation at formation will render observation of high values of L impossible except for Van Valdenburg's equipment. Theoretically, Van Valdenburg should have been able to observe the maximum value of L. However, he states that he was concerned with meteors fainter than those which are able to produce luminous trains. By this we must assume that he was concerned with those trains fainter than the eye can detect. Therefore Van Valdenburg must have investigated meteor trains of $+5^M$ and fainter.

A $+5^M$ meteor is one with an electron line density of $10^{14} m^{-1}$ (equation (1.3)) and therefore Figure 3.5 may possibly show why Van Valdenburg did not detect values higher than 4.0. The largest value of L occurs for an electron line density of $2.3 \times 10^{14} m^{-1}$, brighter than $+5^M$ and hence excluded from his analysis.

Summarising the foregoing, in general if plasma resonance is going to occur, it will appear shortly after the formation of the meteor train. The effect will last perhaps 20 or 25 msecs whereupon L will drop to unity. The equipment used in this experiment will barely detect such a short duration event. A 20 or 25 msec duration corresponds to a rise time of about 10 or 12 msec. The rise time of a typical meteor echo is of the order of 50 msec.

Also, the enhanced resonance predicted by Lebedinec and Sosnova will occur when the train is overdense and one would expect this to have the effect that the overdense train would screen the forward-scattered wave from the resonance. Therefore, any resonance observed on forward-scatter would possibly be less pronounced than on back-scatter. Therefore in keeping with the foregoing discussion it was decided to calculate the simpler of the two reflection coefficients, $g_{//}$.

Making the substitution $\rho = r/r_d$, equation (3.5) becomes

$$\frac{d^2P_n(\rho)}{d\rho^2} + \frac{1}{\rho}\frac{d\,P_n(\rho)}{d\rho} + \left[\epsilon(r)\ (kr_d^2) - \frac{n^2}{\rho^2}\right] P_n(\rho) = 0 \quad ---(3.12)$$

and $\epsilon(r)$ is shown by McKinley (1961) to be given by

$$\epsilon(r) = 1 - 81\frac{N_e}{f^2} \quad ----------(3.13)$$

where f is the frequency of the incident radio wave and N_e is given by equation (3.1). Substitution of equation (3.1) into (3.13) gives

$$\epsilon(r) = 1 - \frac{81\ \alpha\ \exp(-r^2/(4Dt + r_o^2))}{f^2\ \pi\ (4Dt + r_o^2)}\ .$$

Rearranging the above equation and substituting $r_d = (4Dt + r_o^2)^{1/2}$ then

$$\epsilon(r) = 1 - \frac{1.13 \times 10^{-14}\ \alpha\ \exp(-\rho^2)}{(kr_d)^2} \quad ----------(3.14)$$

The reflection coefficient for parallel polarisation is obtained by modifying equations (3.6) and (3.7) and yields

$$g_{//} = \sum_{o}^{\infty} \tau_n \frac{P_n'(\rho)J_n(kr_d\rho) - kr_dJ_n'(kr_d\rho)P_n(\rho)}{-H_n^{(1)}(kr_d\rho)P_n'(\rho) + kr_dH_n^{(1)\prime}(kr_d\rho)P_n(\rho)}\cos(n\theta) \quad -(3.15)$$

To obtain the parallel polarisation reflection coefficients for various electron line densities and scattering angles, equations (3.12), (3.14) and (3.15) were solved.

3.4 The Numerical Integration Method

The solution of the differential equation (3.12) and subsequent solution of the parallel polarisation reflection coefficient given by equation (3.15) was accomplished by a numerical method with the aid of the University of Western Ontario C.D.C. 6400 electronic computer. The integration technique employed was the Runge-Kutta Method (Scarborough, 1966). Bessel functions of the first kind were taken as initial conditions for $P_n(\rho)$ (Lebedinec and Sosnova, 1967). Reflection coefficients were obtained for back-scattering, orthogonal-scattering and two cases of forward-scattering, 160° and 180°. The reflection coefficient $g_{//}$ for the four cases was plotted versus various kr_d values and some typical examples are shown in Figure 3.8 (a,b,c and d). Electron line densities are displayed on the curves.

3.5 The Meteoroid Mass Distribution

Jones and Collins (1970) state that the mass of a meteoroid can be taken to be proportional (at least statistically) to the electron line density it produces on entry into the atmosphere. Therefore,

$$m \propto \alpha \qquad \text{----------(3.16)}$$

The mass distribution of meteoroids deduced from the investigation of faint radio meteors is observed to be of the form

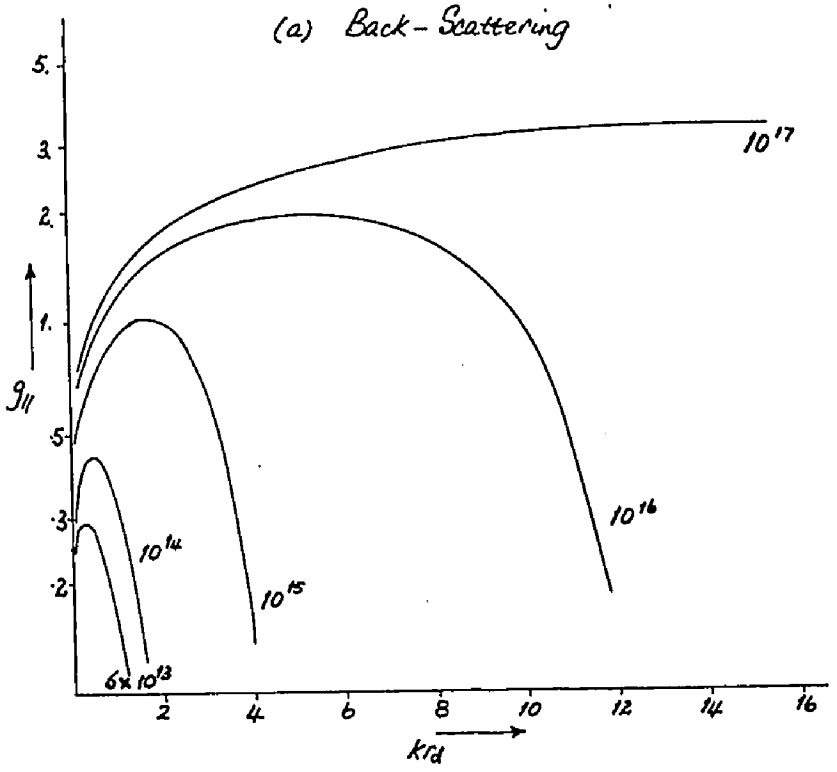

Parallel polarisation reflection coefficient g_{11} versus krd for
(a) Back-Scattering (b) Orthogonal-Scattering

Figure 3.8 (a) and (b)

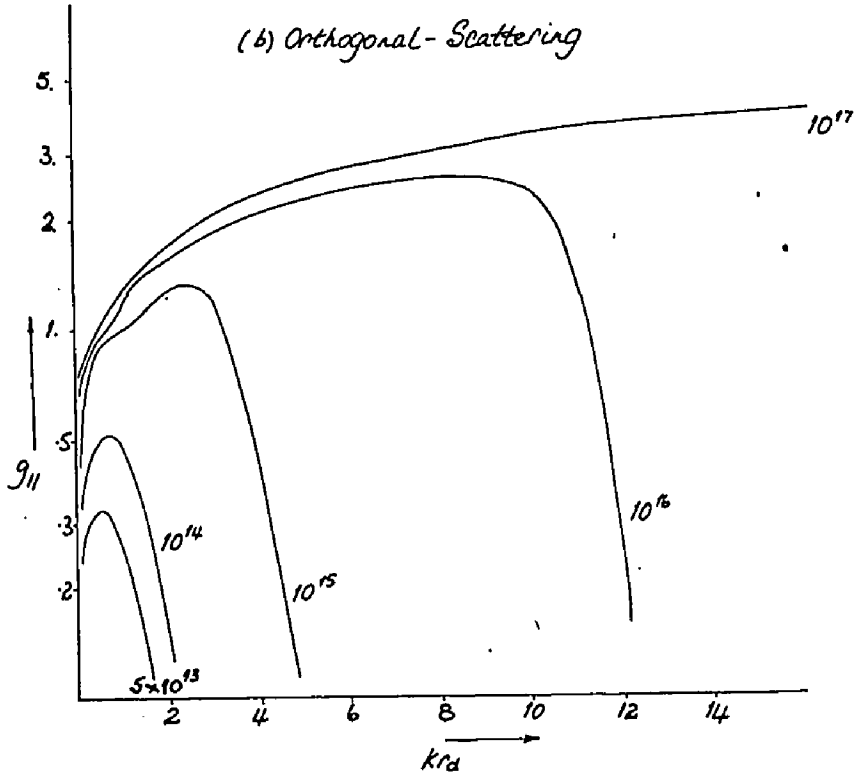

(c) 160° Forward-Scattering

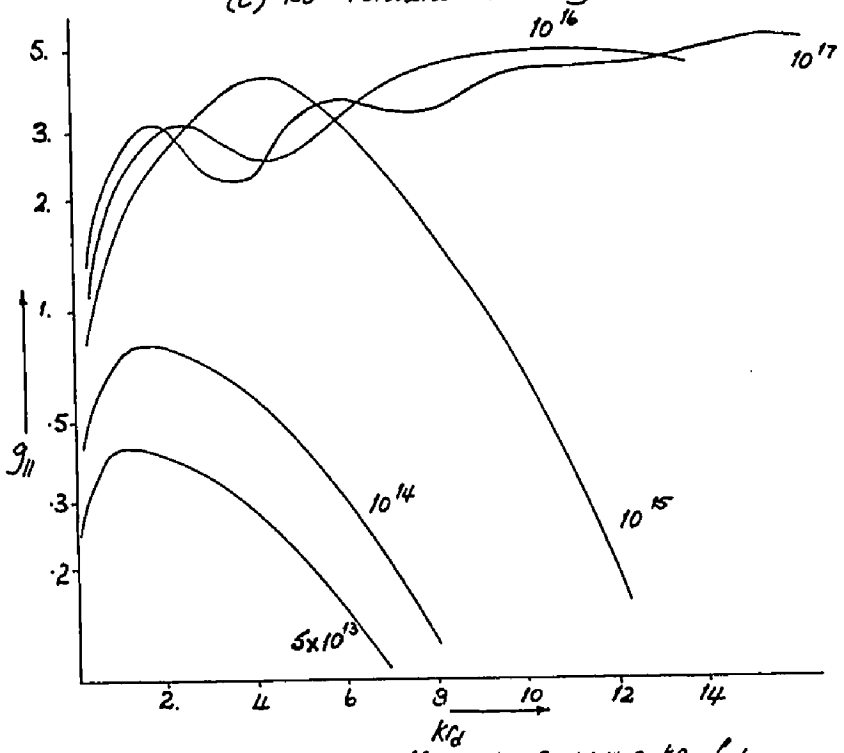

Parallel polarisation reflection coefficients $g_{\parallel}$ versus kr_d for (c) 160° Forward-Scattering (a) 180° Forward Scattering

Figure 3.8 (c) and (a)

(a) 180° Forward-Scattering

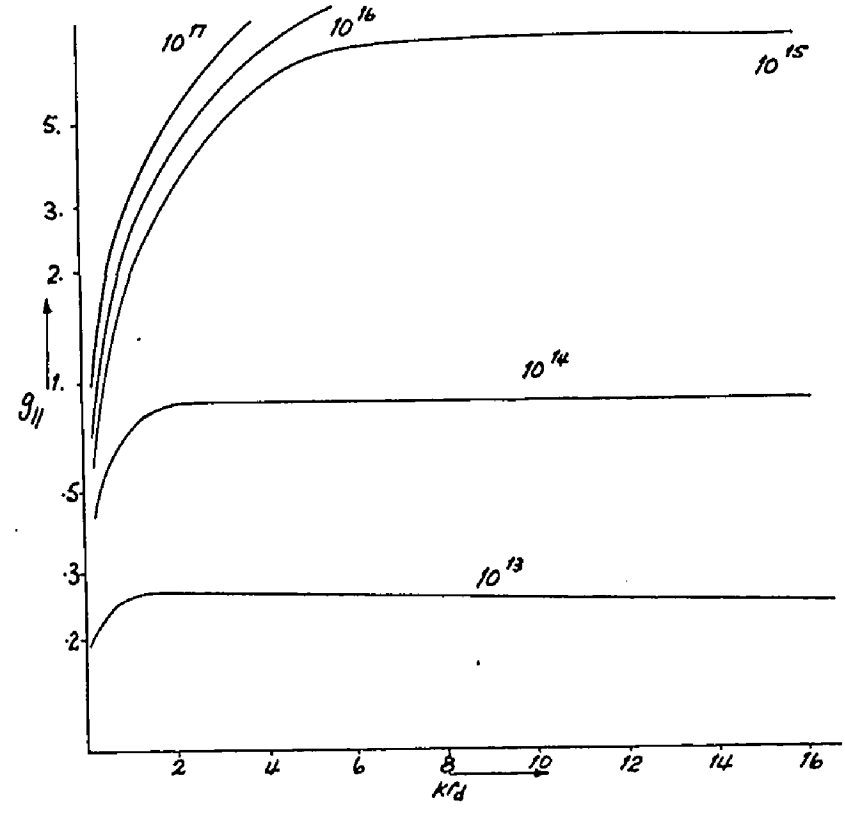

$$N = \text{constant} \times m^{1-s} \quad \text{----------(1.4)}$$

The radio meteor echo amplitude distribution index is defined as

$$\frac{d \log_{10} N}{d \log_{10} A} = 1-s' \quad \text{----------(1.5)}$$

Thus

$$1-s' = \frac{d \log_{10} N}{d \log_{10} m} \Big/ \frac{d \log_{10} A}{d \log_{10} m}$$

but $\dfrac{d \log_{10} N}{d \log_{10} m} = 1-s$ since s is a constant and

therefore we can define

$$\frac{d \log_{10} A}{d \log_{10} m} \equiv \frac{d \log_{10} A}{d \log_{10} \alpha} = \beta$$

and hence $1-s' = \dfrac{1-s}{\beta}$.----------(3.17)

Thus values of the mass distribution index s may be obtained from a consideration of the radio echo amplitude distribution index s' and appropriate values of β.

If, to a first approximation, the maximum value of the reflection coefficient $g_{//}$ is taken to be proportional to the echo amplitude A, then values of β may be obtained from the slope of a graph of $\log_{10} (g_{//})$ versus $\log_{10} (\alpha)$. Equation (1.3) states that the radio magnitude M is proportional to $\log_{10} (\alpha)$ and Figure 3.9 illustrates $\log_{10} (g_{//})$ versus M for the four scattering cases. The slopes of the

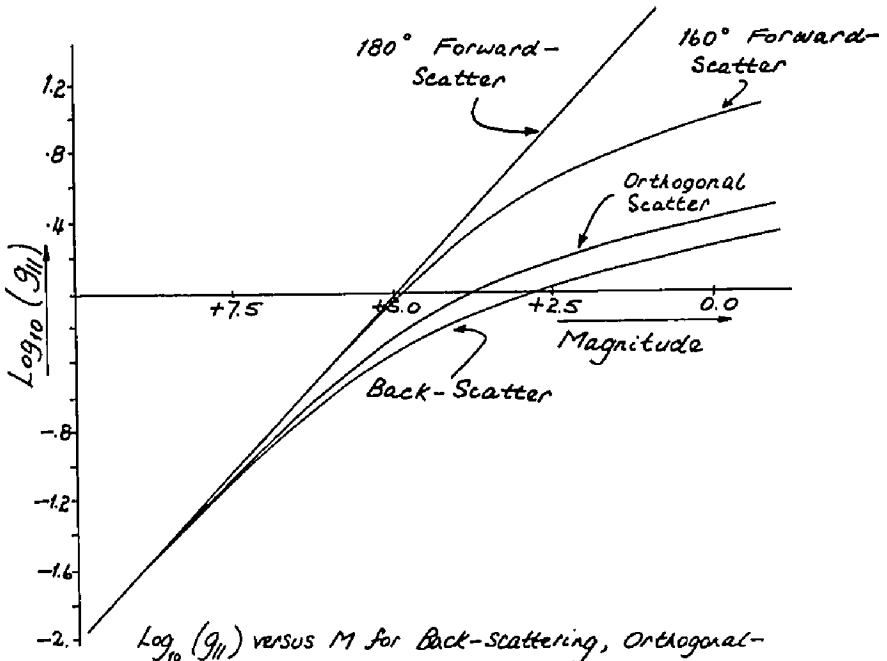

$Log_{10}(g_{11})$ versus M for Back-Scattering, Orthogonal-Scattering, 160° and 180° Forward-Scattering

Figure 3.9

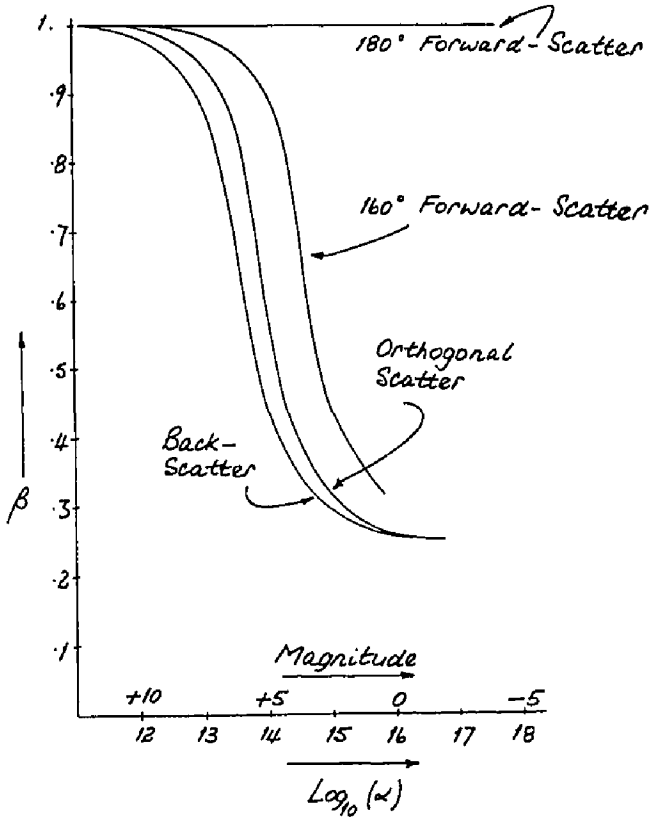

β versus $Log_{10}(\alpha)$ for various scattering angles

Figure 3.10

curves were obtained by a Lagrangian interpolation method (Scarborough, 1966) and values of β were plotted versus $\log_{10}(\alpha)$ (or M) and are illustrated in Figure 3.10.

Figure 3.9 illustrates that the region of curvature between underdense and overdense asymptotes, or regimes, occurs over a magnitude range of approximately $+7^{\underline{M}}$. It is clear then, that equipment sensitivity would have to be in excess of approximately $+9^{\underline{M}}$ for a true asymptote to the underdense region of a $\log_{10}$ N versus $\log_{10}$ A graph to be drawn. For a sensitivity less than this figure, the s' value obtained will be sensitivity dependent.

It can be shown that a relationship of the form

$$s' = s + A^{0.86} \qquad \text{----------(3.18)}$$

is a good approximation for both forward and back-scatter geometries over a limited magnitude range. If values of s' are plotted versus corresponding amplitudes to the power 0.86 the intercept of a line drawn through the data points will intersect the ordinate or s' axis at a value which will be by definition, the value of the meteoroid mass distribution index.

The limit to which equation (3.18) may be applied can be illustrated by the following procedure. From equation (3.17) it can be shown that if s is taken equal to 2, then $s' = \frac{1}{\beta} + 1$. By choice of suitable values of $\log_{10}(\alpha)$, corresponding values of $\log_{10}(g_{//})$ (or $\log_{10}(A)$) can be obtained from Figure 3.9 and similarly values of β from

Figure 3.10. Thus values of s' and $A^{0.86}$ may be calculated and these are shown plotted in Figure 3.11 for both back-scatter and forward-scatter cases.

It is apparent from the figure that a linear relationship between s' and $A^{0.86}$ exists over only a limited region. The relationship becomes non-linear when s' exceeds approximately 2.1 or 2.2 corresponding to radio magnitudes of approximately $+5^M$ and $+7^M$ for forward and back-scatter respectively. Thus in order to use equation (3.18) to determine the mass distribution index, values of s' obtained from meteor echoes brighter than the above magnitudes must be excluded from the analysis. Figure 3.12 illustrates the procedure employed in the determination of s if a linear relationship between s' and $A^{0.86}$ exists.

The equipment used in this experiment did not possess sufficient sensitivity to allow the above approach to be employed and a more general method was sought in order to determine the meteoroid mass distribution index.

First, Figures 3.9 and 3.10 were combined such that β could be expressed as a function of $\log_{10}$ (A). This is illustrated in Figure 3.13 for both scattering cases. Polynomial approximations to the curves were made. It was found that the best fits were of degree 6 and degree 7 for the back and forward-scatter geometries respectively.

Values of s' were determined from adjacent pairs of points exactly as illustrated in Figure 3.12. Each

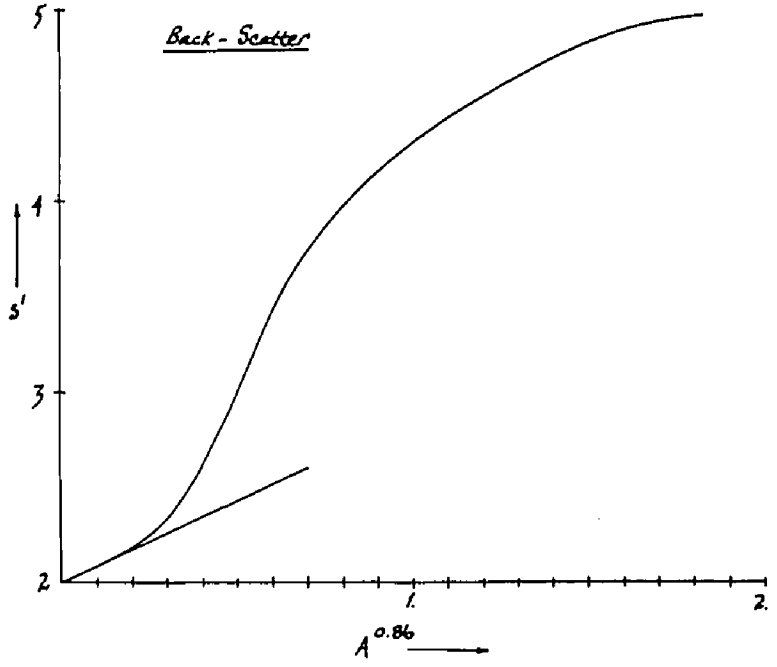

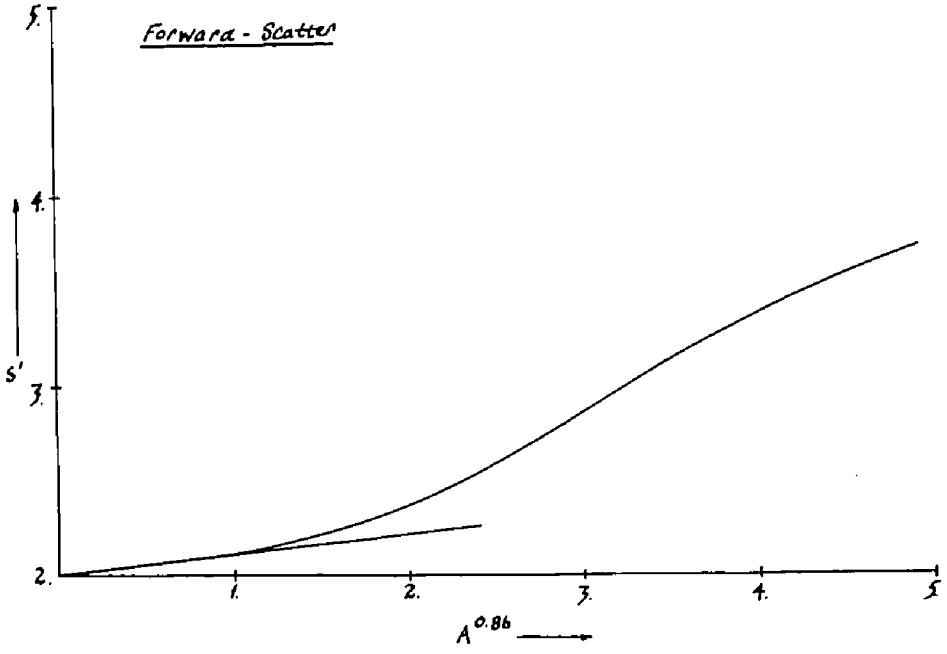

The variation of s' versus $A^{0.86}$ when s = 2 for the case of back-scattering and 160° forward-scattering

Figure 3.11

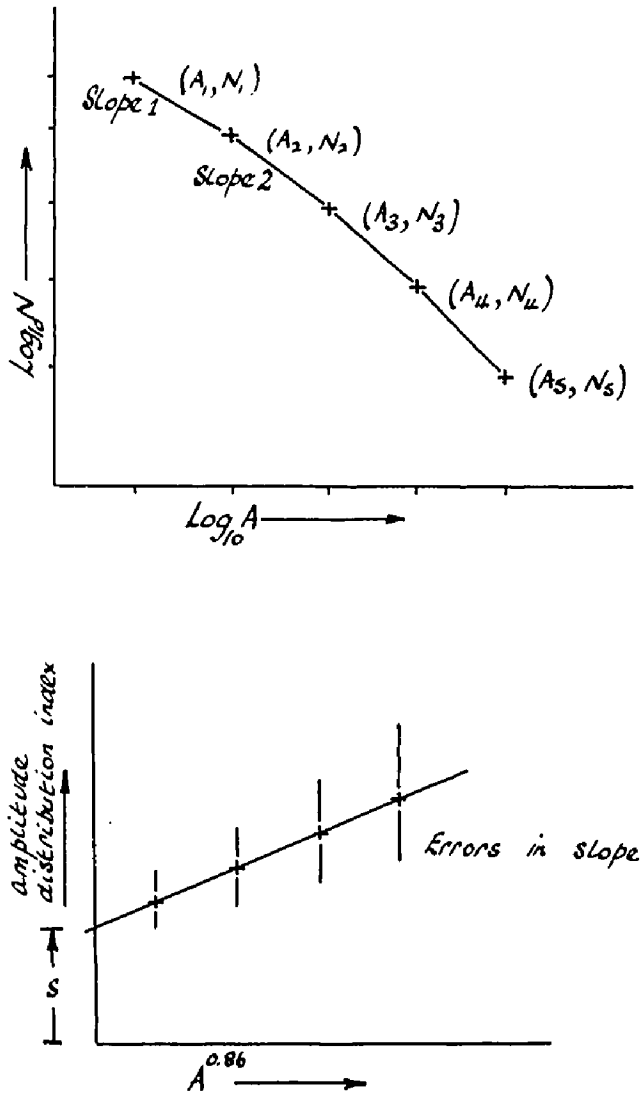

An illustration of the method by which the true mass distribution index is obtained

Figure 3.12

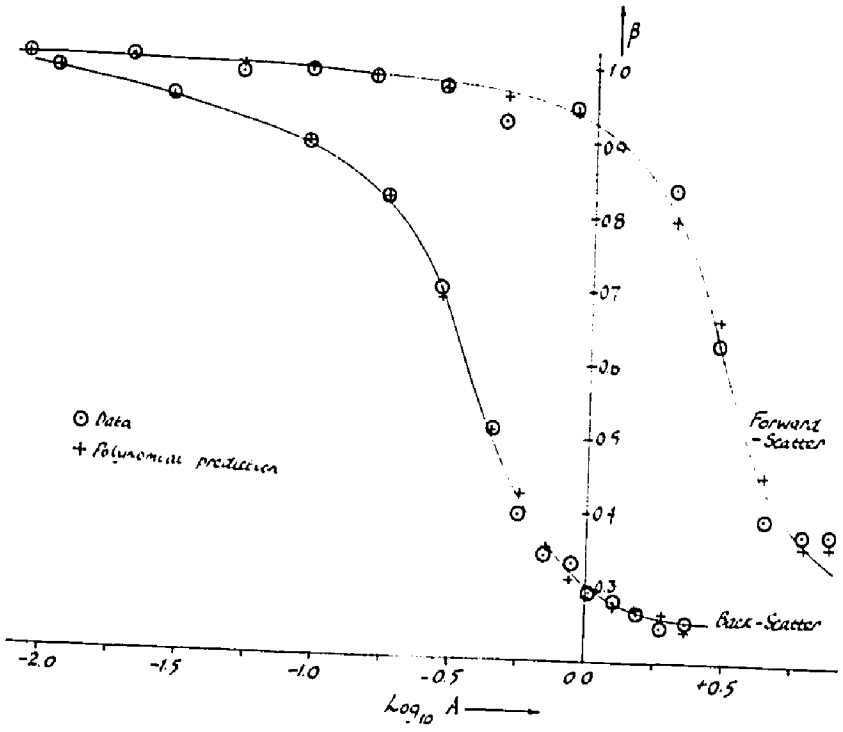

β versus $\log_{10}(A)$ for the case of back-scatter and 160° forward-scatter

Figure 3.13

value of s' was assigned an amplitude (in μv) such that the logarithm of this amplitude was the mean log amplitude of the two data points from which s' was deduced. The ratios of these amplitudes were then calculated and the following procedure adopted.

1. An arbitrary minimum theoretical amplitude was chosen by a consideration of Figure 3.13.

2. Higher amplitude levels were determined by ensuring that they were in the same ratio as the experimental amplitude levels, for the data under consideration.

3. A value of β corresponding to each theoretical amplitude was calculated from the polynominal (which expressed β as a function of the logarithm of the theoretical amplitude).

4. A value of the meteoroid mass distribution index s was determined for each amplitude by application of equation (3.17). Thus for the n^{th} amplitude level $s_n = \beta_n (s_n' - 1) + 1$. Values of s_n' were the empirical values determined previously.

5. The weighted mean value of s was calculated such that $\langle s \rangle = \left(\sum_{o}^{n} s_n/\sigma^2 \right) / \left(\sum_{o}^{n} 1/\sigma^2 \right)$ where σ is the standard deviation in s.

6. χ^2 was calculated where

$$\chi^2 = \sum_{o}^{n} \left((s_n - \langle s \rangle)^2 / \sigma^2 \right)$$

7. The minimum theoretical amplitude was incremented and steps 1 to 7 repeated.

The numerical procedure outlined above was performed by computer. The program concerned the entire range of theoretical amplitudes illustrated in Figure 3.13. The program was arranged so that values of s could be determined from a minimum of two data points up to the maximum number of data points available. The correct value of s determined from a set of data was taken to be that value for which χ^2 was a minimum. Errors in s were determined by the method outlined in Appendix 4.

3.6 A Determination of the Equipment Sensitivity from a Knowledge of the Mass Distribution Index

In Section 3.5, a method was described for determining the true mass distribution index by calculating χ^2 for a set of data located at some minimum theoretical amplitude. Since a minimum χ^2 was taken to be indicative of the true s value, the minimum theoretical amplitude existing at this point can be related to the average equipment sensitivity. Figure 3.9 displays values of $\log_{10}(A)$ versus $\log_{10}(\alpha)$ and by application of equation (1.3) the average radio magnitude may be obtained. The value of M so determined will be that value appropriate to the "most sensitive" value of s'.

The limiting magnitude of a particular scatter system is usually calculated (theoretically) for the most sensitive point in the antenna beam. An estimate of the limiting magnitude may also be made by a consideration of the average magnitude (above) and by the use of certain simplifying assumptions.

According to Kaiser (1960), radio meteors occur in a relatively narrow height range at an altitude of about 100 km which is called the echo surface. Kaiser states that the geometry of the reflection process is such that for a given radiant, the locus of echoing points is approximately a line on the echo surface. The radio meteor echo rate is proportional to the integral $\mathcal{J}$ where

$$\mathcal{J} = \int \alpha_{min}^{1 - s} \, dx$$

and α_{min} is the minimum detectable electron line density the integration being taken along the echo line.

To a first approximation, the limits of the intergration can be taken to be those points at which the reflection mechanism changes from underdense to overdense since $A \sim \alpha^{\frac{1}{4}}$ for overdense echoes whereas $A \sim \alpha$ for underdense. If, also to a first approximation, echo amplitude is assumed proportional to meteoroid mass then differentiation of equation (1.4) with respect to amplitude yields.

$$dN = \text{constant} \times A^{-s}\, dA$$

The echo amplitude will be dependent on the position along the echo line where the meteor occurs. Consider Figure 3.14 where sensitivity is shown as a slowly varying function of x, the distance along the echo line. The most sensitive point on the line occurs when $x = 0$, where the amplitude $A = A_o$, the minimum detectable echo. Most meteor echoes will not occur at this point, but rather some distance along the echo line at x_1 for example. If $A = A_1$ at this point, then in order to be seen $A_1 > A_o$. Therefore A_o and A_1 may be related by the expression

$$A_o = A_1 f(x)$$

$$\text{or} \quad A_o / f(x) = A_1$$

Therefore

$$dN = c A_o^{1-s} f(x)^{s-2} \left[\frac{df(x)}{dx}\right] dx$$

The average value of A_1, $(\bar{A}_1)$ is given by $\dfrac{\int A_1 dN}{\int dN}$

and therefore

$$\bar{A}_1 = A_o \frac{\int f(x)^{s-3} \left[\frac{df(x)}{dx}\right] dx}{\int f(x)^{s-2} \left[\frac{df(x)}{dx}\right] dx} \qquad (3.19)$$

The variation of α_{min} along the echo line may be regarded as Gaussian to a first approximation (Jones and

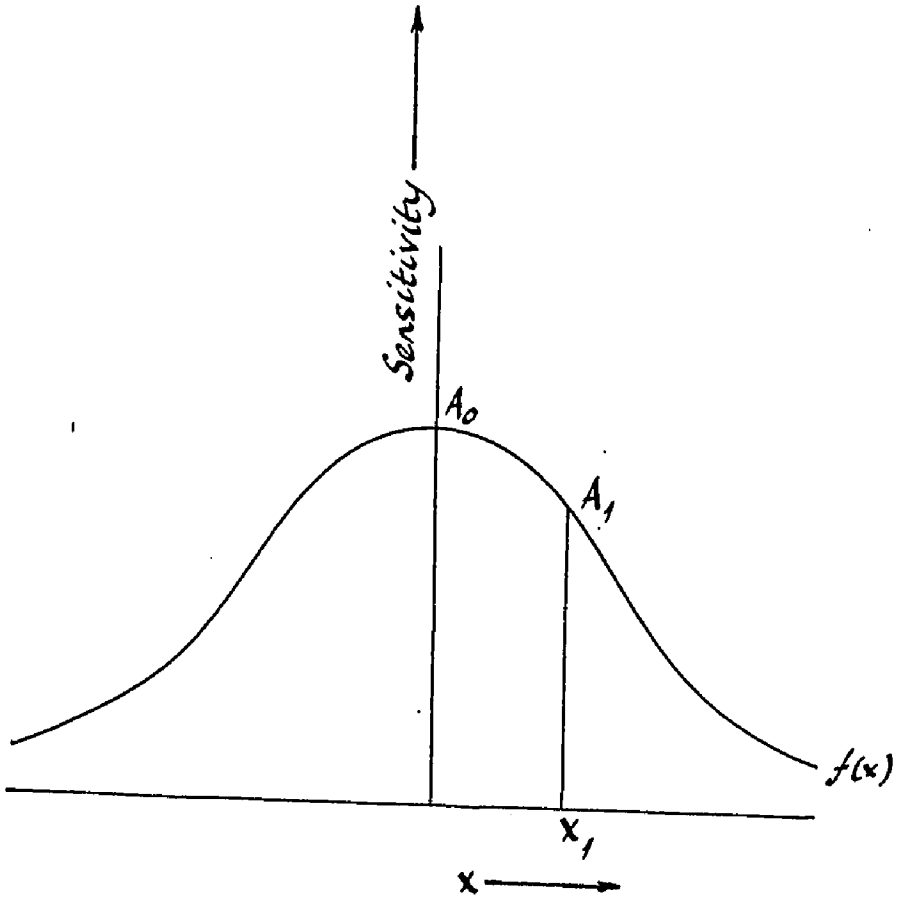

Variation of sensitivity with distance along the echo line

Figure 3.14

Collins, 1970) and therefore

$$\frac{\alpha_o}{\alpha_{min}} = \exp\ (-x^2) = f(x)$$

Replacing f(x) in equation (3.19),

$$\frac{\bar{A}_1}{A_o} = \frac{\int x \exp(x^2(2 - s))\, dx}{\int x \exp(x^2(1 - s))\, dx}$$

α_o is the value of α_{min} at the most sensitive point on the echo line. The lower limit of the integration will occur for $\alpha_{min} = \alpha_o$ or x = 0, the upper limit when $\alpha_{min} = \alpha_T$ at $x = \textcircled{w}$ where $\textcircled{w} = \sqrt{\ln(\alpha_T/\alpha_o)}$

Therefore

$$\frac{\bar{A}_1}{A_o} = \frac{\int_o^{\textcircled{w}} x \exp(x^2(2 - s))\, dx}{\int_o^{\textcircled{w}} x \exp(x^2(1 - s))\, dx}$$

β versus $\log_{10}(\alpha)$ displayed in Figure 3.10 may be expressed by the emperical relation

$$\beta = \frac{1 + \left[\frac{\alpha}{\alpha_T}\right]^n}{1 + 4\left[\frac{\alpha}{\alpha_T}\right]^n}$$

to a good approximation. If $\alpha = \alpha_T$ then $\beta = 0.4$, and this will serve as our definition of α_T. Consideration of Figure 3.10 will show that values of α_T for 160° forward and back-scatter geometries are respectively

2.2×10^{15} and 2.5×10^{14} electrons m^{-1}. s was varied from 1.0 to 3.0 in steps of 0.4 and the integrals were evaluated for α_o corresponding to magnitudes $+0.0^{\underline{M}}$ to $+10.0^{\underline{M}}$ in steps of $0.5^{\underline{M}}$. Values of $\bar{A}_1/A_o$ obtained were plotted versus s and are shown in Figure 3.15 (a and b).

Once a value of the average magnitude has been obtained, the mass distribution index is used to obtain the correction from Figure 3.15, giving an estimate of the limiting magnitude at the most sensitive point on the echo line. The procedure is as follows: selecting the figure appropriate to the scatter geometry, the contour pertaining to the mass distribution index and average magnitude of the equipment under investigation can easily be found. The value of $\bar{A}_1/A_o$ can then be read off. As meteor echo amplitude A can be taken to be approximately proportional to α then $\bar{A}_1/A_o = \bar{\alpha}_1/\alpha_o = z$. It can easily be shown that

$$M_{av} + 2.5 \log_{10} Z = M_o \text{ ----------(3.20)}$$

where M_{av} is the average magnitude and M_o the experimentally determined limiting magnitude at the most sensitive point.

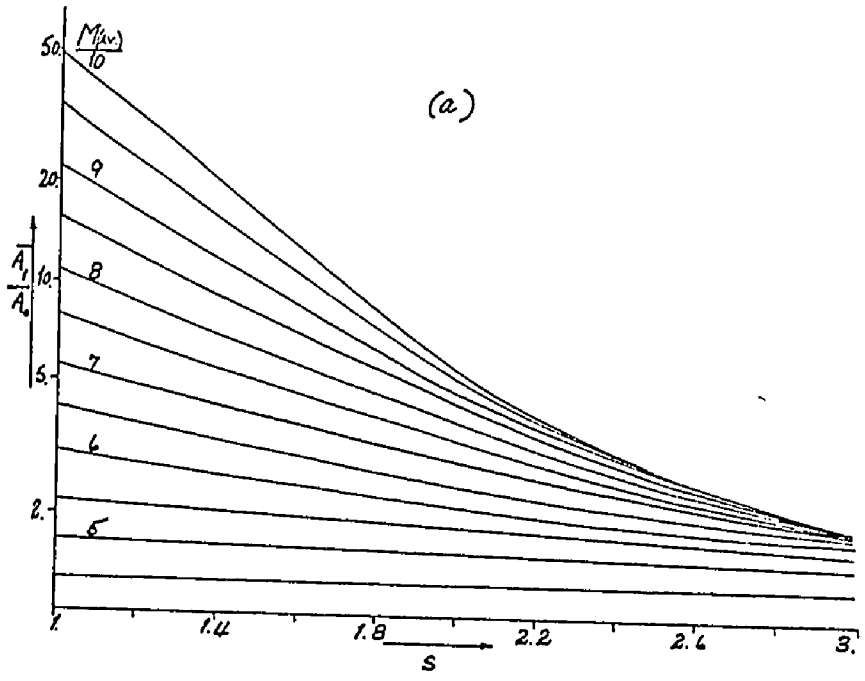

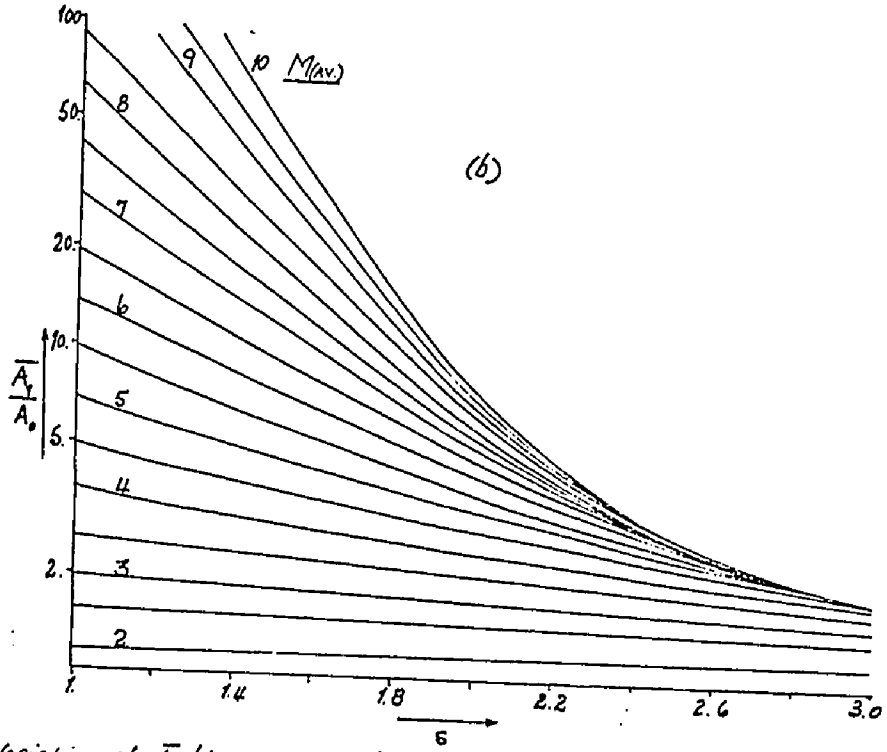

Variation of $\bar{A}_1/A_0$ versus s for (a) Back-Scattering (b) 160° Forward-Scattering

Figure 3.15

Chapter 4

SPORADIC METEOR OBSERVATIONS

4.1 The Diurnal and Seasonal Variation in Sporadic Meteor Activity

Lovell (1954) gives an excellent review of the study of sporadic meteor activity and in this review he points out that there are two main features to consider. First, meteor activity is higher after midnight than before and secondly, the activity in the second part of the year is higher than the first. The Earth's orbital motion leads to an apparent concentration of radiants around the direction of the Earth's path in space, the apex of the Earth's way. Hence an observer in either hemisphere at moderate latitudes would find the largest number of meteoroids entering the atmosphere in the early hours of the morning since at this time the apex points directly overhead. Conversely, during the early evening the observer would find fewest meteor events since at this time the apex points away from him and only meteoroids which catch up with the Earth will be observed.

The seasonal variation in meteor activity was originally thought attributable to the tilt of the earth in its orbit, as illustrated in Figure 4.1. The

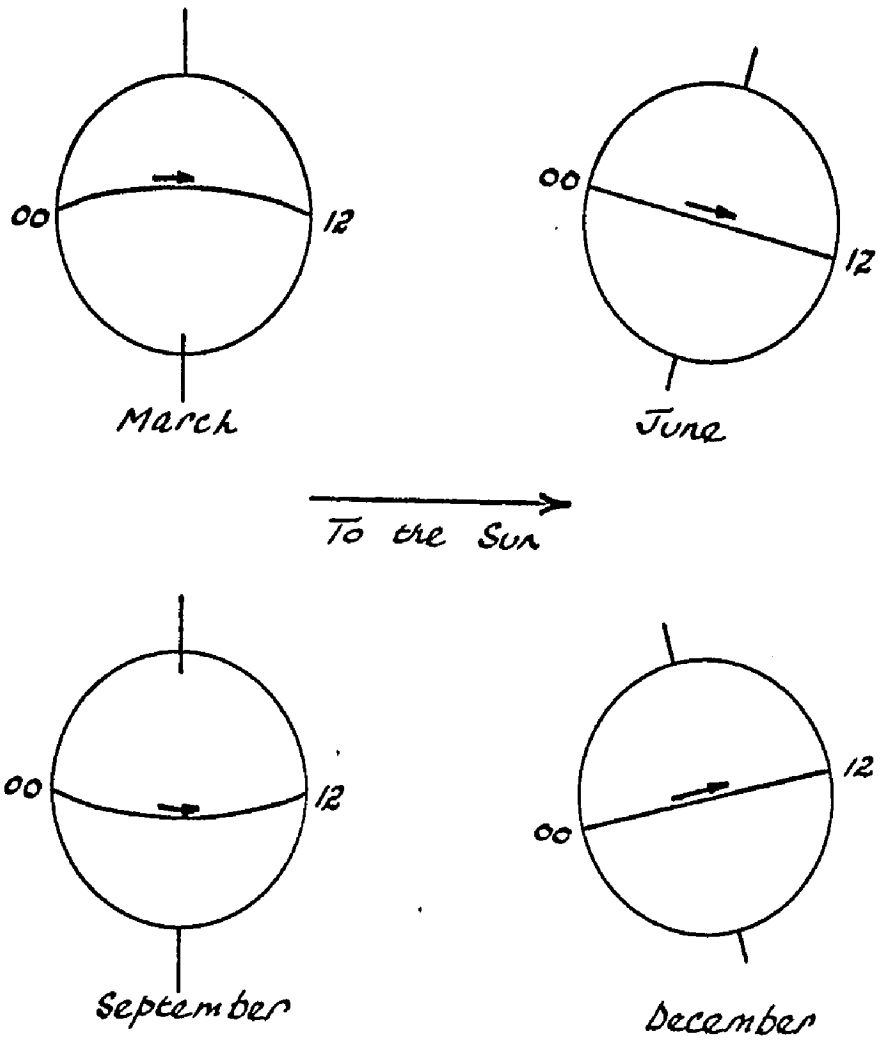

Aspect of the Earth as viewed from the forward side

Figure 4.1

northern hemisphere is tilted away from the apex in spring and towards it in autumn. As a result, it was thought that the rate occurring in the northern hemisphere would be higher in the autumn than in the spring, the converse being true in the southern hemisphere.

According to McKinley (1961) however, observations made in Australia indicate the contrary to be true. The seasonal variation appears very similar to that observed in the northern hemisphere indicating that a real variation in meteoroid distribution does exist.

4.2 Diurnal Rate Curves

Three days of sporadic activity were analysed in this work. The data were obtained from 24 hour recordings on 14/15, 19/20 and 27/28 July 1971. In all, approximately 11,000 meteor echoes were analysed. The mean hourly rate of echoes greater than level 2 (Table 1, section 2.2) is plotted versus the local time at the mid point of the scatter circuit (which is determined from a consideration of the forward-scatter geometry, and is henceforth abbreviated to "L.T.M.P.") and Eastern Daylight Time, for both scatter circuits and is shown in Figure 4.2.

The rate curves can be seen to exhibit the diurnal variation remarked upon in Section 4.1. The

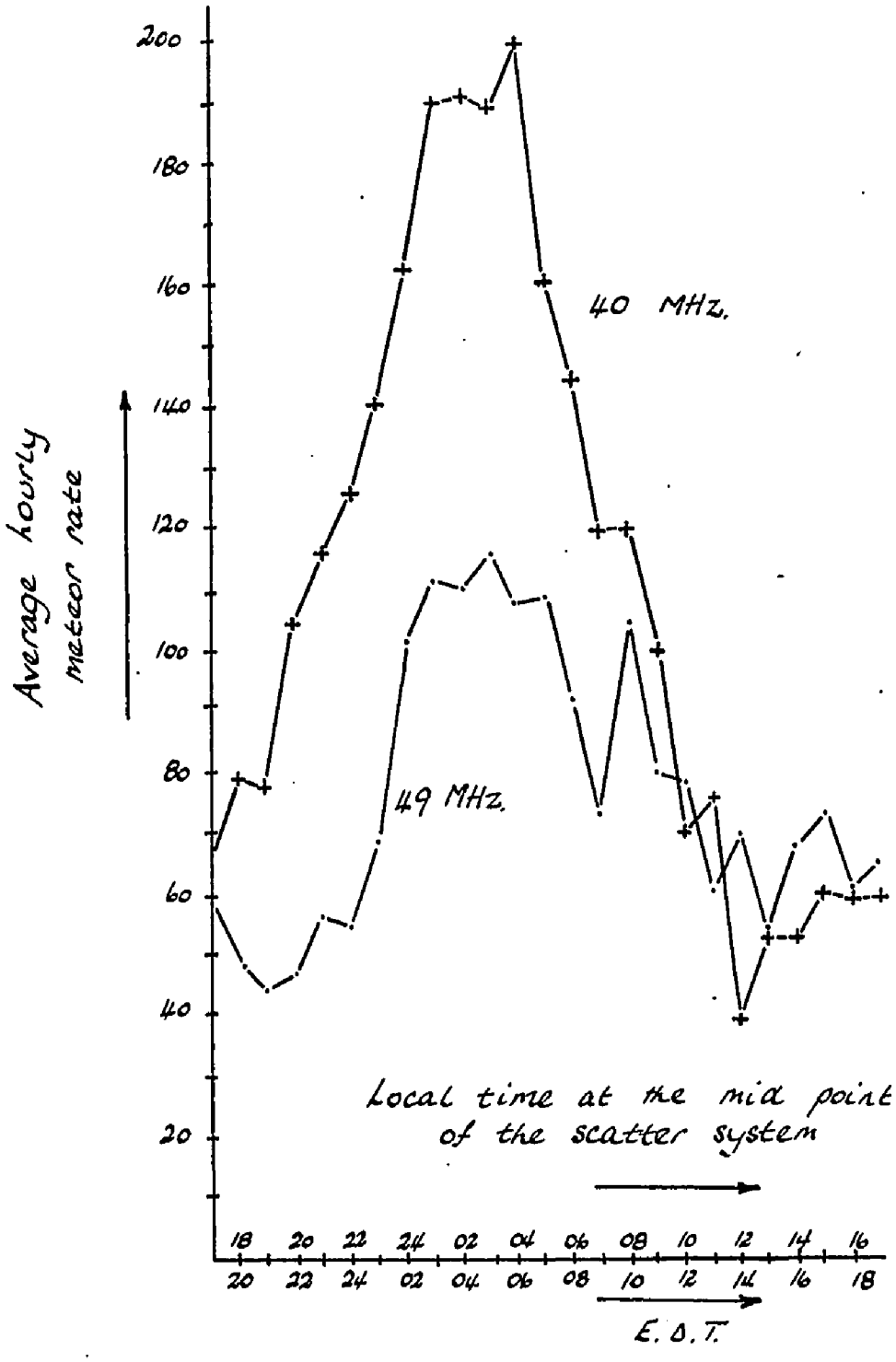

Mean hourly rate of meteor echoes greater than level 2 for both 40 MHz. and 49 MHz. scatter circuits

Figure 4.2

maximum rate for both scatter circuits occurs around 05^{00} EDT with a broad minimum centred at 16^{00} EDT. It is apparent that the maximum rate is different for each scatter circuit. This may be due to differences in the sensitivity of the circuits.

Values of $\log_{10}$ N versus $\log_{10}$ A are shown plotted in Figure 4.3 (a) and (b) for the 49 MHz and 40 MHz data respectively. Three separate cases are shown. First, the logarithm of the total number of meteor echoes for the whole 72 hour period is plotted versus the logarithm of the amplitude in μv; secondly only meteor echoes observed during the day are plotted and thirdly only those occurring during the night. Theory predicts that unless the limiting magnitude of the equipment is in excess of approximately $+9^{\underline{M}}$ then curvature of the graph will occur and such curvature can be seen in the figure.

4.3 The Diurnal Variation of s'

Hughes and Stephenson (1971) using a back-scatter circuit operating at 25 MHz obtained 30,000 meteor echoes from sporadic meteors during the period September 9-14th, 1969. The echo rates were interpreted to give the amplitude distribution index s', which was measured at half hourly intervals throughout the 6

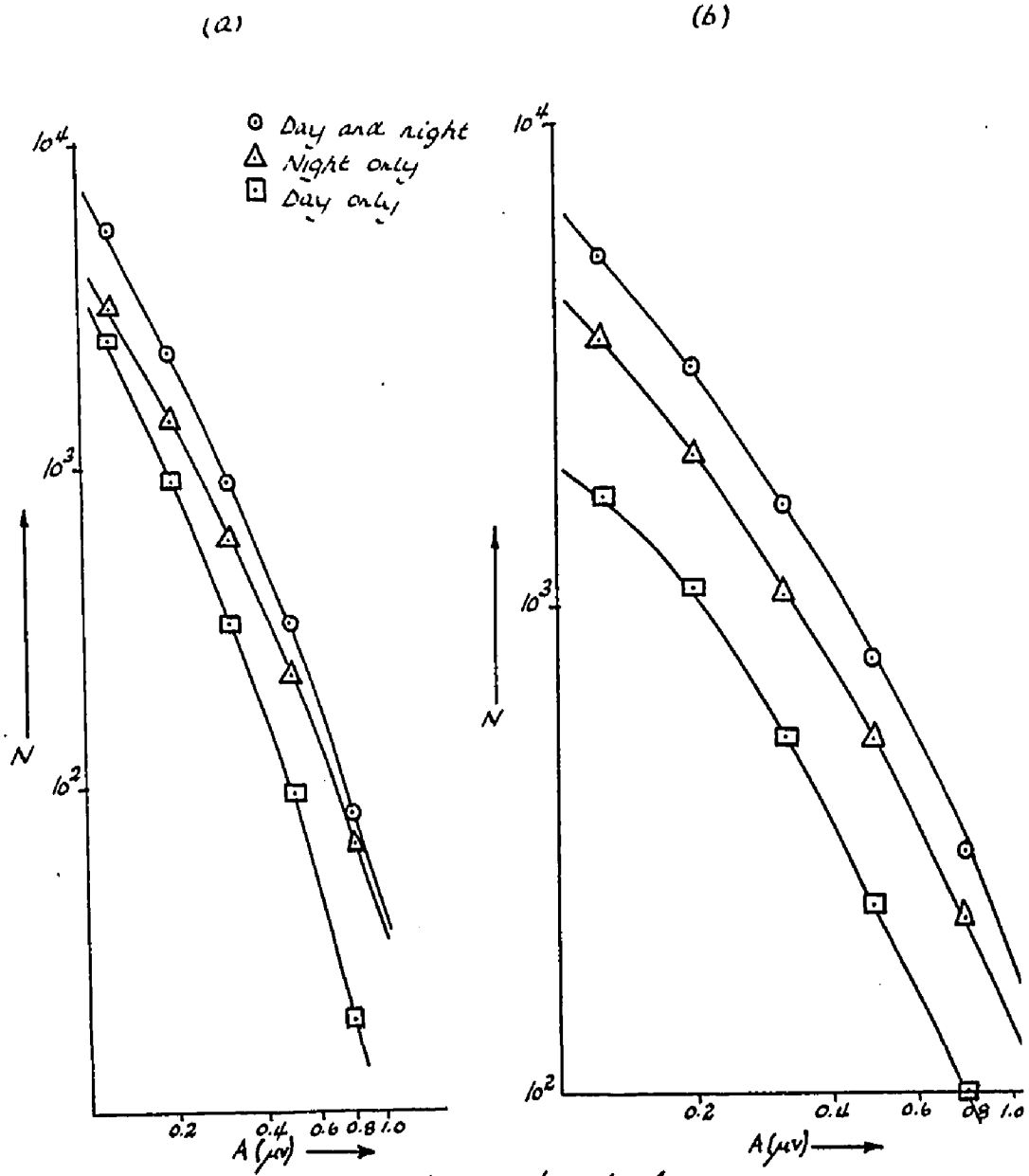

Log_{10} N versus Log_{10} A for

(a) 49 MHz. Sporadic Data

(b) 40 MHz. Sporadic Data

Figure 4.3

days and appeared to exhibit a strong diurnal variation as shown in Figure 4.4.

The data obtained in this experiment were similarly analysed. A value of s' for each hour was obtained from meteor echoes greater than levels 2 and 3 (since level 1 proved unreliable due to noise fluctuation) and the diurnal variation in this value is shown plotted in Figure 4.5(a) and (b) (49 MHz and 40 MHz respectively).

It would appear from the figure that a diurnal variation similar to that obtained by Hughes and Stephenson was seen on the 49 MHz equipment, but appears only weakly on the 40 MHz circuit. The small scale variation in s' is due to the fact that the continuous lines drawn through the data were the result of 3-point averaging. Further smoothing could have been obtained by increasing the number of points involved in the averaging process. Hughes and Stephenson obtained a very smooth curve to their data by fitting an 18th order polynomial, although a fit of a periodic function may have possibly been more appropriate.

It is also apparent from Figure 4.5 that the observed values of s' for 40 MHz are consistently less than those obtained for the 49 MHz data. If differences in sensitivity exist between the two circuits then

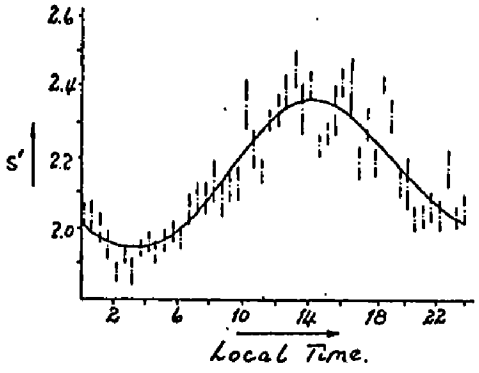

Mean half-hourly values of amplitude distribution index as a function of the time of day for the period September 9th - 14th 1969 (Hughes and Stephenson, 1971)

Figure 4.4.

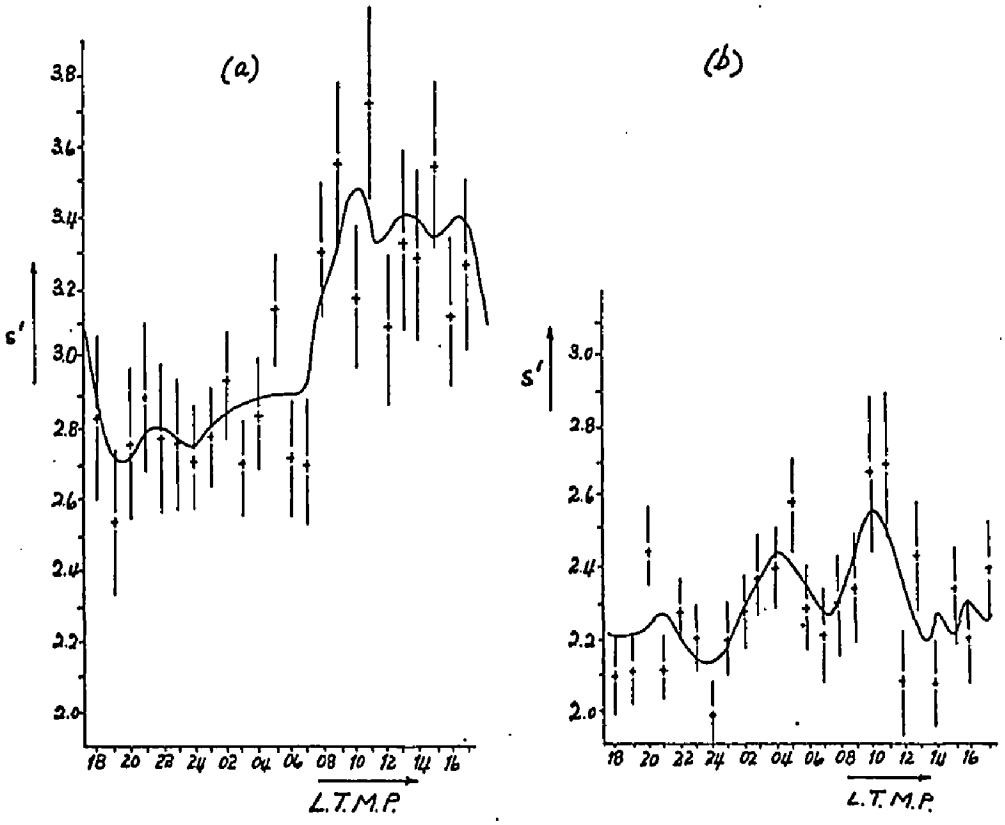

Diurnal variation in s' for

(a) 49 MHz. scatter geometry

(b) 40 MHz. scatter geometry

Figure 4.5

Figure 3.10 shows that each circuit will be associated with a different value of β. Values of β and s' are related by equation (3.17) and it is therefore apparent that equipment sensitivity can affect the value of s' obtained. The larger s' values obtained with the 49 MHz equipment therefore imply that it is less sensitive than the 40 MHz equipment.

Hughes and Stephenson state that the Earth's motion in space causes a variation in the velocity of the average meteoroid with respect to the observed region of the Earth's atmosphere. This variation is from about 60 km s^{-1} at about 04^{00} local time to 25 km s^{-1} at 16^{00} local time, causing a change in the mean echo height distribution from a maximum in the early hours of the morning to a minimum in the evening. Hughes and Stephenson maintain that this variation will be between 97 and 87 km. They based this estimate on results obtained by Šimek and McIntosh (1968) but it appears as if they may have been in error in their interpretation of these results which would render their choice of height variation incorrect.

Figure 4.6 illustrates the data obtained by Šimek and McIntosh (1968). Hughes and Stephenson's choice of between 97 and 87 km can be criticised on the following basis. It would appear from the figure that

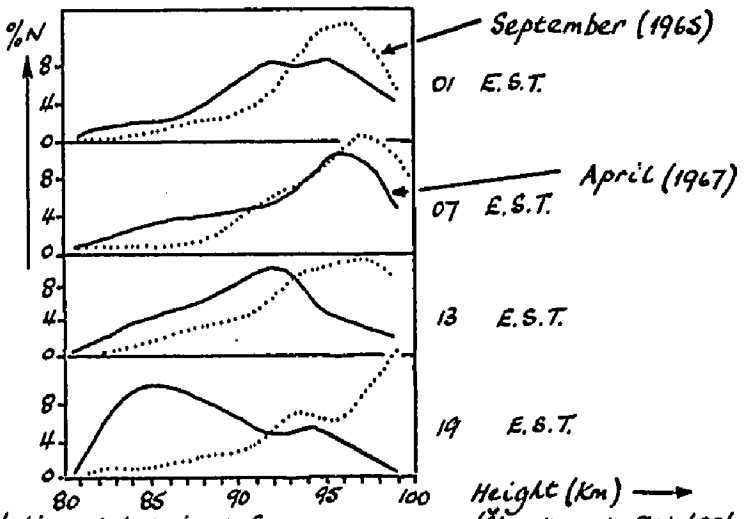

Echo height distribution determined from decay rates (Šimek and McIntosh, 1968)

Figure 4.6

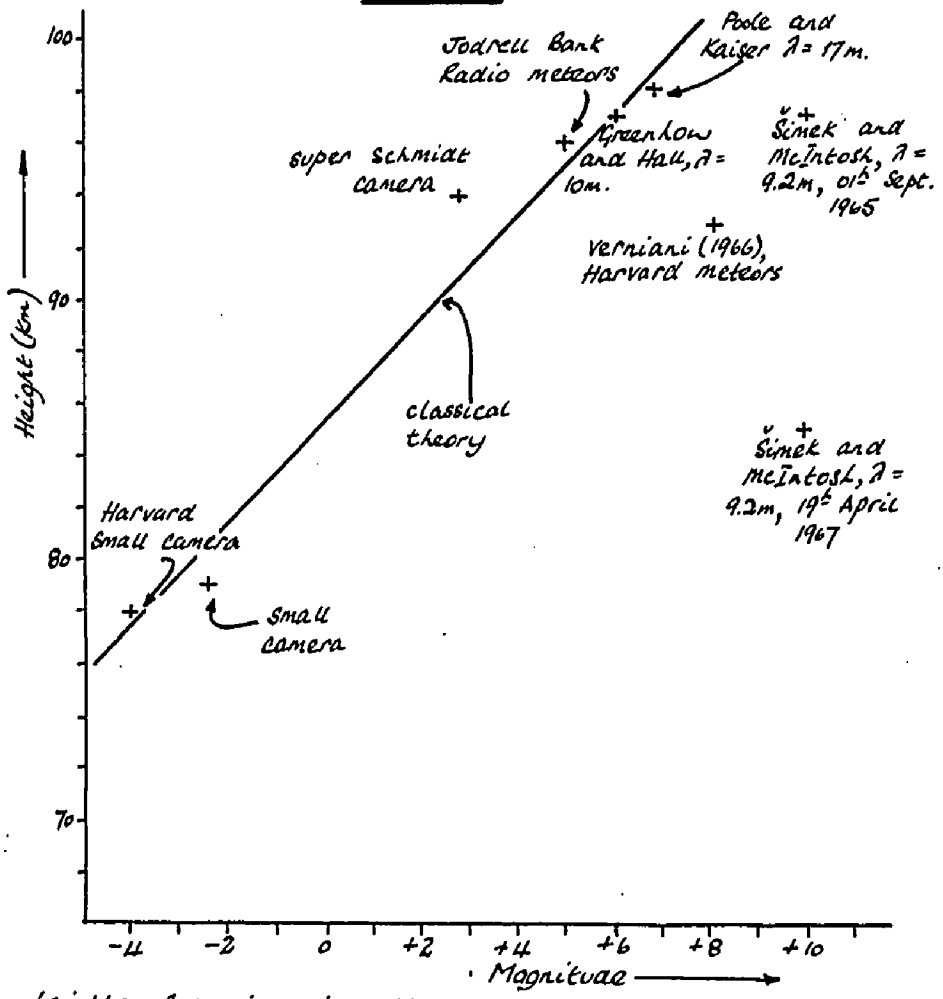

The heights of maximum ionisation versus limiting magnitude for several authors

Figure 4.7

the minimum value was chosen using data obtained in April 1967 whilst the maximum was obtained using data gathered in September 1965. It must be agreed that this would constitute a rather unusual basis on which to establish a maximum/minimum relationship and therefore a revision of the variation will be considered.

According to the classical theory of meteor ionisation, if m is the mass of the meteoroid, and ρ_{air} the air density at the point of maximum ionisation then according to Kaiser (1953) one may write

$$\rho_{air} \propto m^{1/3}$$

or

$$\ln \rho_{air} \propto \frac{1}{3} \ln m \qquad \text{----------(4.1)}$$

But $\rho_{air} \propto p_{at}$

where p_{at} is the atmospheric pressure given by

$$p_{at} = p_{at}(o) \exp - (h_{max}/H_s) \qquad \text{----------(4.2)}$$

where h is the meteor height and the subscript "max" refers to the point of maximum ionisation. H_s is the scale height being the vertical distance through which the measured parameter (pressure) changes by exp(-1).

Taking logs of equation (4.2) and substituting this into equation (4.1).

$$-\frac{h_{max}}{H_s} \propto \frac{1}{3} \ln m \qquad \text{----------(4.3)}$$

But $m \propto \alpha$, and equation (1.3) states

$$M = 40 - 2.5 \log_{10} \alpha$$

so by changing to natural logarithms

$$M = 40 - \text{constant} \times \frac{2.5}{2.3} \ln m$$

and therefore $(2.3/2.5)M_R \propto -\ln m$.

Substituting this value into equation (4.3) we obtain that

$$h_{max} \propto \frac{H_s}{3}\left[\frac{2.3}{2.5}\right]M \text{ ----------(4.4)}$$

Taking the scale height to be about 7 km at approximately 100 km (Jones, 1970) equation (4.4) will reduce to

$$\frac{d(h_{max})}{dM} \simeq 2.1$$

Therefore, according to classical theory, if the height of maximum meteor ionisation were to be plotted versus the radio or optical magnitude, the resulting graph should be a straight line of slope 2.1. Such a graph was drawn using data supplied by Greenhow and Hall (1960), Verniani (1966), Šimek and McIntosh (1968) and Poole and Kaiser (1967) and is shown in Figure 4.7. It can be seen that most of the data appears to agree fairly well with the theoretical line.

Hughes and Stephenson point out that there is inherent in their equipment a "registration time" this being the time between the actual occurrence of the

echo and the commencement of the automatic analysis. They state that this registration time, τ_R, is 40 msec and if one considers that the time taken for the meteoroid to cross the first or principal Fresnel zone is only of the order of 25 msec one can immediately see that an error will enter the analysis. The echo will have had an additional 15 msec to decay before the analysing equipment recognises the event as a meteor echo. McKinley (1961) shows that the amplitude of an echo may be expressed by

$$A = A_o \exp - \left[\frac{16\pi^2 Dt}{\lambda^2}\right] \exp - \left[\frac{4\pi^2 r_o^2}{\lambda^2}\right] \text{-------(4.5)}$$

Attenuation can be seen to be introduced by two causes; first, the finite initial radius and secondly, diffusion of the meteor train as the meteoroid passes along its path. We shall concern ourselves with this diffusion over the registration time and neglect the effects of the initial radius. Equation (4.5) therefore becomes

$$A \propto A_o \exp - \left[\frac{16\pi^2 Dt}{\lambda^2}\right] \text{----------(4.6)}$$

The unattenutated echo A_o will be proportional to α to a first approximation and therefore,

$$A \propto \alpha \exp - \left[\frac{16\pi^2 D\tau_R}{\lambda^2}\right] \text{----------(4.8)}$$

However, at the point of maximum ionisation

$$\rho_{air} \propto m^{\frac{1}{3}} \propto \alpha^{\frac{1}{3}} \propto D^{-1}$$

and therefore $$D = D_o \left[\frac{\alpha_o}{\alpha}\right]^{\frac{1}{3}} \text{----------(4.9)}$$

Substitution of equation (4.9) into (4.8) yields

$$A \propto \alpha \exp - \left[\frac{16\pi^2 D_o (\alpha_o/\alpha)^{\frac{1}{3}} \tau_R}{\lambda^2}\right] \text{----------(4.10)}$$

and

$$\ln A \propto \ln \alpha - \frac{16\pi^2 D_o \tau_R}{\lambda^2}\left[\frac{\alpha_o}{\alpha}\right]^{\frac{1}{3}} \text{----------(4.11)}$$

We define β such that

$$\beta = \frac{d \ln A}{d \ln \alpha} \equiv \frac{d \log_{10} A}{d \log_{10} \alpha}$$

Differentiating equation (4.11) with respect to $\ln \alpha$

$$\frac{d \ln A}{d \ln \alpha} = \beta = 1 + \frac{16\pi^2 D \tau_R}{3\lambda^2}$$

The substitution of numerical values into the above equation yields, for the equipment of Hughes and Stephenson $\beta = 1 + 0.0152\ D$ ----------(4.12)

If the maximum and minimum heights of meteor ionisation taken from Figure 4.7 are approximately 105 and 95 km respectively, then Greenhow and Hall (1960) indicate that values of D of 20.0 $m^2 s^{-1}$ and 6.3 $m^2 s^{-1}$ respectively, are appropriate for these heights (Figure 4.8).

Both D and the height of meteor ionisation vary with GMT in a manner shown in Figure 4.9. Typical

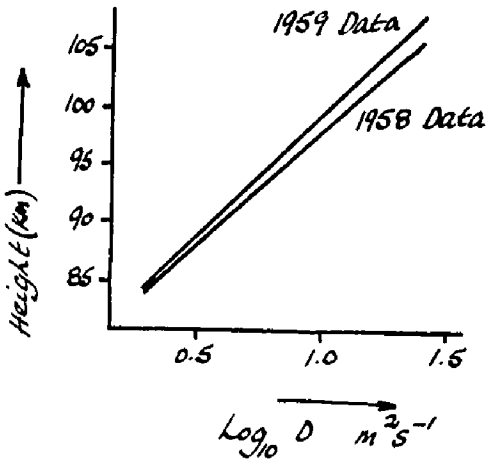

Diffusion Coefficient versus height
after Greenhow and Hall (1960)

Figure 4.8

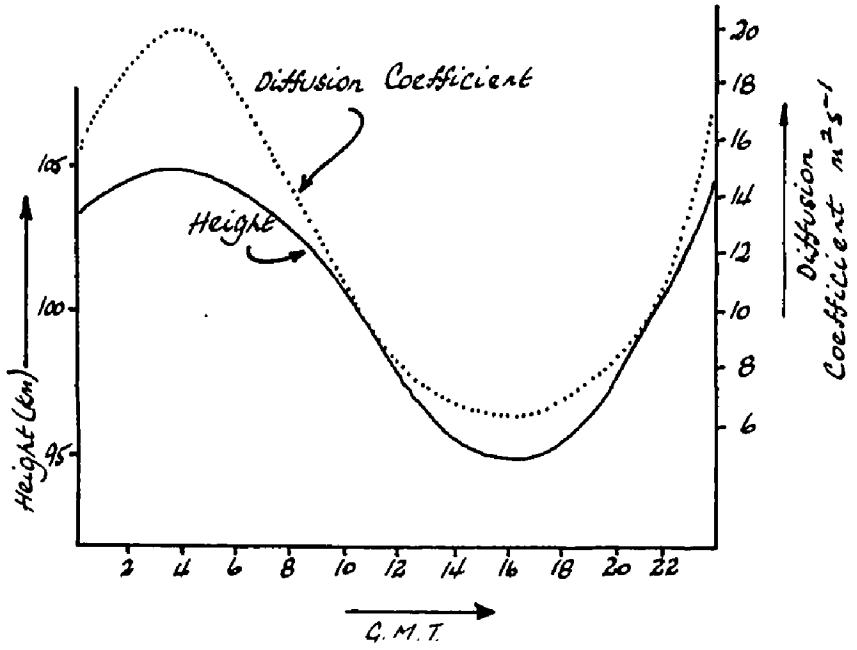

The variation of diffusion coefficient and
height with G.M.T.

Figure 4.9

values of s were selected (2.3, 2.4 and 2.5) and a consideration of these values and equations (4.12) and (3.17) allowed the variation of s' to be calculated. This variation is shown in Figure 4.10 and Table 3. The figure also shows the variation obtained by Hughes and Stephenson for purposes of comparison.

It has therefore been demonstrated that using a relatively crude approach, a diurnal variation in s' similar to that of Hughes and Stephenson can be obtained. A more judicious choice of heights of maximum and minimum ionisation would result in better correlation in the data for particular values of s. This was not attempted since the purpose of the foregoing was merely to indicate where errors in analysis may have played a part. It would therefore be relatively safe to suggest that perhaps the diurnal variation as detected by the above authors can be attributed to another cause, the significant decay of the echo in the registration time.

Having plausibly explained the apparent diurnal variation in s' as obtained by Hughes and Stephenson, we must now turn to an explanation of the same phenomena as observed in this experiment. This variation cannot be attributed to the same causes as that of Hughes and Stephenson for two reasons. First, no registration time exists in the apparatus used and secondly, as the

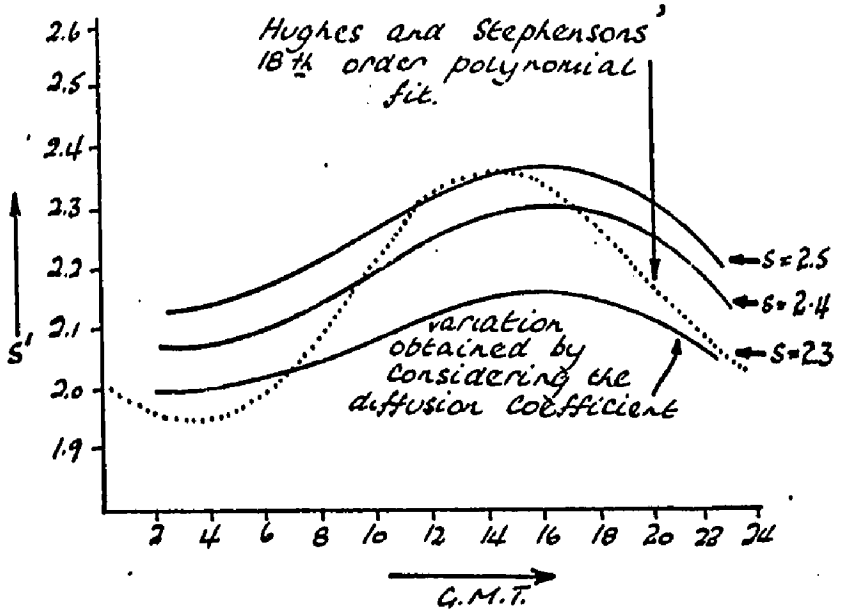

The diurnal variation in s' obtained by Hughes and Stephenson (1971), and also by a consideration of the effect of a varying diffusion coefficient

Figure 4.10

Table 3

Height in Km	Diffusion Coefficient $m^2 s^{-1}$	β value	s' value		
			s = 2.3	s = 2.4	s = 2.5
95	6.3	1.10	2.18	2.27	2.36
100	10.0	1.15	2.13	2.22	2.30
105	20.0	1.30	2.00	2.08	2.15

experiment was carried out by use of forward-scattering, the assumption that the train is instantly formed is a good approximation as pointed out in Appendix 2.

The cause of the apparent diurnal variation as observed in this work may well be absorption in the Earth's upper atmosphere. Davies (1965) states that daytime absorption at high frequencies occurs mainly in the D region between 60 and 90 kms. This is below the so-called meteor region of the atmosphere which is usually thought to exist at approximately 100 km. If an absorbing region were to occur below the meteor region, then equipment sensitivity would be reduced. It has already been demonstrated that a reduction in sensitivity will correspond to an increase in s', and therefore a study of the variation of s' may in some way give a measure of the absorption present in the atmosphere.

In order to study the effect of absorption it is necessary to study the variation of s' in the absence of absorption so that a comparison of s' values for absorption and no-absorption periods may be made. In section 4.5, the method employed is fully explained and a value of the absorption at 49 MHz for mid July 1971 presented as an example.

4.4 The Sporadic Meteoroid Mass Distribution Index

If the effects of absorption are to be avoided, only echoes occurring between about 22^{00} and 08^{00} L.T.M.P. should be considered, since daytime absorption is by far the most common (Davies, 1965). Amplitude distribution indices calculated from the slopes of adjacent pairs of points of $\log_{10}N$ versus $\log_{10}A$ were obtained for this period for both scatter circuits. These s' values were plotted against the mean log amplitude (in μv) and are illustrated in Figure 4.11.

It was pointed out in Section 3.5 that if equipment sensitivity is in excess of approximately $+7^{M}_{-}$ or $+5^{M}_{-}$ for back-scattering and forward-scattering respectively, then the mass distribution index s can be determined by the relation

$$s' = s + A^{0.86}$$

If sensitivity does not exceed the above values, a more general approach is necessary. Values of s determined by both methods should agree for data collected by the use of high sensitivity equipment.

Values of s were determined for the 1971 sporadic meteor data, collected utilising 40 and 49 MHz forward-scatter circuits. The scatter equipment was of relatively low sensitivity and therefore the general approach outlined in Section 3.5 was used in the

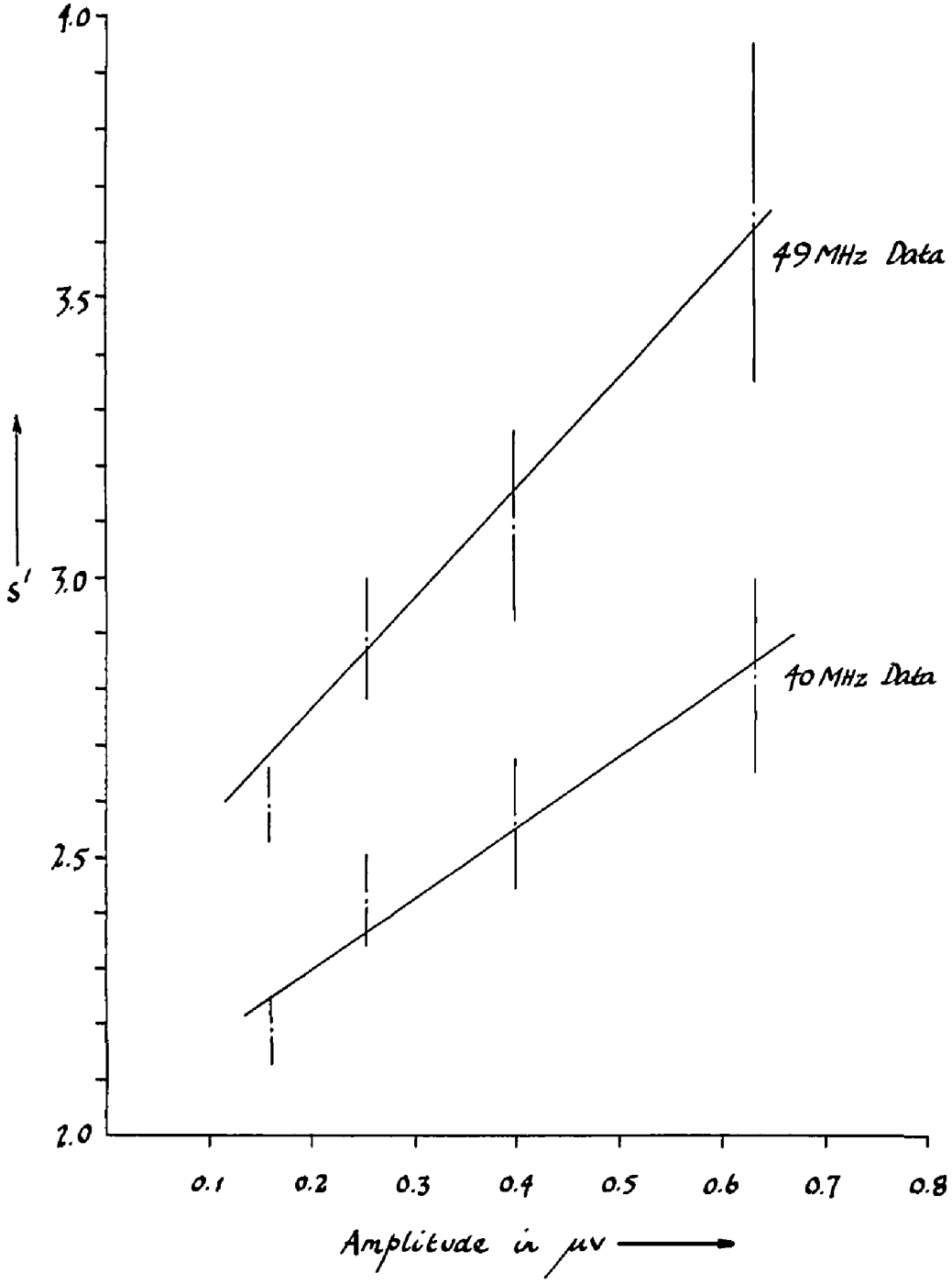

s' as a linear function of amplitude for 49 MHz and 40 MHz sporadic meteoroid data, 1971.

Figure 4.11

determination. Sporadic meteor data obtained in September 1968 on both a 49 MHz forward-scatter circuit and a 40 MHz back-scatter circuit were similarly analysed. The mass distribution index for meteors occurring during the night was

1971 49 MHz forward-scatter - 2.63 ± 0.02

1971 40 MHz forward-scatter - 2.18 ± 0.04

1968 49 MHz forward-scatter - 2.82 ± 0.06

1968 40 MHz back-scatter - 2.27 ± 0.07.

Values of s determined using 49 MHz forward-scatter equipment appear higher than values determined by both forward and back-scatter operating at 40 MHz, which agree well with the theoretical value derived by Dohnanyi (1970) of s = 2.17. The value of s' calculated for the lowest two amplitude levels for the 49 MHz circuits is approximately 2.9(1968) and 2.7(1971). If $s \simeq 2.2$ then β under these conditions will be of the order of 0.63(1968) and 0.70(1971). These values correspond to electron line densities of approximately 4.5×10^{14} and 3.5×10^{14} m^{-1}, or average radio magnitudes of $+3.3^{M}$ and 3.6^{M} respectively.

The value of the transition electron line density has been taken as 2×10^{15} m^{-1} corresponding to a radio magnitude of the order of $+2.0^{M}$. The equipment was calibrated such that successive amplitude levels were 0.5^{M} apart in 1971 and approximately 0.4^{M} in 1968

and since there are four measured values of s' in each case, it can be seen that the magnitude associated with the transition electron line density falls within the range of amplitude levels. In other words, a certain proportion of recorded echoes may have been from overdense meteor trains.

The distortion of long enduring trains by winds results in a systematic decrease in s', which reduces the curvature of the d $\log_{10}$ N/d $\log_{10}$ A curve. If the analysis described in the previous section is adopted, this will lead to a value of s which is too large since the correction of the s' values increases with increasing curvature of the d $\log_{10}$ N/d $\log_{10}$ A curve.

In an attempt to minimise the possible effect of overdense echoes, it was decided to calculate s using the values of s' existing at the two minimum amplitudes. This was only done for the 49 MHz forward-scatter data; elsewhere, the maximum number of s' values available were utilised.

Values of s obtained from 2 data points are listed below in comparison to values of s determined from the maximum number of values of s' available (4)

1971 s(4) - 2.63 ± 0.02 s(2) - 2.55 ± 0.001

1968 s(4) - 2.82 ± 0.06 s(2) - 2.48 ± 0.002

It can be seen that although the value of s has been reduced, it is still larger than values obtained with other frequencies and scattering geometries.

McIntosh and Šimek (1969) in a comprehensive analysis of the mass distribution of meteoroids, analysed some 18,000 meteor echoes. The data obtained by these authors is particularly useful in that it permits an estimate of s to be made by both the aforementioned techniques. This is made possible as the limiting magnitude of their 33 MHz back-scatter equipment is in excess of $+10\frac{M}{-}$.

Figure 4.12 shows values of s' calculated from adjacent pairs of data points plotted versus amplitude (in arbitrary units). The three points nearest the origin lie within the region +10 > M > +7 and therefore can be plotted versus $A^{0.86}$ to determine a value of s. This is shown in Figure 4.13. A weighted least squares fit was performed (Topping, 1955) and the value of s so determined was 2.00 ± 0.03.

The more general approach was then applied to the same three data points (since χ^2 would not minimise in the range of values of theoretical amplitude available, for any number of points greater than three) and a value

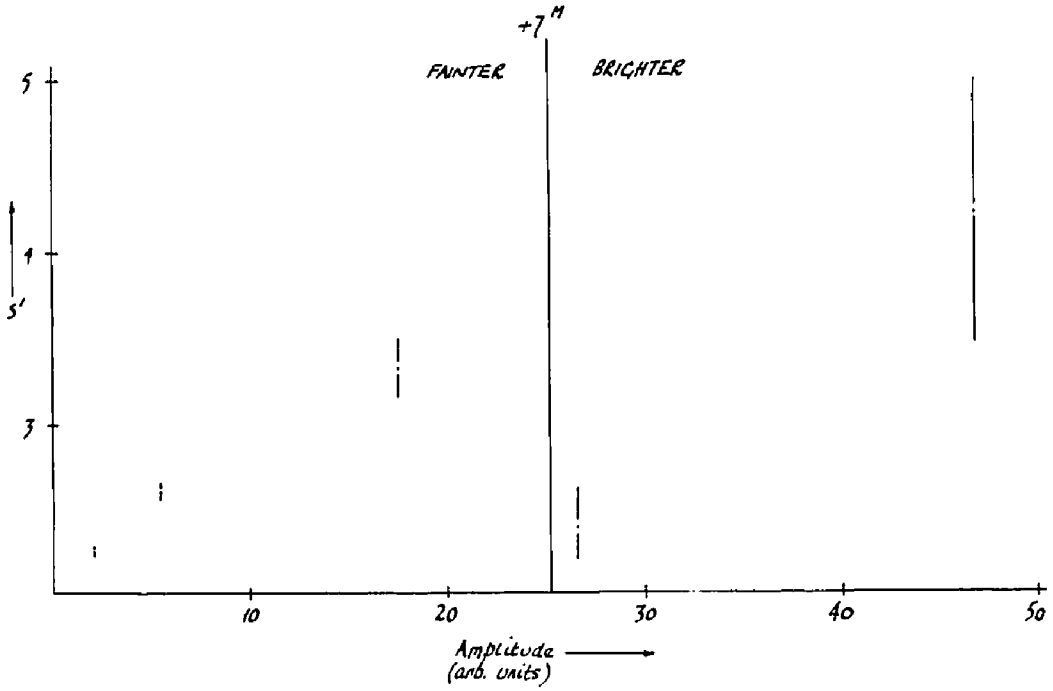

s' versus amplitude for the sporadic meteor data of McIntosh and Šimek (1969)

Figure 4.12

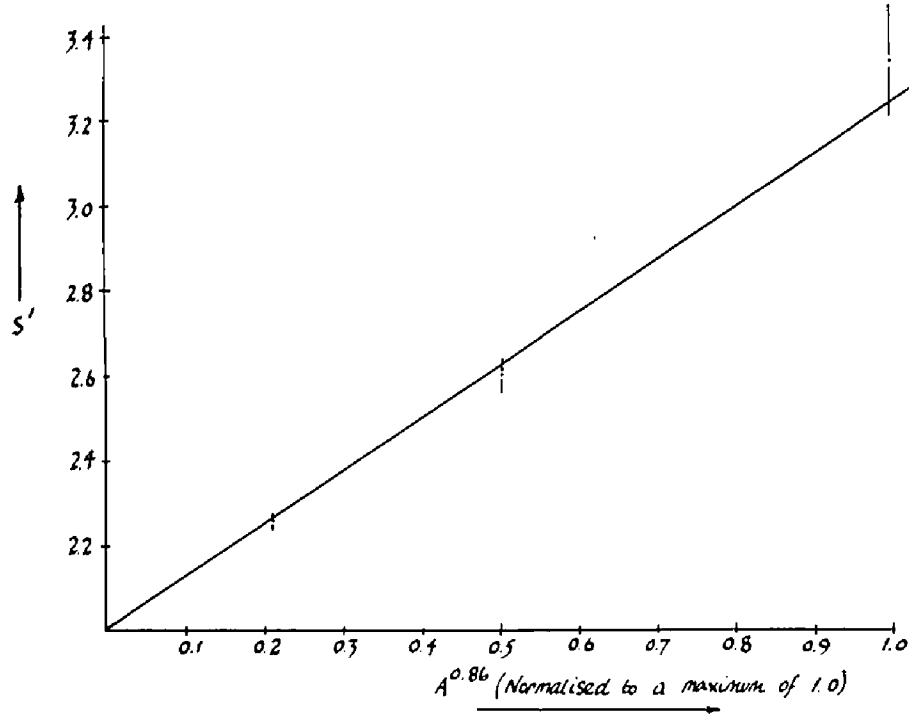

s' versus $A^{0.86}$ for the sporadic meteor data of McIntosh and Šimek (1969)

Figure 4.13

of s equal to 2.14 ± 0.03 was obtained. The agreement between these two values of s is somewhat disappointing. It is felt that the reason for disagreement is perhaps as follows. The exponent 0.86 in the relation $s' = s + A^{0.86}$ may contain error. It is the average value, determined for both forward and back-scatter cases. (Back-scatter 0.874, forward-scatter 0.858) If s' is plotted versus $A^{0.874}$, the value of s obtained is only slightly larger than 2.00 and still below 2.14 determined by the general approach.

An estimate of the error in the exponent is quite difficult to attempt considering the approximations and assumptions made in its derivation. It is therefore very difficult to justify any alteration in the value of the exponent.

Table 4 summarises the mass distribution indices obtained for the sporadic meteor data dealt with in this chapter. Fair agreement in the value of s obtained can be seen for all but the 49 MHz forward-scatter data.

4.5 The Measurement of Atmospheric Absorption

Figure 4.14 shows a flat Earth forward-scattering arrangement. Radio waves from the transmitter Tx enter the absorbing region of width x and are received at the receiving station Rx, approximately 1500 km (say) from the transmitter.

Table 4

Scatter Equipment	mass distribution index		
	general method		$A^{0.86}$
	Night only	24 hr.	
49 MHz Forward-Scatter, 1968	2.48±.001	2.60±.001	
40 MHz Back-Scatter, 1968	2.27±.07	2.28±.05	
33 MHz Back-Scatter, 1967		2.14±.03	2.00±.03
49 MHz Forward-Scatter, 1971	2.55±.001	3.09±.003	
40 MHz Forward-Scatter, 1971	2.18±.04	2.05±.09	
Theoretical, Dohnanyi (1970)	2.17		

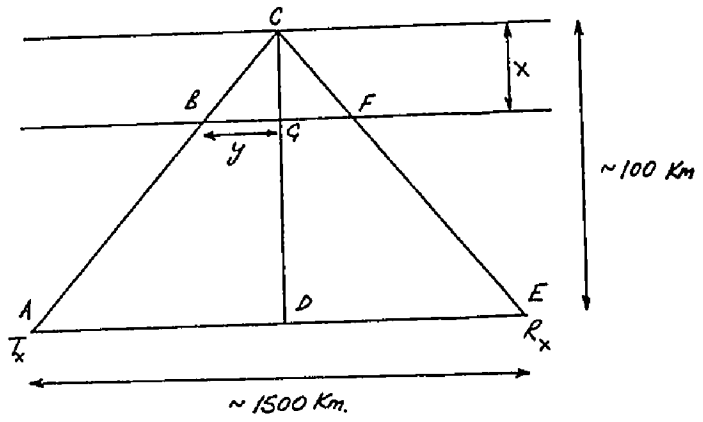

Typical Forward-scatter arrangement.
T_x is the transmitter and R_x the receiver

Figure 4.14

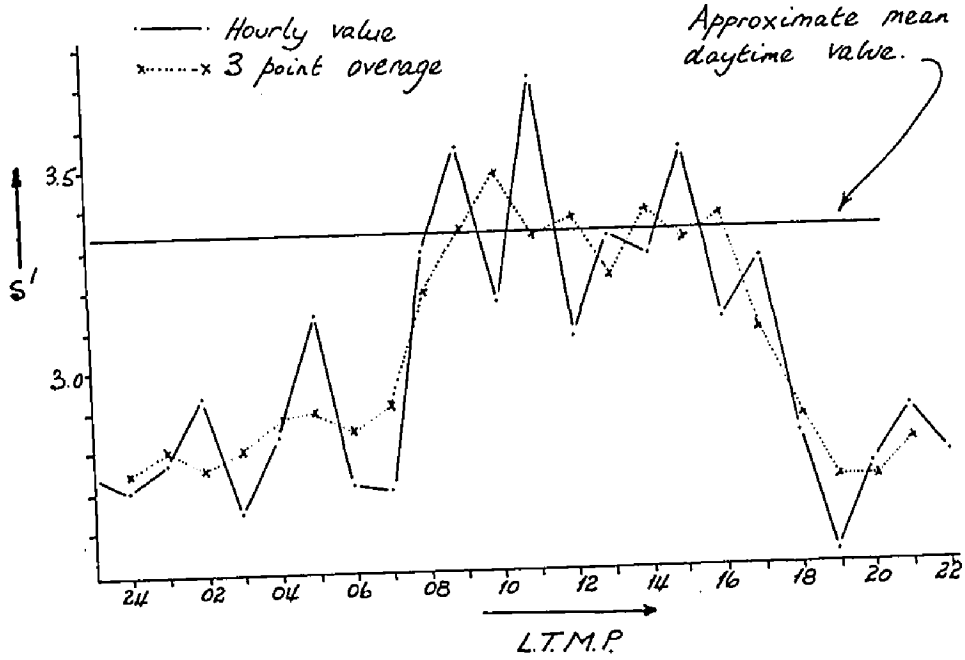

Diurnal variation in s' for the 49 MHz. scatter circuit

Figure 4.15

If absorption of the radio wave occurs, equipment sensitivity will be reduced. Figure 3.10 shows that a decrease in sensitivity (being directly proportional to the logarithm of the minimum detectable electron line density) will correspond to a decrease in β and hence and increase in the value of s'. To a first approximation, values of s' calculated from adjacent pairs of data points can be plotted linearly versus amplitude. This is shown in Figure 4.11, the straight line through the data being a least squares fit. From the figure, it can be seen that a most sensitive value of s' for the 49 MHz scatter circuit (as an example) is 2.65, occurring at an amplitude of 0.159 μv, (A_o where the subscript "o" refers to no absorption) Figure 4.15 shows the diurnal variation in s' for the 49 MHz scatter circuit and it can clearly be seen that a value of s' of approximately 3.33 is an average daytime value for the data considered. Figure 4.11 shows that an s' of 3.33 corresponds to an amplitude of 0.48 μv (A_a, where the subscript "a" refers to the presence of absorption) a measure of absorption can be obtained by comparing these two amplitudes. The absorption relation can be written

$$\text{Absorption} = 20 \log_{10} \left[\frac{A_a}{A_o}\right]$$

Since A_a/A_o = 3.02 the mean absorption measured over the three days will be approximately 9.6db. As measurements were made by forward-scattering this absorption occurred at oblique incidence and must be converted to normal incidence for comparison with conventionally obtained absorption measurements.

From Figure 4.14 it can be shown that BC, the oblique path length is equal to approximately 7.6x. A signal reflected at normal incidence passing through the absorbing region (once) would therefore give an absorption value of approximately 0.63 db (at 49 MHz). An attempt was made to correlate this value with data supplied by Air Force Cambridge Research Laboratories Geophysical and Space Data Bulletin (3rd quarter, 1971) but no absorption measurements appeared for mid July 1971. Therefore, direct comparison between the value obtained in this thesis, and values obtained independently could not be made.

However, Lusignan (1960) indicates that D region absorption in July (measured by riometer operating at 27.5 MHz) attains a value of slightly over 1db for several hours on either side of 12^{00} local time. Davies (1965) also mentions that for a 30 MHz riometer, an absorption value of 1db is fairly typical for the D region, during the day. Absorption is inversely pro-

portional to the square of frequency (Davies, 1965) and therefore,

$$\frac{\text{Absorption @ 30 MHz}}{\text{Absorption @ 49 MHz}} \propto \left[\frac{49 \text{ MHz}}{30 \text{ MHz}}\right]^2$$

According to this expression, absorption at 49 MHz should be approximately 0.4 db. The two absorption values can be seen to be in fair agreement, thus apparently supporting the method discussed.

To obtain absorption measurements directly, a graph of s' versus absorption could be drawn following the method outlined above. A measurement of the value of s' at any desired time would permit an estimate of absorption to be made.

Chapter 5

SHOWER METEOR OBSERVATIONS

5.1 The Perseid Shower

5.1a Introduction

Lovell (1954) states that the Perseid shower is one of the most regular visible meteoric events. The period of activity extends from approximately July 25th until August 17th with a maximum rate occurring around August 12th (McKinley, 1961). Lovell goes on to say that the shower is particularly noteworthy since its orbit was originally computed by Schiaparelli in about 1865, leading to the connection between it and Comet 1862 III: this was the first occasion on which any plausible relation was established between meteoroids and other celestial objects.

5.1b Orbital Elements of the Perseid Stream

Lovell (1954) points out that many measurements of the elements of the Perseid stream have been made. Table 5 (after Lovell, 1954) compares these orbital elements with those of Comet 1862 III.

The close connection between the orbit of the comet and the stream is also evident in Figure 5.1 after Lovell

Table 5

Observers	☊	ω	i	e	q	a	Period (yrs)
Comet 1862 III	137° 27′	152° 46′	113° 34′	———	0.9626	———	121.5
Schiaparelli	138° 16′	151° 28′	115° 57′	assumed parabolic	0.9643	———	———
Whipple	141° 28′	155° 21′	119° 42′	0.9577	0.9680	22.89	109.5
Cepiecka	140° 21′	150° 53′	112° 12′	0.9474	0.9606	18.11	———
Hawkins and Almond	139° 30′	153° 0′	114° 0′	0.93	0.97	14.4	———

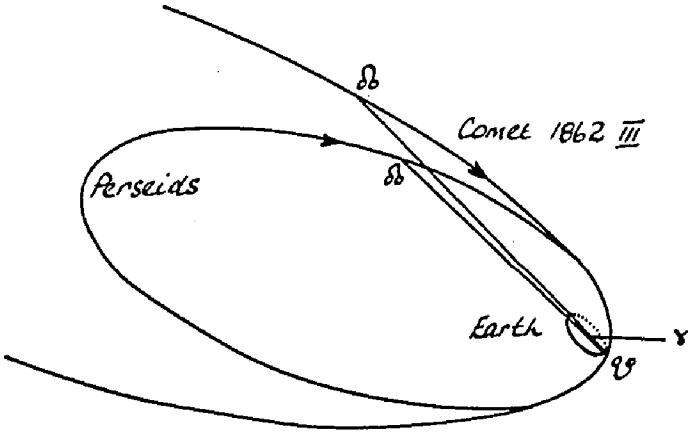

The orbit of the Perseid meteor stream determined by radio echo observations compared with the orbit of Comet 1862 III (Projection is on the plane of the comet's orbit) after Lovell (1964)

Figure 5.1

(1954), where the shower orbit is projected on to the plane of the orbit of the comet.

McKinley (1961) states that the right ascension and declination of the Perseid stream are respectively 46° and +58°. The local time of transit of the shower radiant is 05^{40}.

5.1c Hourly Rate Curves

Hourly Rate Versus Time

Data collection was planned for the period 14th July until 20th August 1971. During this time, 3 complete 24 hour observations on 14th/15th, 19th/20th and 27th/28th July were made along with 20 nights of observation between 30th July and 20th August. The record obtained on 8th/9th August was found to be useless due to equipment failure.

Computations outlined in Appendix 3 indicate that the maximum rate of Perseid shower meteors should occur at approximately 04^{00} LTMP (06^{00} EDT). Consequently, data collection was commenced at approximately 20^{00} EDT on each night of recording and was not finished until about 08^{00} EDT the following morning.

Shortly before the commencement of the shower, a failure occurred in the 40 MHz equipment. Further observation of the shower at this frequency proved impossible. Thus all further references to meteor activity refer to observations made at 49 MHz only.

Figure 5.2 shows the hourly meteor rate versus LTMP. Two separate cases are shown in the figure. The dashed curve is an average value of the sporadic activity, calculated for two days preceding the shower (7/8th, 9/10th August) and the solid curve shows the effects of both shower and sporadic activity. This curve is an average value of the total meteor rate calculated for the nights of maximum activity of the shower, (11th, 12th, and 13th August).

The sporadic activity shows a broad maximum around 24^{00} to 03^{00} LTMP but the shower + sporadic activity appears displaced slightly to a maximum between about 01^{00} to 05^{00} LTMP presumably due to the influence of the shower.

Hourly Rate Versus Date

Figure 5.3 illustrates the variation in meteor echo rate for the period of observation of the shower. Data are shown plotted for each hour of observation between 02^{00} and 05^{00} LTMP inclusively. In the figure, the curves for the hourly rate of meteor echoes greater than levels 2 and 4 are displayed. The shower was expected to be active between about 03^{00} and 05^{00} LTMP on the 11th, 12th and 13th August and it can be seen that such an increase in activity does occur.

The Perseid shower also appears to be masked by a

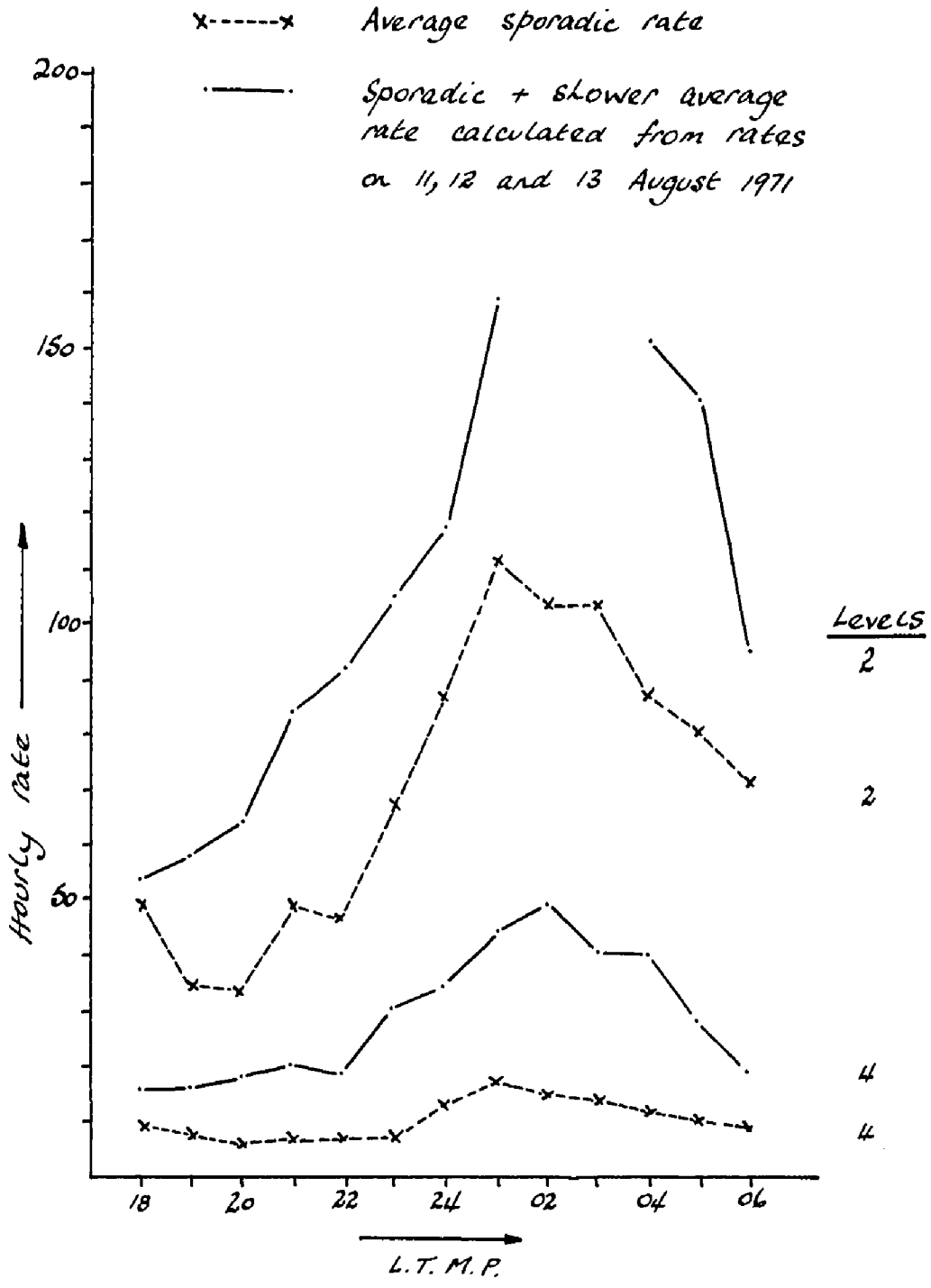

Variation of the hourly meteor rate during the Perseid shower, 1971

Figure 5.2

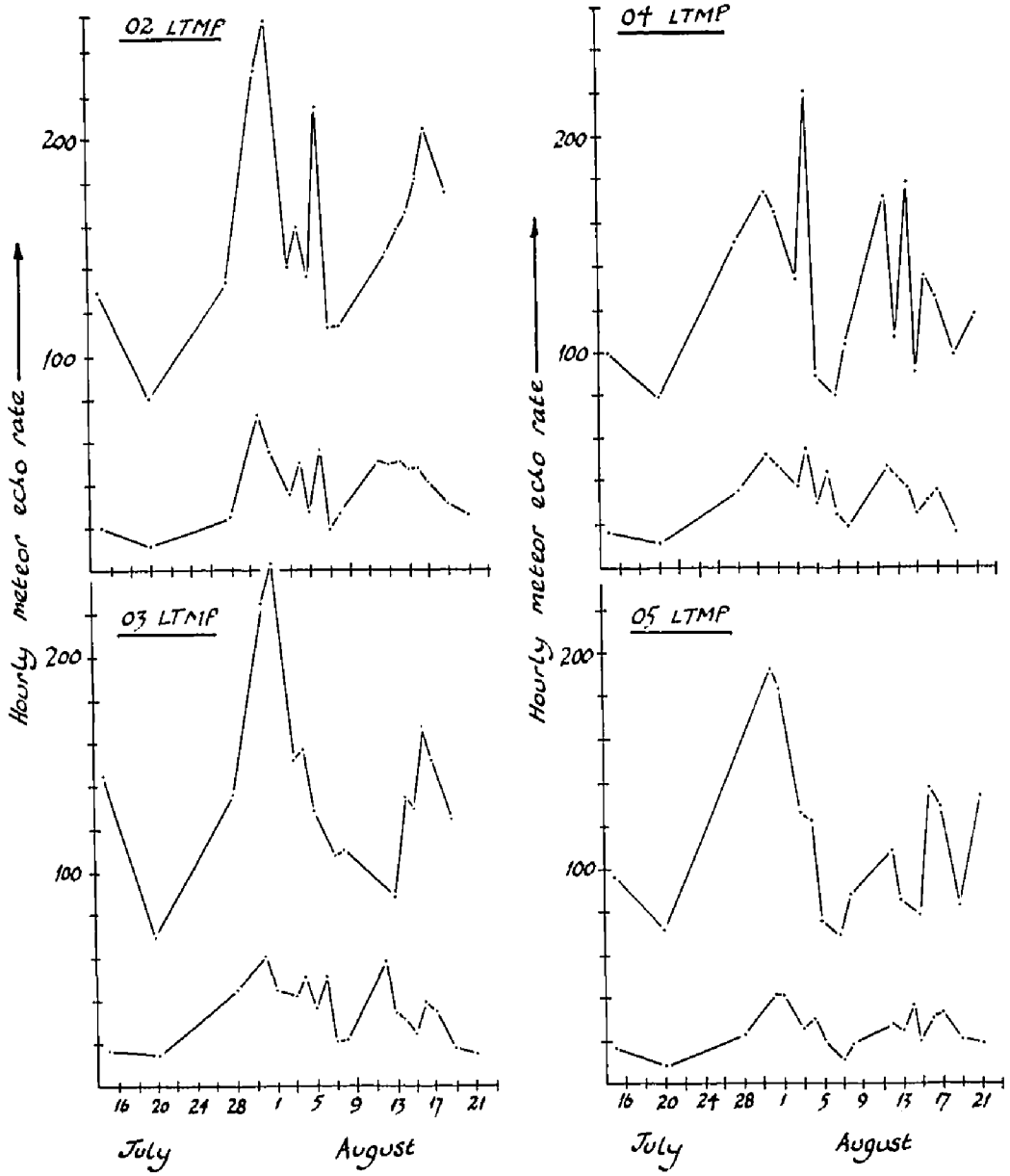

Variation in meteor echo rate for several hours of observation

Figure 5.3

considerable increase in meteor activity occurring approximately between July 30th and August 3rd with a maximum on July 31st. The maximum rate of meteor echoes occurs at approximately 02^{00} LTMP. This activity has subsequently been identified as the δ-Aquarid shower (maximum rate on about 29th July, 02^{10} local time of transit of shower radiant, declination 00° (Mckinley, 1961). Investigation was carried out on this shower and is discussed in a later section.

Due to the relatively low Perseid shower meteor rate it was not possible to investigate the diurnal variation. Since extensive investigations of this shower have been completed (Webster, 1963) a further comprehensive analysis appears unwarranted. Therefore investigation of the shower was primarily concerned with the attempt to obtain a true value of the mass distribution index for the shower maximum, that is for the three nights of maximum activity.

5.1d Determination of the Amplitude Distribution Index s'

A value of s' was obtained by measuring the slope of the line having the best fit through data points for the three most sensitive levels (levels 2, 3 and 4). Figure 5.4 illustrates the diurnal variation in s' for combined shower plus sporadic activity at 04^{00} LTMP. The figure shows one important feature. There is a

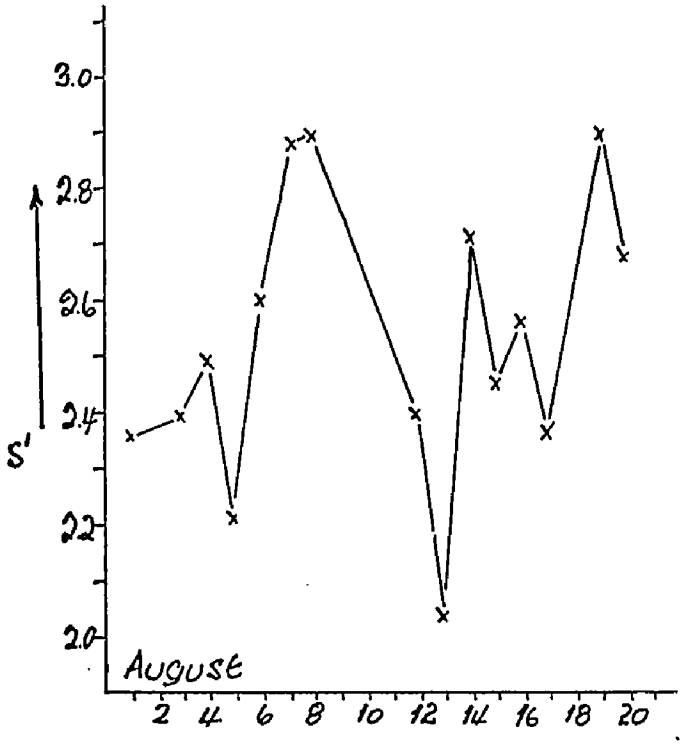

Diurnal variation in s' for the period of the Perseid shower, 1971 (04^{00} L.T. M.P.)

Figure 5.4

The variation in s' for the Perseid shower after Webster (1963)

Figure 5.5

decrease in the value of s' at the maximum of the shower this being a further indication that the Perseid shower was observed. Previous observations of the shower indicate that it contains a high percentage of larger meteoroids (Webster 1963, McKinley 1961). Thus when Perseid meteoroids are incident on the Earth's atmosphere, the increased rate of large meteors have the effect of decreasing the value of the amplitude (and mass) distribution index.

Figure 5.5 shows the diurnal variation in s' for the shower, determined by Webster (1963). Comparison of Figures 5.4 and 5.5 indicates that they both display the same essential features. Both show a relatively high value of s' around August 8th falling to a minimum on August 13th. The value of s' then commences to increase to a maximum on August 15th, the subsequent development of both figures remaining much the same. It should be mentioned that Webster's data is plotted for Perseid shower meteors alone, the effects of the sporadic background having been removed.

The sporadic rate of meteor echoes occurring on 49 MHz forward-scatter was removed from the total meteor rate so that the effect of the shower could be estimated. Figure 5.6 shows the resulting total number of shower meteor echoes versus amplitude in μv, plotted logarithmically.

5.1c The Determination of the Mass Distribution Index s

The index s of the Perseid meteoroids is deter-

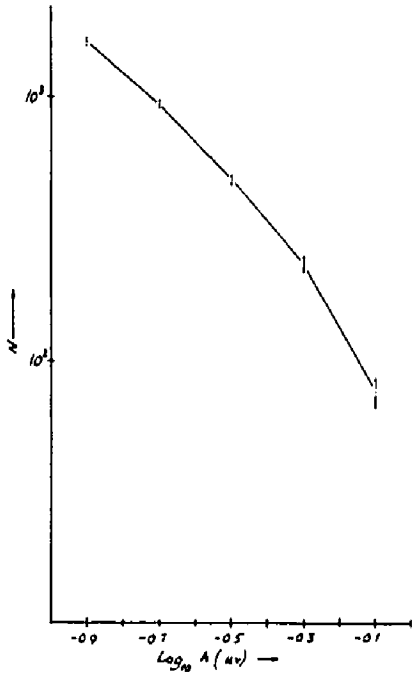

Log_{10} N versus Log_{10} A (μv) for the total number of Perseid slower meteors

Figure 5.6

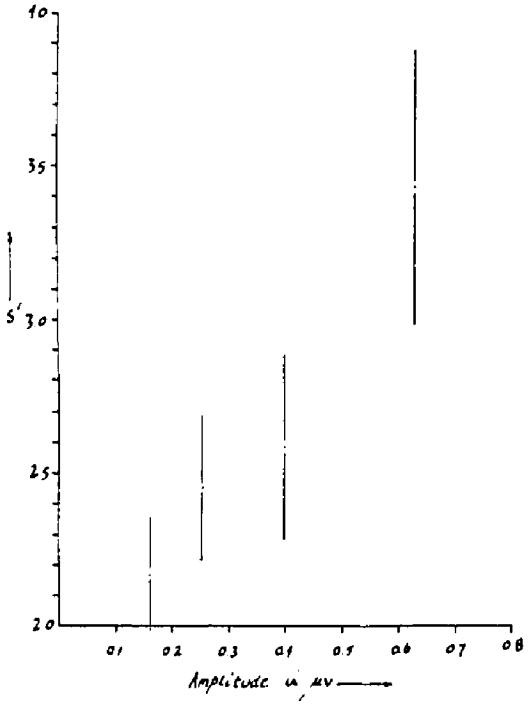

Values of s' versus amplitude for the 1971 Perseid meteor echoes

Figure 5.7

mined in exactly the same manner as was the value of s for sporadic meteoroids. Approximately 1600 Perseid meteor echoes were analysed. Slopes from adjacent pairs of points were obtained as before giving values of s'. These values were plotted versus the corresponding mean amplitude and are shown in Figure 5.7.

The number of Perseid meteor echoes occurring on the day of peak activity was 669 (13th August, 1971). Analysis was performed on these in order to obtain s for the peak of the shower. Webster (1963) obtained 13,600 Perseid shower meteors utilising a 17 MHz back-scatter radar. 1612 Perseid meteors occurred on the day of peak activity and these meteors were similarly analysed in order to obtain some correlation in the value of s.

Although the 49 MHz forward-scatter circuit employed in this experiment was of low sensitivity and seems to give poor results in the determination of s for sporadic meteors, it is felt that values of s for the Perseid meteors are realistic for the following reasons. The average geocentric velocity of sporadic meteoroids is about 40 kms^{-1} whilst the velocity of the Perseid shower meteoroids is about 60 kms^{-1}, since the Perseid stream is in a retrograde orbit (McKinley, 1961). Consequently, Perseid meteoroids will ablate

higher in the atmosphere than will sporadic meteoroids. The effect of this will be that the rate of diffusion will increase from approximately 5 to 16 $m^2 s^{-1}$ (Greenhow and Hall 1960) and consequently there will be less observational selection in favour of overdense meteors.

The 17 MHz back-scatter equipment of Webster (1963) had a limiting magnitude of about $+8^{M}$. Predetermined levels were approximately 0.8^{M} apart and consequently level 5 is associated with an electron line density approximately equal to the transition value. To avoid effects of overdense echoes, analysis was only performed on data obtained from levels 1 to 4 inclusively. Similarly, in the case of 49 MHz forward-scatter data, level 6 was disregarded.

Values of s obtained are summarised in Table 6. It can be seen that fair agreement between the 49 MHz forward-scatter data and 17 MHz back-scatter data is obtained for both the day of peak activity and for the effect of the total Perseid shower.

The forward-scatter s values appear somewhat larger than those obtained by back-scatter. As already mentioned, due to the relatively high geocentric velocity of Perseid meteoroids, ablation of meteoric material will occur higher in the atmosphere than it will for the

Table 6	
Data	s
1971 49 MHz. Forward-scatter Peak-Day	1.79 ± 0.02
1963 17 MHz Back-Scatter Peak-Day	1.69 ± 0.02
1971 49 MHz. Forward-scatter Total shower	2.12 ± 0.05
1963 17 MHz Back-Scatter Total Shower	1.81 ± 0.02

sporadic meteoroids, for example. Consequently, due to the decrease in atmospheric density with increase in height, the initial radius effect will be greater. The differences in values of s obtained may be indicative of the effect of an increase in the initial radius.

5.2 The δ-Aquarid Shower

5.2a Introduction

According to McKinley (1961) the period of activity of the δ-Aquarid shower lasts from approximately July 15th until August 18th with a maximum occurring on about July 29th. Lovell (1954) maintains that there are no spectacular past occurrences of the shower during the period of observation by trained observers in the nineteenth century. He also mentions that previous observation of the shower indicates a rapid rise to maximum activity followed by a slow decline. McKinley (1961) reports that the equivalent visual hourly rate of the shower is only 10 (the equivalent visual hourly rate is the rate that a single naked eye observer would see assuming a clear dark night and a radiant elevation of 45°. The rate includes the effects of sporadic meteors).

5.2b Orbital Elements of the δ-Aquarid Stream

McKinley (1961) gives the right ascension and declination of the δ-Aquarid shower as 339° and 00° respectively. Lovell (1954) states that various estimates of the orbital elements of the stream have been made and these are displayed in Table 7. Lovell goes on to say that the mean orbit of the stream is very similar to that of the Arietid shower in June.

5.2c Hourly Rate Curves

The maximum rate of δ-Aquarid meteors was expected

to occur one hour before transit (Appendix 3) at about 01^{00} LTMP and since the data collection was commenced at 20^{00} EDT (18^{00} LTMP) and not finished until about 08^{00} EDT (06^{00} LTMP) the ζ-Aquarid maximum period was well bracketed. Figure 5.8 displays the observed hourly rate of sporadic meteors compared to one night of shower plus sporadic activity at the height of the shower.

The sporadic background was determined from data obtained on the 14th/15th and 19th/20th July 1971. The maximum shower rate occurred on the nights of 30th/31st July and 31st July/1st August with activity scarcely being above the sporadic level on succeeding nights. A fairly broad maximum in activity was evident and approximately 1,600 ζ-Aquarid shower meteor echoes were obtained and analysed.

5.2d The Determination of the Mass Distribution Index

The mass distribution index of the two days of peak activity of the ζ-Aquarid shower was determined in exactly the same manner as that of the Perseid shower. The value of s deduced for the shower is 2.11 ± 0.29. It is hard to determine how meaningful this result is for the following reason. ζ-Aquarid meteors have an average velocity of 41 kms^{-1}, about the same as sporadic meteors. Since the mass distribution of the ζ-Aquarid meteoroids is approximately the same as that of sporadic

Table 7

	Ω	π	ω	i	e	q	a	V_h
McIntosh (28 July 1934)	304.7	104.3		65 8	1.0	0.039		para-bolic
Watson	305			56	1.0	0.039		
Hoffmeister (3 Aug.)	310.0	97.0	147.0	23.7	0.926	0.118	1.599	34.64
Lindblad (29 July)	305.6		152 2	28.4	0.956	0.080	1.807	35.4
Almond (28 July)	304.6	101	156	24	0.96	0.06	1.5	
Comet 1948 n	233 0		183.8	13 25	0.809	0 558	2.9 11	
1566 Icarus	87 77		20.87	23.02	0 83	0.187	1.078	

V_h — heliocentric velocity km s^{-1}

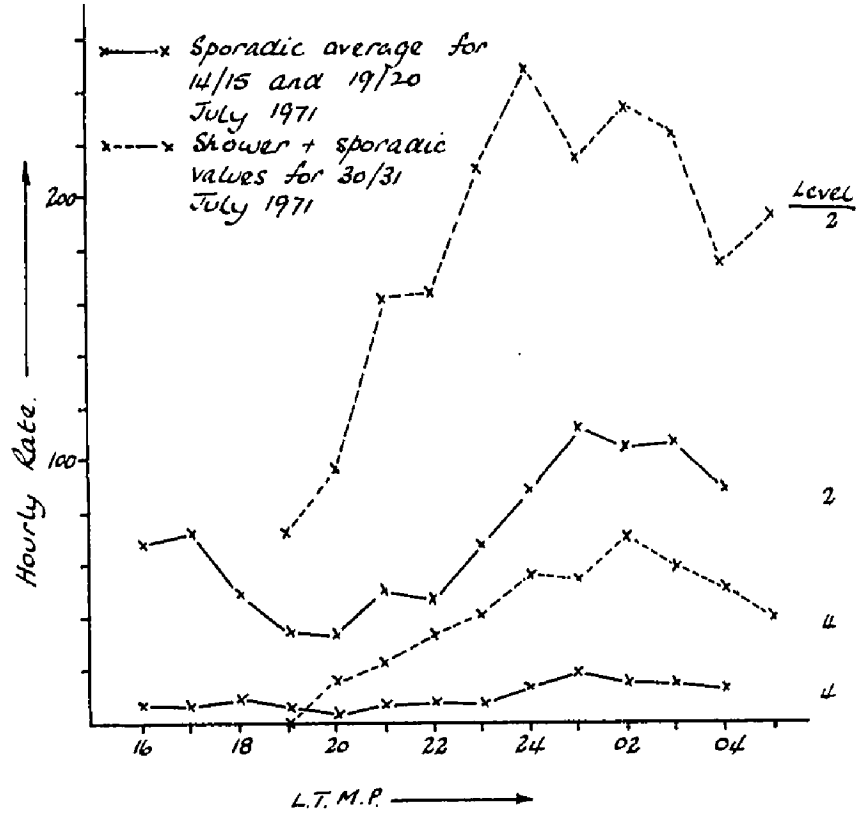

Observed hourly rate of sporadic meteor echoes compared to the activity at the height of the δ-Aquarid shower.

Figure 5.8

meteoroids, heights of ionisation must be approximately the same for both cases. Therefore the δ-Aquarid meteors would also be subject to observational selection. Figure 5.9 shows the variation in $\log_{10}$ N versus $\log_{10}$ A(μv) for the δ-Aquarid meteors and Figure 5.10, the variation in s' versus A(μv).

To avoid the possible effects of observational selection in favour of overdense echoes, the value of s was determined from s' values associated with levels 2,3,4 and 5.

Lovell (1954) states the previous visual observation of the δ-Aquarid shower indicates that a maximum of activity occurs at solar longitude 124° (July 28th, 1971). He goes on to point out that some radio echo observations made in 1949 indicate a maximum at solar longitude 126°, July 30th, 1971. Unfortunately, no data collection was made at this time, and therefore it is hard to confirm this date. From the data available, it appears as though the maximum (radio) rate of δ-Aquarid shower meteors occurs at solar longitude 127°, July 31st/August 1st, 1971.

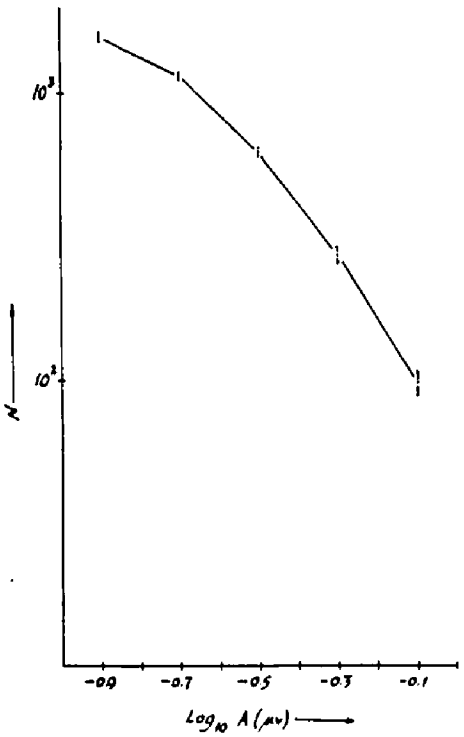

Log_{10} N versus Log_{10} A (μv) for the total number of δ-Aquarid shower meteors

Figure 5.9

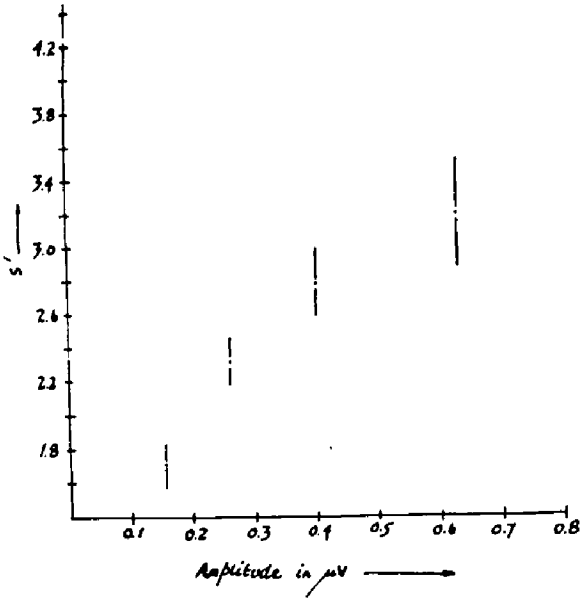

Values of s' versus amplitude for the 1971 δ-Aquarid meteor shower

Figure 5.10

5.3 The Arietid Shower

5.3a Introduction

The advent of radar enabled a systematic study of meteor events unhampered by clouds or daylight. Daytime observations were of particular importance since they yielded information on meteor streams falling on the sunlight side of the Earth. According to Lovell (1954), in 1949 and 1950 the orbits of the main daytime streams were first clearly delineated and it is now known that the dominant streams of the summer sequence are the Arietids and Zeta-Perseids in early June and the β-Taurids in late June. Lovell goes on to state that a number of less active streams, not all recurrent comprise the activity of May and July.

5.3b Orbital Elements of the Arietid Stream

Details of the orbital elements are shown in Table 8 following Lovell (1954). He points out that the stream may intersect the orbit of the Earth again before perihelion passage and the predicted radiant of the return coincides with the δ-Aquarid shower. Lovell maintains that it is possible that the two showers are connected and produced by one extended meteor stream. Figure 5.11 shows the similarity of the Arietid and δ-Aquarid streams projected on the plane of the ecliptic (Lovell, 1954).

5.3c Activity

The Arietid shower is one of the most active showers of the summer sequence. McKinley (1961) gives the

Table 8

Date	R.A.	Dec.	V_0	a	e	q	i	ω	π	$\delta\delta$
1950 June 1	38.4	15.5		1.5	0.94	0.09	3	28	98	70.3
June 8 (mean)	43.8	21.9	37.7	1.5	0.94	0.10	18	29	106	77.0
June 18	51.1	31.1		1.5	0.92	0.12	34	33	120	86.6
1951 May 30	39.3	20.7		1.6	0.91	0.15	11	38		67.3
June 8 (mean)	43.4	23.9	38.7	1.6	0.94	0.09	21	29	106	76.8
June 18	47.1	26.7		1.6	0.97	0.06	40	22		85.4
1952 June 9	45.5	21.7	38.5	1.6	0.95	0.09	13	29	106	77.5

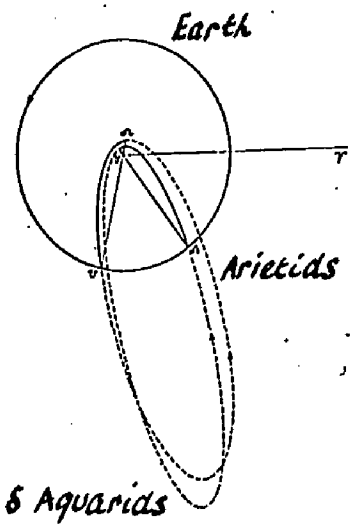

Mean orbit of the δ-Aquarid stream and the day-time Arietid stream projected on the plane of the ecliptic (Lovell, 1954)

Figure 5.11

equivalent visual hourly rate of the shower as 60 which can be compared to the rate of the Perseid and Geminid showers which he gives as approximately 50. McKinley goes on to state that the shower has a peak of activity on June 7th with a duration from May 29th until June 19th. The approximate local time of transit of the shower radiant is also given to be 10^{00} local time.

5.3d The Diurnal Variation in Meteor Rate

According to calculations given in Appendix 3, the maximum rate of Arietid shower meteors was predicted to occur at the local time of transit of the radiant, approximately 12^{00} EDT. Accordingly, data collection was planned for a considerable period preceding and including the shower. Results were obtained for 20th May 1971 and for the period 25th May until 18th June 1971 inclusively. A thunderstorm in the vicinity of the Delaware field site on June 7th permitted only 3 hours of data collection, between the hours of 10^{30} and 13^{30} EDT. Two other records occurring during the shower were rendered useless by equipment failure. An attempt was made to record the shower utilising both the 40 MHz and the 49 MHz scatter circuits but only the results recorded on 49 MHz were eventually found to be useful.

Data collection was commenced as early as possible during the day, usually around 07^{30} EDT and was continued

until about 16^{30} EDT. Data were analysed exactly as before. The maximum rate of Arietid shower meteors occurred around 11^{00} EDT on June 7th. This estimate is complicated by a lack of data for the hours preceding this time due to the aforementioned thunderstorm. Figure 5.12 (a and b, for 40 and 49 MHz forward-scatter respectively) displays the diurnal variation in rate for 11^{00} EDT, the peak of activity on June 7th 1971 being immediately obvious.

The Arietid shower was also investigated in 1968 using 40 MHz back-scatter and 49 MHz forward-scatter equipment. The results of this investigation are shown in Figure 5.12 (c and d, for 49 MHz forward-scatter and 40 MHz back-scatter respectively). The data shown in the figure were obtained at approximately 11^{00} EDT. Similarities between Figure 5.12 (a) and (c) are immediately apparent. Examination of the forward-scatter results of Figure 5.12(c) show the peak of the shower occurs on June 7th 1968 with a subsidiary maximum on June 2nd. A minimum of activity exists on June 4th. Figure 5.12 (a) displays results almost identical with this except that the subsidiary maximum occurs on June 3rd 1971 and the minimum on June 5th.

5.3e Determination of the Amplitude Distribution Index s'

The amplitude distribution index was determined

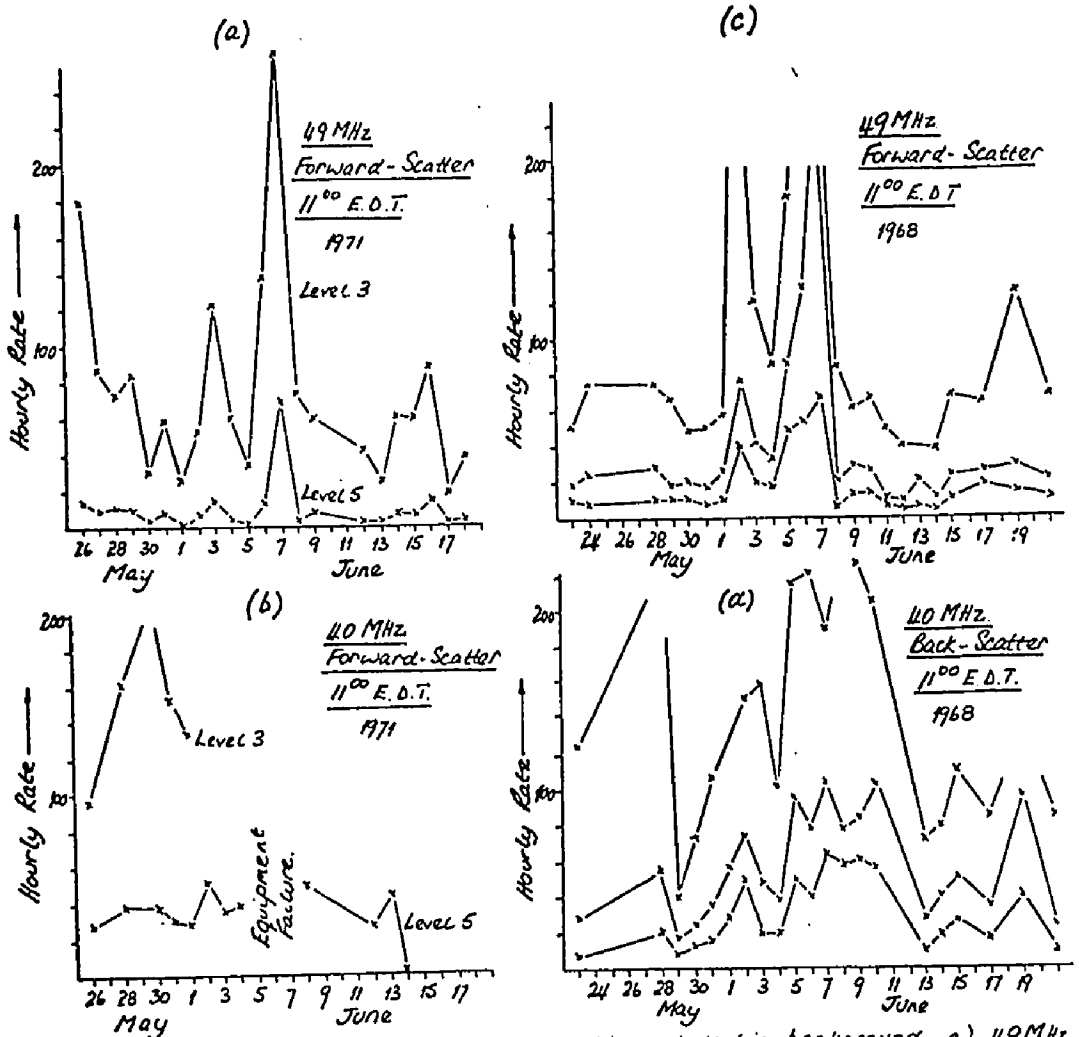

The activity of the Arietid shower including sporadic background. a) 49 MHz. Forward-Scatter 1971. b) 40 MHz. Forward-Scatter 1971. c) 49 MHz. Forward-Scatter 1968 d) 40 MHz. Back-Scatter 1968

Figure 5.12

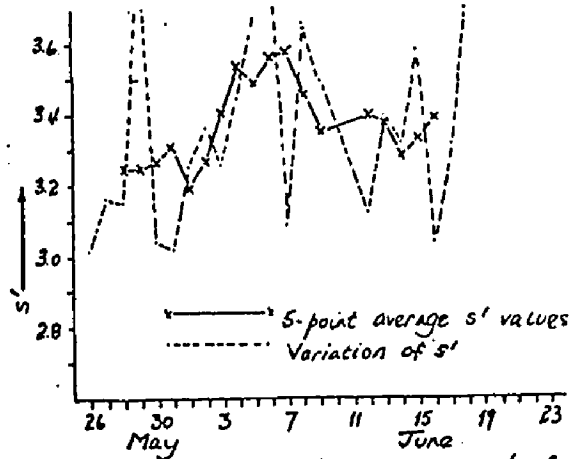

Variation of amplitude distribution index s' for the 1971 Arietid meteor shower investigated at 49 MHz. forward-scatter

Figure 5.13

throughout the period of investigation of the shower. McKinley (1961) states that the Arietid stream contains an abundance of smaller meteoroids a consequence of this being that an increase in the amplitude distribution index is expected as the Earth passes through the stream. Figure 5.13 displays the variation of s' through the course of the (1971) shower for 11^{00} EDT (49 MHz data). An increase in the value of s' occurs around June 7th indicating the presence of the shower. The values of s' displayed in the figure are values deduced from the combined effects of both the shower and sporadic meteoroids.

5.3f The Determination of the Mass Distribution Index s

The level of meteor activity existing on 30th, 31st May and 1st June 1971 was taken to be due to the effects of the sporadic meteor background. The average background rate was removed from the total rate occurring around June 7th, (the height of activity of the shower) which left the effect due to the shower meteors.

The same procedure was employed in the analysis of the 1968 data. Data recorded in 1968 consisted of one hour per day only (10^{30} - 11^{30} EDT). Data recorded in 1971 consisted of 9 hours per day however (07^{30} - 16^{30} EDT) and it was decided to take full advantage of this and to include the effects of all shower meteors

occurring within this time. In all, nearly 600 1971 shower echoes were analysed, approximately 400 occurring at 11^{00} EDT the other 200 at 12^{00} and 13^{00} EDT. The analysis will yield only an average value of the meteoroid mass distribution of the shower, the number of echoes occurring per day being too few to permit an investigation of the evolution of the index.

The dates of sporadic activity for the 1968 investigation of the Arietid shower were taken to be the 29th, 30th and 31st May 1968. Forward-scatter activity was a maximum from 4th June until 7th June inclusively whilst the back-scatter maximum occurred between 4th June and 10th June inclusively. Forward-scatter analysis yielded just over 500 echoes whilst back-scatter yielded slightly less than 900.

Analysis of adjacent pairs of data points was performed as previously described and values of the slopes were obtained. Interpretation of the Arietied shower data proved very difficult, and Figures 5.14 and 5.15 illustrate why this is so. 1968 meteor data is shown in Figure 5.14. Values of $\log_{10}N$ are plotted versus $\log_{10}A(\mu v)$ for both back-scatter and forward-scatter meteor echoes and it is immediately obvious that the characteristic curve is not in evidence. This is further pointed out in Figure 5.14(b) where

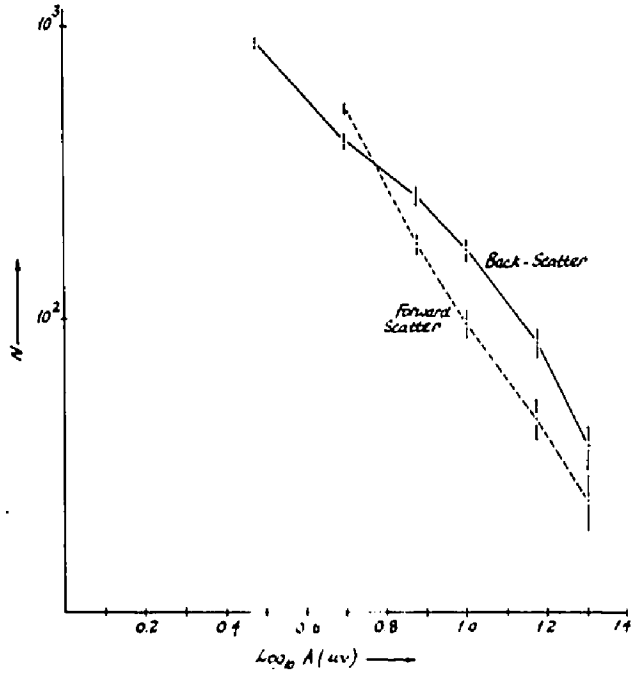

1968 Arietid Meteors 49 MHz Forward-Scatter and 40 MHz Back-Scatter

(a)

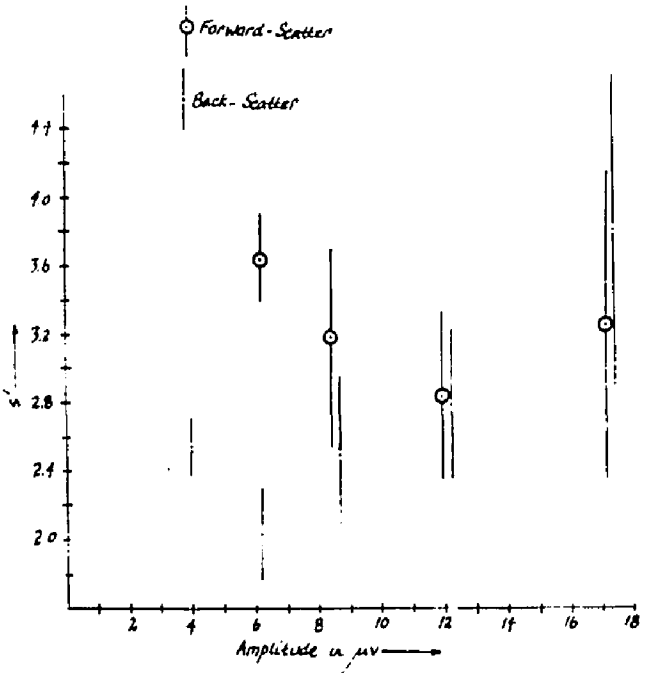

Values of s' versus amplitude for the 1968 Arietid Meteor meteors recorded on 49 MHz Forward-Scatter and 40 MHz Back-Scatter

(b)

Figure 5.14

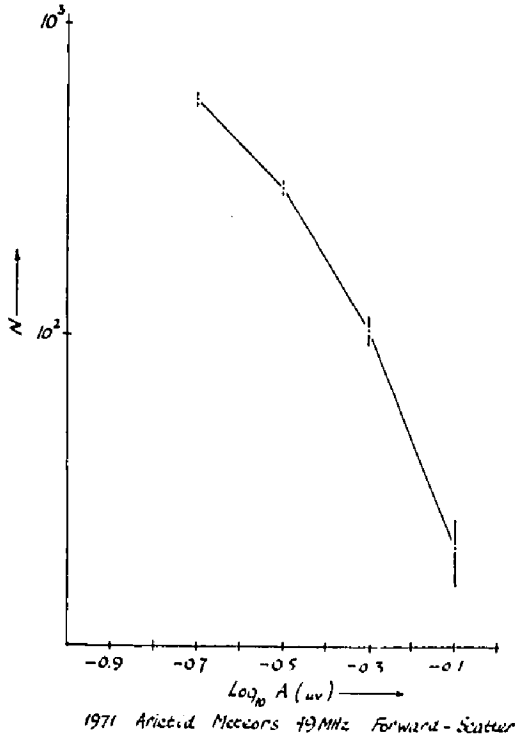

1971 Arietid Meteors 19 MHz Forward-Scatter

(a)

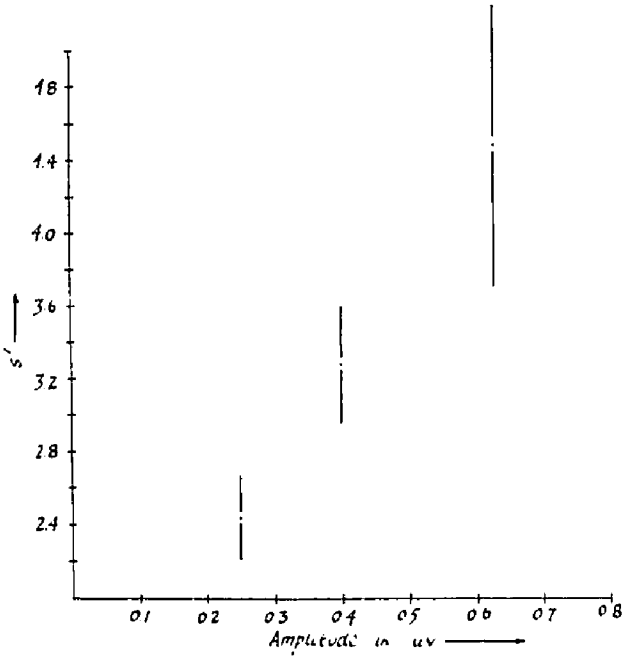

Values of s' versus amplitude for the 1971 Arietid shower meteors

(b)

Figure 5.15

values of s' are plotted versus the corresponding amplitude in μv.

Figure 5.15 (a and b) are plotted for the 1971 data and it can be seen that this data appears more consistent. Due to the high noise level no meteor data for either level 1 or 2 could be plotted. Ignoring level 6, a value of $s = 1.86 \pm 0.02$ was obtained for 1971 Arietid radio meteors.

The Arietid shower occurs during the daytime. It was pointed out in section 4.5 that daytime absorption will effect equipment sensitivity, especially forward-scatter. Geomagnetic and solar data provided by the Journal of Geophysical Research* indicate that June 7th 1971 was an especially magnetically quiet day with a Kp index of 0+ around noon. The Kp index for the same day in 1968 was 3-. Observation of the Arietid shower in 1971 may have been made possible by the unusually low atmospheric absorption.

---

* J. Geophys. Res., 1971, 76, 7020
  J. Geophys. Res., 1968, 73, 6868

Chapter 6

SUMMARY AND CONCLUSIONS

6.1 Summary

A theoretical study of the reflection of radio waves from meteor trains at various scattering angles and electron line densities was completed and is presented in Chapter 3. This study indicated that previous estimates of the value of s based on a measurement of the slope at the underdense asymptote of the amplitude distribution, may be in error. This is due to the curvature of the so-called transition region which exists over a much greater range than had been anticipated ($+2\frac{M}{-}$ to $+9\frac{M}{-}$ approximately).

Chapter 3 contains illustrations of the methods by which values of the mass distribution index are obtained. The experimental investigation in this work concerned the observation of both shower and sporadic meteor activity, and Chapter 4 illustrates how the theory was applied to sporadic meteor data whilst Chapter 5 concerns the shower data.

A determination of D region absorption from a knowledge of the variation of s' with A is also presented in Chapter 4. The absorption value obtained for

mid July 1971 appears to agree quite well with the accepted value of approximately 0.4db at 49 MHz.

A further consequence of the theory developed in Chapter 3 is that an estimate of the approximate equipment sensitivity is possible. This estimate is not based on any of the usual parameters and will thus provide a completely independent check.

6.1a Sporadic Meteor Observations

A complete summary of all the sporadic meteor data is shown in Figure 6.1. Neglecting the perhaps unreliable 49 MHz values, fair agreement between experimental and theoretical values of s can be observed. The weighted mean values of mass distribution index for the sporadic meteoroid population are 2.20 ± 0.04 for night-time data and 2.17 ± 0.05 for the 24 hour data.

This is in excellent agreement with the theoretically calculated value of 2.17 obtained by Dohnanyi (1970) and must therefore give considerable support to the theory that the sporadic meteoroid population is continually being fed by perturbed shower particles.

6.1b Shower Meteor Observations

The analytical procedure was also employed in the investigation of several showers and values of s so obtained are shown in Table 9. The table also includes data for the Geminid meteor shower (Webster,

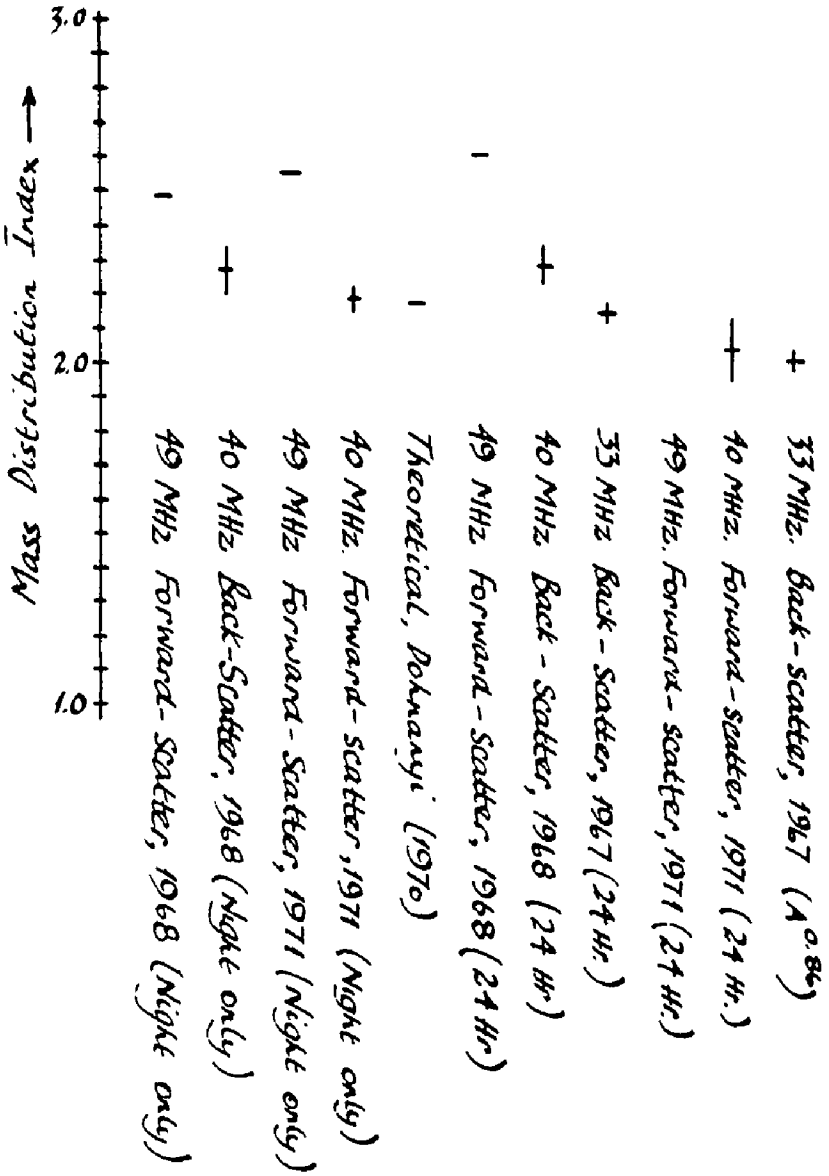

(Errors are indicated by vertical lines through the points)

Sporadic Meteoroid s Values

Figure 6.1

Table 9	
Data	s
1971 Perseids, 49 MHz Forward-Scatter (Peak Day)	1.79 ± 0.02
Webster (1963), Perseids 17 MHz. Back-scatter (Peak Day)	1.69 ± 0.02
1971 Perseids, 49 MHz. Forward-Scatter (Total shower)	2.12 ± 0.05
Webster (1963), Perseids 17 MHz Back-scatter (Total shower)	1.81 ± 0.02
Webster (1963), Geminids, 17 MHz Back-Scatter (Peak Day)	1.58 ± 0.05
Webster (1963), Geminids, 17 MHz. Back-scatter (Total shower)	1.38 ± 0.01
1968 Arietids, 49 MHz, Forward-Scatter (Total shower)	
1968 Arietids, 40 MHz. Back-Scatter (Total shower)	
1971 Arietids, 49 MHz. Forward-scatter (Total shower)	1.86 ± 0.02
1971 δ-Aquarids, 49 MHz Forward scatter (Total shower)	2.11 ± 0.29

1963) which has not been mentioned so far. Reasonable agreement in s values obtained from data collected by the author (49 MHz forward-scatter) and Webster (1963) (17 MHz back-scatter) is seen for the Perseid shower.

The values of s determined for the Arietid and δ-Aquarid showers may be unreliable due to the sensativity of the 49 MHz forward-scatter system. Arietid shower s values may be particularly unreliable because, as the shower occurs during the daytime, equipment sensitivity may suffer from absorption, a very common phenomenon at this time of year (Davies, 1965).

6.1c Equipment Sensitivities

Section 3.6 dealt with a method in which approximate values of limiting and average equipment sensitivity could be obtained. The theory was applied to both the shower and the sporadic activity and values of sensitivity obtained are shown in Table 10. The average value of equipment sensitivity is displayed in Table 11.

It is apparent that agreement between theoretically and experimentally determined values of limiting magnitude is not perfect especially for forward-scatter geometry where the experimental values appear consistently less than the theoretically predicted. The apparent loss in sensitivity may be due to imperfect ground conditions

Table 10

Scatter Equipment		Sporadics (All day)	Sporadics (night)	Perseids (Peak Day)	Perseids (Total shower)	Geminids (Peak Day)	Geminids (Total shower)
1971 49 MHz Forward-Scatter	$\log_{10}(\alpha_{min})$	13.84	14.16	14.14	14.12		
	M_{AV}	5.4	4.6	4.6	4.7		
	ΔM	0.8	1.0	1.3	1.2		
	M_0	6.2	5.6	5.9	5.9		
1971 40 MHz. Forward-Scatter	$\log_{10}(\alpha_{min})$	14.15	13.98				
	M_{AV}	4.6	5.1				
	ΔM	1.2	1.2				
	M_0	5.8	6.3				
1963 17 MHz Back-Scatter	$\log_{10}(\alpha_{min})$			13.19	12.96	12.96	13.55
	M_{AV}			7.0	7.6	7.6	6.1
	ΔM			1.4	1.5	1.7	1.1
	M_0			8.4	9.1	9.3	7.2
1968 49 MHz Forward-Scatter	$\log_{10}(\alpha_{min})$	14.43	14.49				
	M_{AV}	3.9	3.8				
	ΔM	0.8	0.8				
	M_0	4.7	4.6				
1968 40 MHz Back-Scatter	$\log_{10}(\alpha_{min})$	13.12	13.02				
	M_{AV}	7.2	7.4				
	ΔM	1.1	1.1				
	M_0	8.3	8.5				
1967 33 MHz Back-Scatter	$\log_{10}(\alpha_{min})$	13.03					
	M_{AV}	7.4					
	ΔM	1.2					
	M_0	8.6					

Table 11

Scatter Equipment	Magnitude		
	Theory	Experimentally Determined	
		Sporadic	Shower
1971 49 MHz Forward-Scatter	6.55	5.8	5.9
1971 40 MHz Forward-Scatter	6.95	6.1	
1963 17 MHz Back-Scatter	8.6		8.7
1968 49 MHz Forward-Scatter	5.75	4.7	
1968 40 MHz Back-Scatter	7.80	8.4	
1967 33 MHz Back-Scatter	9.75	8.6	

at the receiving site as indicated in Appendix 1. By virtue of the geometry of the reflection process, a closer approximation to a flat ground plane is more easily realised in the case of back-scattering than in forward-scattering since the beam elevation is much greater in the former case. Consequently, obstructions in the neighbourhood of the antennas are much less likely to have an effect.

The limiting magnitude of the 1971 49 MHz forward-scatter equipment determined from sporadic meteor observations appears large. If s is equal to approximately 2.2 and s' for the most sensitive level approximately 2.7 then $\beta \simeq 0.7$. This corresponds to an electron line density of $\alpha \simeq 3.6 \times 10^{14}$ or $M_{av} \simeq 3.6$. ΔM will be approximately 0.8 and therefore $M_o \simeq 4.4$, approximately 1.4^{M} less than the general approach indicates.

Limiting magnitudes determined by a consideration of either β ($\beta = (s - 1)/(s' - 1)$ or $\log_{10} A_{min}$ (theoretical)(the general approach mentioned in Chapter 3) agree well except for 49 MHz forward-scatter circuitry. It may be that the failure of the general approach in predicting a value of s consistent with other results for the 49 MHz forward-scatter systems, is also the reason for the high values of M_o which were

obtained.

6.2 Conclusions

Values of s determined by the back-scatter technique are assumed by many investigators to be low due to the initial radius effect. By virtue of the reflection process, s values obtained by forward-scattering should not be thus affected and consequently should result in a somewhat larger value.

The s values determined for sporadic meteors apparently do not show much variation with scatter geometry. Investigation carried out on the Perseid meteors apparently shows quite the opposite and values of s obtained by forward-scattering are consistently larger than those obtained by back-scattering. This may be due to the increased height of ionisation of Perseid meteoroids.

The effect of a finite initial radius is not taken into account in the theory developed in Chapter 3. Similarly, strictly speaking the method developed should only be applied to data obtained from underdense meteor echoes since it contains no compensation for such effects as wind-shears.

It is believed however that reliable values of s have been obtained for the majority of data.

6.3 Suggestions for Future Work

Reflection coefficients for the scattering of E.M. waves by columns of ionisation should be calculated for the case of transverse polarisation of the electric vector if only to confirm the theoretical results of Lebedinec and Sosnova (1967).

An extensive investigation of all the major showers by both forward and back-scattering should result in both a reliable value of s and in a better understanding of the effects of a finite initial radius.

APPENDIX 1

ANTENNA ORIENTATION

AT THE DELAWARE RADIO OBSERVATORY

Figure A1.1 illustrates the conditions when a reflected E.M. wave eminating from the meteor region is received at the antenna. $\hat{\theta}$ is the angle of elevation of the antenna beam and by considering the geometry of the forward-scatter path, it can be shown that this angle is 4.1°.

The wave reflected from point D in Figure A1.1 suffers a 180° change of phase and in order for both the direct and reflected waves to arrive at the antenna in phase, CE must equal $\lambda/2$. Now λ_{49} (where the subscript refers to the forward-scatter frequency in MHz) is approximately 20 ft. and λ_{40} 24 ft. The antenna height above the reflection point should therefore be 68 and 84 ft. for the 49 and 40 MHz equipment respectively.

Knowing the antenna height and angle of elevation of the beam it is possible to calculate the position of the reflection point. BD_{49} is approximately 950 ft. and BD_{40} 1180 ft. The linear extent of the reflection point must also be considered.

Consider Ray 1 and Ray 2 in Figure A1.1 where Ray 1 is reflected at point F and Ray 2 at the reflection point D. The distance FD = x, BD = d and AD = R. The total effect at the antenna A will depend on phase differences along the wavefront HD after reflection, and in particular if

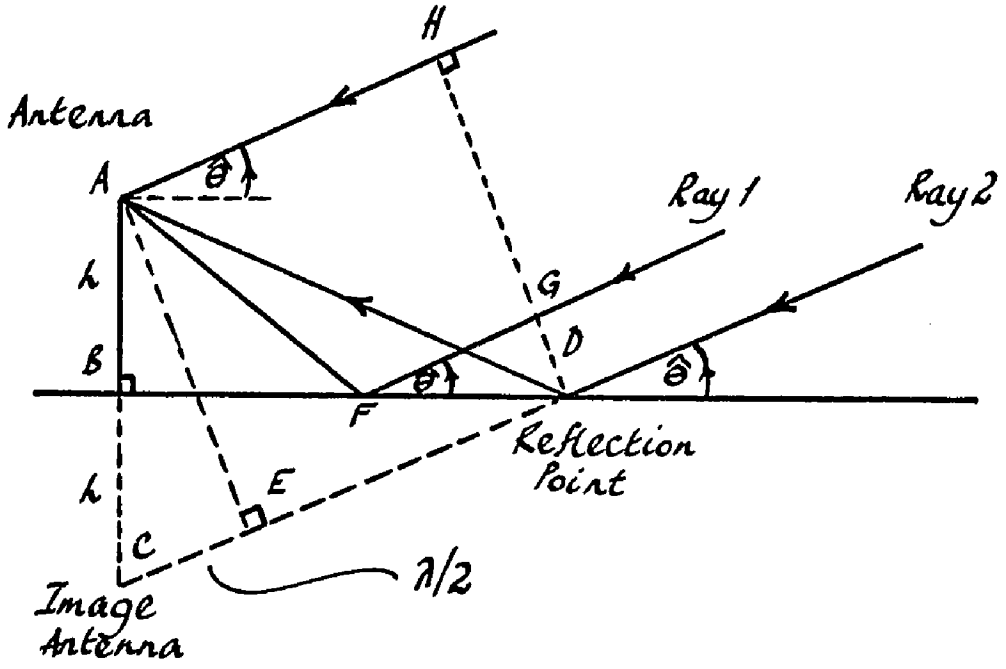

Ideal Antenna Conditions

Figure A 1.1

$$AF + FG - AD = \lambda/2$$

this will define the extent of the first Fresnel Zone.

It can be shown that

$$\sqrt{R^2 + (d-x)^2} + x\cos\hat{\theta} - R = \lambda/2$$

which reduces to

$$x \simeq 2\,\frac{(d - R\cos\hat{\theta})}{\sin^2\hat{\theta}}$$

but since for low elevations $R \simeq d$ then

$$x = \frac{2d\,(1 - \cos\hat{\theta})}{\sin^2\hat{\theta}}$$

and hence $x \simeq d$.

Since $d \simeq 950'$ at 49 MHz forward-scatter and 1180' at 40 MHz, the region of flat ground necessary for good reflection in front of the antennas can be seen to be considerable for an angle of elevation of approximately 4°.

APPENDIX 2

THE BASIS FOR THE INSTANTANEOUSLY FORMED TRAIN APPROXIMATION

When a radio wave is incident on a very underdense meteor train McKinley (1961) shows that the ratio of the total scattered amplitude from the diffusing electrons (A), to the total amplitude which would be obtained if all the electrons where in phase at the train axis (A_o) for the forward-scatter case can be expressed as

$$\frac{A}{A_o} = \frac{2\pi \int_o^\infty N_e \, J_o(4\pi r/\lambda \sec\phi) \, r dr}{2\pi \int_o^\infty N_e \, r dr}$$

N_e is the electron volume density, r the distance from the meteor train axis and J_o the zero order Bessel function. When the integration is carried out, McKinley shows that,

$$\frac{P_R(t)}{P_R(0)} = \left[\frac{A}{A_o}\right]^2 = \exp -\left[\frac{32\pi^2 Dt}{\lambda^2 \sec^2\phi}\right] \exp -\left[\frac{8\pi^2 r_o^2}{\lambda^2 \sec \phi}\right]$$

where $P_R(t)$ is the power received from the diffusing electrons and $P_R(o)$ the total power received from all electrons radiating in phase on the train axis.

Rearranging the above equation, one can see that

$$A = A_o \exp -\left[\frac{16\pi^2 Dt}{\lambda^2 \sec^2\phi}\right] \exp -\left[\frac{4\pi^2 r_o^2}{\lambda^2 \sec^2\phi}\right] \text{--------(A2.1)}$$

Therefore, the amplitude is a function of both diffusion (D) and the initial radius (r_o). The effect of r_o is not serious in the case of forward-scattering since if we consider $\lambda \simeq 7$ metres, $\phi \simeq 80^o$ and $r_o \simeq 1$ metre (Baggaley, 1970), then due to the inclusion of the $\sec^2 \phi$ term

$$\exp - \left[\frac{4\pi^2 r_o^2}{\lambda^2 \sec^2 \phi}\right] = 0.968 \simeq 1$$

It can be appreciated that, in the case of back-scattering where $\sec^2 \phi = 1$, the amplitude of the echo may be attenuated due to the effect of the initial radius of the meteor train.

It is known that the majority of the meteor echo comes from the first Fresnel zone. Diffusion of the meteor train will only become a factor if the meteoroid passes through the first Fresnel zone sufficiently slowly.

McKinley (1961) shows that the decay time of an underdense forward-scatter meteor echo may be expressed by the relation

$$\tau = \frac{\lambda^2 \sec^2 \phi}{16\pi^2 D} \qquad \text{(A2.2)}$$

By rearranging equation (A2.1) (neglecting the initial radius effect) and substituting equation (A2.2)

$$A = A_o \exp - \left[\frac{t}{\tau}\right] \qquad \text{(A2.3)}$$

The decay time of a typical underdense echo is approximately 0.5 secs. t in equation (A2.3) is the time taken for the meteoroid to cross the first Fresnel zone. If we consider the first Fresnel zone to be

approximately 2 km (see Manning and Eshelman, 1959) and a typical meteoroid velocity to be in the region of 40 km s^{-1} then t ≃ 50 msecs. Therefore equation (A2.3) will reduce to

$$A = A_o \exp - (0.05/0.5) = 0.91\ A_o$$

The assumption that the meteor train is instantaneously formed is therefore a valid one as little attenuation of the echo occurs.

APPENDIX 3

A CALCULATION OF THE TIME OF OCCURRENCE OF THE MAXIMUM SHOWER METEOR RATE FROM A KNOWLEDGE OF THE LOCAL TIME OF TRANSIT OF THE RADIANT

Hines (1955) states that observational factors can affect the number of shower meteors detected. He maintains that in the case of forward-scattering the factors can be expressed as functions of the shower radiant and produce a weight factor which changes as the radiant moves during the course of a day.

Assuming an isotropic antenna gain, Hines shows that there is a net observability factor which can be calculated for any forward-scatter network. Data for the Winnipeg/ London scatter circuit was substituted into his equations. Figure A3.1 shows the observability contours thus derived. The contours shown on the chart are normalised to a maximum meteor rate of 100 per hour. At the centre of the figure is the North celestial pole and radiants will move in a circle about this pole during the course of the day, intersecting the meteor rate contours. The time of transit of a shower radiant is the local time at which the radiant is highest in the sky. The maximum rate need not, and in fact often does not occur at the time of transit. The mass distribution index s used for Figure A3.1 was 2. Similar diagrams were obtained for s values of 1.5, 2.5, 3 and 4 but very little difference was observed in the positioning of the contours.

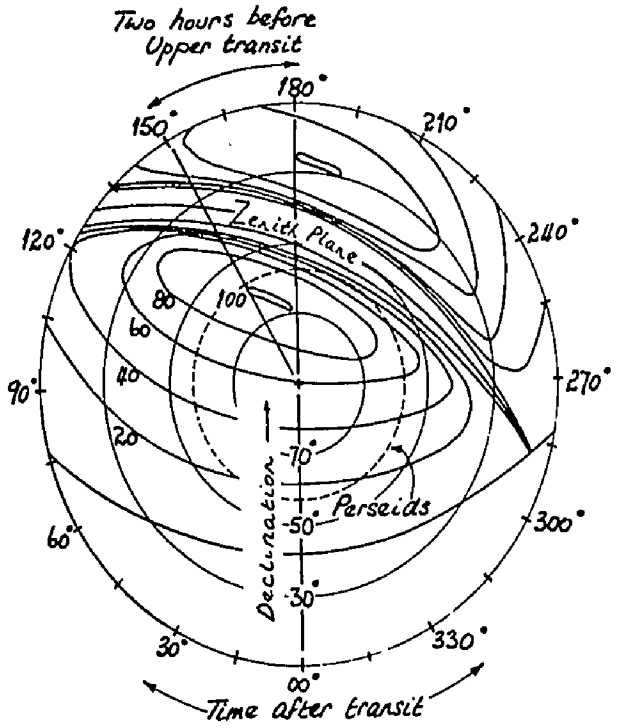

Observability contours for the Winnipeg / London scatter circuit

Figure A3.1

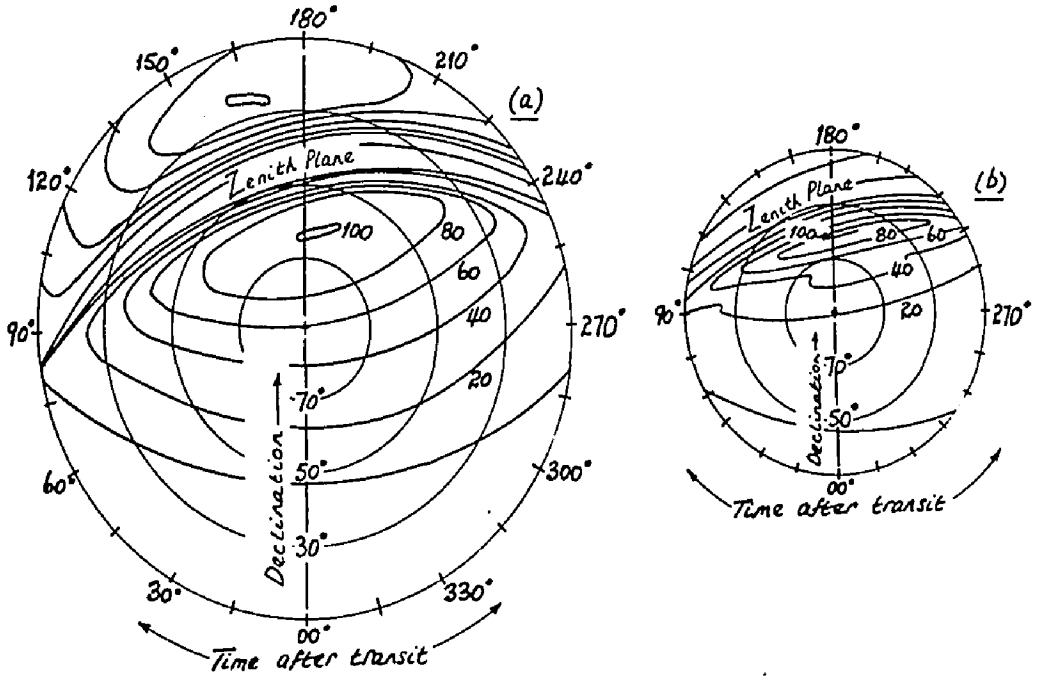

Observability contours for the Ottawa / Cedar Rapids scatter circuit including the effects of a) an isotropic antenna
b) a real antenna pattern (Forsyth, Hines and Vogan, 1955)

Figure A3.2

Hines further developed his analysis to take into account a more realistic antenna pattern and Figure A3.2(b) (after Forsyth, Hines and Vogan, 1955) shows the results of this for the Ottawa/Cedar Rapids forward-scatter network. Figure A3.2(a) was calculated for this same network using an isotropic antenna pattern. Comparison of Figures A3.2(a) and (b) shows that although the majority of contours are displaced with respect to one another, the position of the maximum rate contour is virtually at the same point. Thus optimum meteor observation conditions can be calculated at least approximately for a particular radiant with no knowledge of the actual antenna pattern.

As an example in the use of the aforementioned contour charts we shall consider the Perseid radiant having a declination of 57° and local time of transit 05^{40}. The path followed by the Perseid radiant around the North celestial pole is shown plotted in Figure A3.1 and it can be seen from the figure that the radiant will be in a favourable position to give a maximum rate approximately 30° (or 2 hours) before the time of transit.

The time of maximum rate (approximately 04^{00} local time at the mid-point) must be converted to E.D.T. or E.S.T. It can be shown that local time at the mid-point is approximately 1 hour ahead of E.S.T. and 2 hours ahead of E.D.T. The Perseid shower is a summer shower and therefore if the maximum is calculated to occur 2 hours before transit, and

the time of transit of the shower is 06^{00} the maximum rate will occur at approximately 06^{00} E.D.T.

APPENDIX 4

DATA POINT ERRORS AND WEIGHTS

Errors

Since s' is defined by the relation

$$s' = \frac{d \log_{10} N}{d \log_{10} A} + 1$$

then

$$s' \simeq \frac{\log_{10}(N_1/N_2)}{\log_{10}(A_2/A_1)} + 1$$

where N_1 and N_2 are the number of meteor echoes exceeding amplitudes A_1 and A_2.

The error in a random number N can be calculated from random walk theory and can be shown to be $\sqrt{N}$. If N_1 is constrained whilst N_2 varies between $N_2 + \sqrt{N_2}$ and $N_2 - \sqrt{N_2}$ then since $\ln(1 \pm \frac{1}{\sqrt{N}}) \simeq \pm \frac{1}{\sqrt{N}}$ it can be shown that

$$\text{slope}(1) = \frac{\ln(N_1/N_2)}{\ln(A_2/A_1)} \pm \frac{\frac{1}{\sqrt{N_1}}}{\ln(A_2/A_1)}$$

A similar result is obtained by keeping N_1 constant and letting N_2 vary. The r.m.s. error in the slope and hence in s' will therefore be

$$\pm \left[\frac{1}{N_1} + \frac{1}{N_2} \right]^{\frac{1}{2}} \Big/ \ln (A_2/A_1)$$

The error in shower values of s' will be different however. Shower data is obtained by the subtraction of two large numbers, the total number of meteor echoes

minus the average sporadic background. It is possible to show that the error in s' in this case will be

$$\pm \frac{\left[\frac{1}{N_1} + \frac{1}{N_2} + 2\left(\frac{N_1(\text{Sporadic})}{N_1^2} + \frac{N_2(\text{Sporadic})}{N_2^2}\right)\right]^{\frac{1}{2}}}{\ln A_2/A_1}$$

where N_1 and N_2 are the numbers of shower meteors exceeding the sporadic rate of N_1(sporadic) and N_2(sporadic) respectively.

Topping (1955) shows that each observation can be given a weight proportional to the reciprocal of its standard deviation. The observations were weighted accordingly whenever necessary. Errors in values of s were obtained by considering the standard error of the weighted mean. Topping shows that this can be expressed as

$$\pm \sqrt{\frac{\sum \frac{1}{\sigma_s^2}(s - \bar{s})}{(n-1)\sum \frac{1}{\sigma_s^2}}}$$

where σ_s is the standard deviation of s.

APPENDIX 5

FORMULATION OF AN EXACT SCATTERING THEORY

According to Herlofson (1951) when no ionised column is present, a plane wave is a solution of Maxwell's equations everywhere and is propagated without deformation. When an ionised column is introduced, the electromagnetic field must still satisfy Maxwell's equations but in the region where charges are present, the current due to the motion of these charges must be added to the displacement current and this will distort the previous plane wave in this region. It will then be impossible to match a pure plane wave outside the column to the distorted field inside and still satisfy Maxwell's equations. The distortion inside the column will make itself felt in the wave pattern outside, due to the continuity of the field vectors. This disturbance will fall off with increasing distance from the column and at a large distance there is left only a diverging cylindrical wave. (The original plane wave is identified with the incident wave due to the radio transmitter and the diverging cylindrical wave with the echo from the meteor train).

The current due to the motion of the charges must first be calculated. Herlofson maintains that it is sufficient to consider the force of the electric vector of the applied radio wave and neglect the Lorentz force due to

motion in the geomagnetic field since the gyrofrequency is of the order of 1 MHz whilst observations were carried out at a frequency of between 40 and 50 MHz. Similarly collisions may be neglected since the electron collision frequency at heights greater than 80 km is negligible compared to the frequencies used.

The equation of motion for an electron can be written

$$m_e \frac{\partial \bar{v}_e}{\partial t} = e_e \bar{E} \qquad \text{(A5.1)}$$

where m_e and e_e are the electronic mass and charge respectively, and $\bar{E}$ is the electric vector. We shall assume that all vectors in the radiation field depend on time through a factor $\exp(2\pi jft) = \exp(j\omega_e t)$. If N_e is the volume density of electrons the current density due to $\bar{E}$ will be

$$\bar{J} = N_e e_e \bar{V}_e \qquad \text{(A5.2)}$$

Since $\bar{V}_e = \bar{V}_{oe} \exp(j\omega_e t)$ then it follows from equations (A5.1) and (A5.2) that

$$\bar{J} = \frac{N_e e_e^2 \bar{E}}{j\omega_e m_e} \qquad \text{(A5.3)}$$

Ampères law states that

$$\nabla \times \bar{H} = \frac{4\pi}{c} \bar{J} + \frac{1}{c} \frac{\partial \bar{D}_e}{\partial t} \qquad \text{(A5.4)}$$

where $\bar{D}_e$ is the displacement vector given by

$$\bar{D}_e = \bar{E} + 4\pi \bar{P} \qquad \text{(A5.5)}$$

and $\bar{P}$ is the polarisation vector. Viewed microscopically $\bar{P} = 0$ and therefore differentiation of equation (A5.5) with respect to time give

$$\frac{\partial \bar{D}_e}{\partial t} = \frac{\partial \bar{E}}{\partial t} \qquad \text{(A5.6)}$$

and since $\bar{E} = \bar{E}_o \exp(j\omega_e t)$

then $$\frac{\partial \bar{E}}{\partial t} = j\omega_e \bar{E}$$

and therefore equation (A5.6) is

$$\frac{\partial \bar{D}_e}{\partial t} = j\omega_e \bar{E} \quad .$$

Substitution of this into equation (A5.4) gives

$$\nabla \times \bar{H} = \frac{4\pi}{c} \bar{J} + \frac{j\omega_e \bar{E}}{c} \qquad \text{(A5.7)}$$

and substitution of equation (A5.3) into equation (A5.7) gives

$$\nabla \times \bar{H} = \frac{j\bar{E}}{c}\left[\omega_e - \frac{4\pi N_e e_e^2}{\omega_e m_e}\right] \qquad \text{(A5.8)}$$

Jackson (1967) states that the dielectric constant of a plasma may be expressed by the relation

$$\epsilon(r) = 1 - \frac{\omega_p^2}{\omega_e^2 + j\omega_e \Gamma} \qquad \text{(A5.9)}$$

where ω_p refers to the plasma frequency and Γ is the damping constant. Damping may be neglected and therefore,

$$\epsilon(r) = 1 - \frac{\omega_p^2}{\omega_e^2} \qquad \text{(A5.10)}$$

Jackson also shows that

$$\omega_p^2 = \frac{4\pi N_e e_e^2}{m_e}$$

and therefore equation (A5.10) becomes

$$\omega_e(\epsilon(r)-1) = -\frac{4\pi N_e e_e^2}{m_e \omega_e}$$

Substituting this into equation (A5.7), the first of our equations is

$$\nabla \times \overline{H} = j\epsilon(r)k\overline{E} \quad \text{----------(A5.11)}$$

Faraday's law is

$$\nabla \times \overline{E} + \frac{1}{c}\frac{\partial \overline{B}}{\partial t} = 0 \quad \text{----------(A5.12)}$$

Now $\overline{H} = \overline{B} - 4\pi \vec{\kappa} \overline{M}$

or $\frac{\partial \overline{H}}{\partial t} = \frac{\partial \overline{B}}{\partial t}$

since $\vec{\kappa} \overline{M} = 0$ for a meteor train.

But $\overline{H} = \overline{H}_o \exp(j\omega_e t)$

and therefore equation (5.12) will become

$$\nabla \times \overline{E} = -jk\overline{H} \quad \text{----------(A5.13)}$$

This is the second of our two basic equations. For the following analytical discussion we introduce a rectangular system of coordinates with the z-axis along the axis of the ionised column and we assume the E.M. wave to be incident in the negative x direction (see Figure A5.1). When the electric vector is parallel to the column of ionisation the situation is described as parallel polarisation and if it is

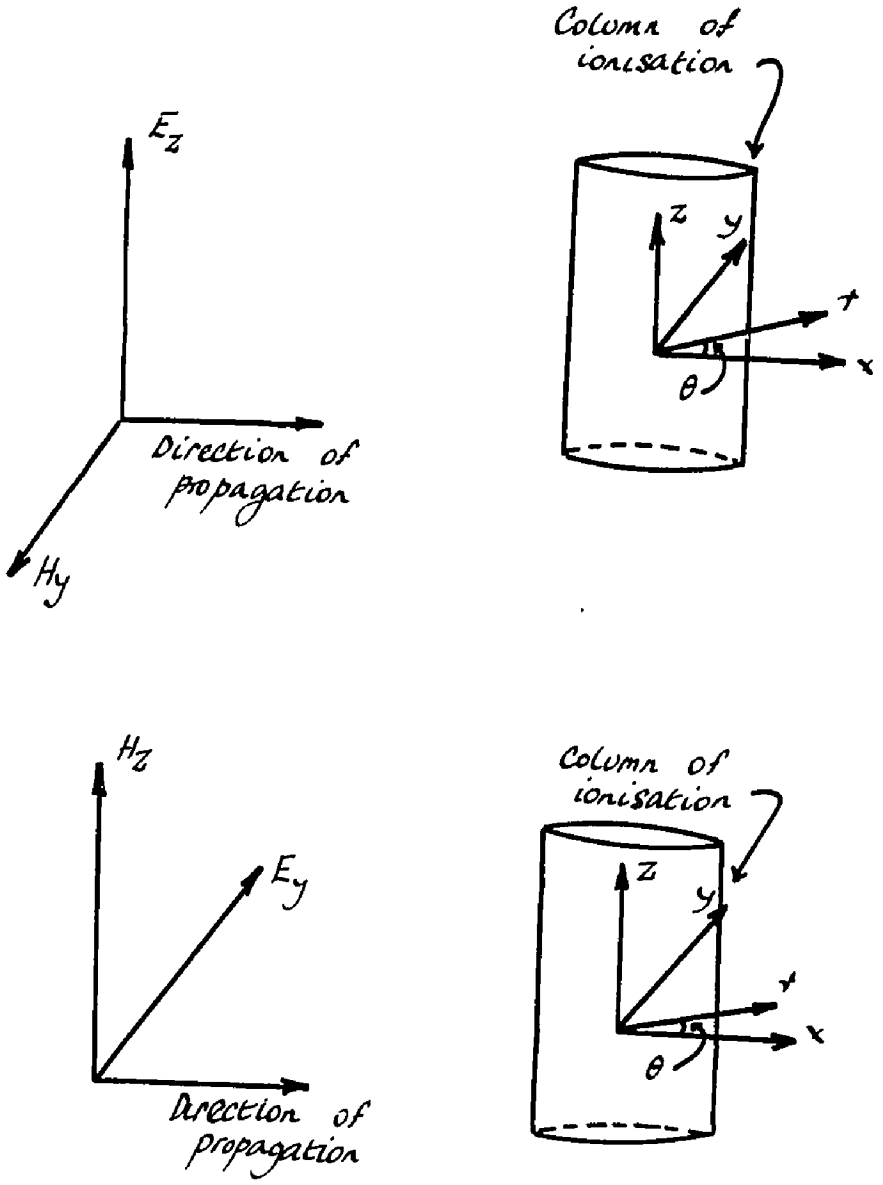

Geometry of plane waves normally incident on a column of ionisation a) parallel electric polarisation

b) transverse electric polarisation

Figure A5.1

perpendicular to the column, transverse polarisation.

Elimination of the magnetic vector in equations (A5.11) and (A5.13) will give the case of parallel scattering. By rearranging equation (5.13) and substituting equation (A5.11) it follows that

$$\nabla \times (\nabla \times \overline{E}) = \epsilon(r)k^2\overline{E} \quad \text{----------(A5.111)}$$

Now $\nabla \cdot \overline{D}_e = 4\pi\rho$

The total charge enclosed in a volume within the meteor train can be considered to be zero since the original atoms are electrically neutral. Considerable forces are set up to prevent charge separation

$$\therefore \quad \nabla \cdot \overline{D}_e = 0$$

$$\therefore \quad \nabla \cdot (\overline{E} + 4\pi\overline{P}) = 0$$

and therefore $\nabla\overline{E} = 0$.

Thus, equation (A5.14) will become

$$\nabla^2\overline{E} + \epsilon(r)k^2\overline{E} = 0 \ .$$

The electric vector only exists in the z direction (parallel polarisation) and therefore

$$\nabla^2 E_z + \epsilon(r)k^2 E_z = 0 \quad \text{----------(A5.15)}$$

Elimination of the electric vector in equations (A5.11) and (A5.13) will give

$$\nabla \times \overline{H} = j\epsilon(r)\, k\overline{E}$$

$$\nabla \times \left[\frac{1}{j\epsilon(r)k}\ (\nabla \times \bar{H})\right] = \nabla \times \bar{E} = -jk\bar{H}$$

$\epsilon(r)$ is a function of r and therefore

$$\nabla \times \left[\frac{1}{\epsilon(r)}\ (\nabla \times \bar{H})\right] = k^2\bar{H} \quad \text{----------(A5.16)}$$

It follows that

$$k^2\bar{H} = \left[\nabla \frac{1}{\epsilon(r)}\right] \times (\nabla \times \bar{H}) + \frac{1}{\epsilon(r)} \left[\nabla(\nabla\cdot\bar{H} - \nabla^2\bar{H})\right]$$

$$\nabla \frac{1}{\epsilon(r)} = -\frac{1}{(\epsilon(r))^2}\ \nabla \epsilon(r)$$

and by rearrangement

$$-\frac{\nabla\epsilon(r)}{\epsilon(r)} \times (\nabla \times \bar{H}) + (\nabla(\nabla\cdot\bar{H}) - \nabla^2\bar{H}) - k^2\epsilon(r)\bar{H} = 0$$

$$\bar{H} = \bar{B} - 4\pi\ \bar{\hat{M}}$$

and therefore $\nabla\cdot\bar{H} = 0$, since $\nabla\cdot\bar{B} = 0$.

Hence $$\frac{\nabla\epsilon(r)}{\epsilon(r)} \times (\nabla \times \bar{H}) + \nabla^2\bar{H} + k^2\epsilon(r)\bar{H} = 0\ .$$

If the magnetic field possesses only a z component (transverse electrical polarisation)

$$\left[\frac{\nabla\epsilon(r)}{\epsilon(r)} \times (\nabla \times \bar{H})\right]_z + \nabla^2 H_z + k^2\epsilon(r)H_z = 0 \quad \text{-----(A5.17)}$$

Equation (A5.17) can be written

$$\nabla^2 H_z - \frac{1}{\epsilon(r)}\ \frac{d\epsilon(r)}{dr}\ \frac{\partial H_z}{\partial r} + k^2\epsilon(r)H_z = 0 \quad \text{------(A5.18)}$$

Summarizing the two basic equations we have obtained up until this point for parallel polarisation

$$\nabla^2 E_z + \epsilon(r) k^2 E_z = 0 \quad \text{----------(A5.15)}$$

and for transverse polarisation

$$\nabla^2 H_z - \frac{1}{\epsilon(r)} \frac{d\epsilon(r)}{dr} \frac{\partial H_z}{\partial r} + k^2 \epsilon(r) H_z = 0 \quad \text{-------(A5.18)}$$

Cylindrical coordinates r and θ can be introduced into the above equations. Equation (A5.15) becomes

$$\frac{1}{r} \frac{\partial}{\partial r} \left[r \frac{\partial E_z}{\partial r} \right] + \frac{1}{r^2} \frac{\partial^2 E_z}{\partial \theta^2} + \epsilon(r)\ k^2 E_z = 0$$

and equation (A5.18) becomes

$$\frac{1}{r} \frac{\partial}{\partial r} \left[r \frac{\partial H_z}{\partial r} \right] + \frac{1}{r^2} \frac{\partial^2 H_z}{\partial \theta^2} - \frac{1}{\epsilon(r)} \frac{d\epsilon(r)}{dr} \frac{\partial H_z}{\partial r} + k^2 \epsilon(r) H_z = 0$$

----------(A5.19)

Try a solution to equation (A5.19) of the form $H_z = \sum T(r) \Theta(\theta)$, and in particular the n^{th} term such that $H_{z_n} = T_n(r)\ \Theta(\theta)$.

Therefore equation (A5.19) becomes

$$\frac{1}{r} \Theta_n(\theta) \frac{dT_n(r)}{dr} + \Theta_n(\theta) \frac{d^2 T_n(r)}{dr} + \frac{T_n(r)}{r^2} \frac{d^2 \Theta_n(\theta)}{d\theta^2} -$$

$$\frac{\Theta_n(\theta)}{\epsilon(r)} \frac{d\epsilon(r)}{dr} \frac{dT_n(r)}{dr} + k^2 \epsilon(r)\ T_n(r)\ \Theta_n(\theta) = 0 \quad .$$

Dividing through by $1/T_n(r)\ \Theta_n(\theta)$

$$\frac{r^2}{T_n(r)}\left[\frac{1}{r}\frac{dT_n(r)}{dr}+\frac{d^2T_n(r)}{dr^2}-\frac{1}{\epsilon(r)}\frac{d\epsilon(r)}{dr}\frac{dT_n(r)}{dr}\right]$$

$$+k^2\epsilon(r)r^2+\frac{1}{\Theta_n(\theta)^2}\frac{d^2\Theta_n(\theta)}{d\theta^2}=0$$

and by separation of the variables

$$\frac{r^2}{T_n(r)}\left[\frac{1}{r}\frac{dT_n(r)}{dr}+\frac{d^2T_n(r)}{dr^2}-\frac{1}{\epsilon(r)}\frac{d\epsilon(r)}{dr}\frac{dT_n(r)}{dr}\right]$$

$$+k^2\epsilon(r)r^2=n^2 \qquad \text{----------(A5.20)}$$

$$\frac{1}{\Theta_n(\theta)}\frac{d^2\Theta_n(\theta)}{d\theta^2}=n^2 \qquad \text{----------(A5.21)}$$

The solution to equation (A5.21) is

$$\Theta_n(\theta) = \exp(-jn\theta)$$

and therefore $$H_{z_n} = T_n(r)\exp(-jn\theta)$$

$$= T_n(r)[\cos(n\theta) - j\sin(n\theta)]$$

Therefore $$H_z = \sum_{0}^{n} T_n(r)[\cos(n\theta) - j\sin(n\theta)]$$ is a solution of equation (A5.19). As the primary wave is incident along the negative x direction, the wave field is symmetric about the x-z plane and it is sufficient to

retain the cos term only in the Fourier series solution

$$\text{Hence} \quad H_z = \sum_{o}^{n} T_n(r) \cos(n\theta) \text{ --------(A5.22)}$$

Equation (A5.20) upon rearrangement is

$$\frac{d^2T_n(r)}{dr^2} + \frac{dT_n(r)}{dr}\left[\frac{1}{r} - \frac{1}{\epsilon(r)}\frac{d\epsilon(r)}{dr}\right] + \left[\epsilon(r)k^2 - \frac{n^2}{r^2}\right]T_n(r)$$

$$= 0 \text{ ----------(A5.23)}$$

A similar equation may be developed for the case of parallel polarisation of the electric vector. Commencing at equation (A5.15) and following exactly the same procedure as just outlined, one can show that

$$E_z = \sum_{o}^{n} P_n(r) \cos(n\theta) \text{ ----------(A5.24)}$$

and

$$\frac{d^2P_n(r)}{dr^2} + \frac{1}{r}\frac{dP_n(r)}{dr} + \left[\epsilon(r)k^2 - \frac{n^2}{r^2}\right]P_n(r) = 0 \text{ --(A5.25)}$$

The radial extent of the ionisation of the meteor train after diffusion is determined by the value of the dielectric constant $\epsilon(r)$. This value is given by equation (A5.10) or equation (3.13) (McKinley, 1961)

$$\epsilon(r) = 1 - 81\frac{N_e}{f^2}$$

$$\epsilon(r) = 1 - \frac{8l\ \alpha\ \exp(-r^2/(4Dt + r_o^2))}{f^2\pi(4Dt + r_o^2)}$$

The radius of the column of ionisation is determined to be the distance measured from the centre of the column to the point where $\epsilon(r)$ attains a value of 0.9999 or greater. That is to say the point at which the electron volume density becomes very small.

Consider a plane wave incident along the negative x direction polarised with the electric vector parallel to the axis of the meteor train. The total field anywhere is a combination of the incident and reflected or scattered wave.

For any value of n, P_n or T_n can be expressed in terms of Bessel functions of the first kind and Hankel functions of the first kind. Therefore

$$P_n(r) = a_n J_n(kr) + b_n H_n^{(1)}(kr) \text{ ----------(A5.26)}$$

where a_n and b_n are the relative amplitudes of the incident and reflected waves respectively. The first derivative of $P_n(r)$ must be continuous at the matching radius r and therefore

$$P_n'(r) = a_n k J_n'(kr) + kb_n H_n^{(1)\prime}(kr) \text{ ----------(A5.27)}$$

Therefore, from equations (A5.26) and (A5.27)

$$\frac{b_n}{a_n} = \frac{J_n(kr)\ P_n'(r) - k\ J_n'(kr)\ P_n(r)}{k\ P_n(r)\ H_n^{(1)\prime}(kr) - P_n'(r)\ H_n^{(1)}(kr)} \qquad \text{(A5.28)}$$

The reflection coefficient for parallel polarisation is written as

$$g_{//} = \sum_{o}^{n} A_n \cos(n\theta) \qquad \text{(A5.29)}$$

At large distances from the z-axis, the series in equation (A5.24) describes a plane incident wave, and a diverging cylindrical wave. The incident wave is given by

$$E_{inc} = \exp(jkx) = \exp(jkr\cos\theta)$$

$$= J_o(kr) + 2 \sum_{}^{n}{}' j^{(n)} J_n(kr) \cos(n\theta)$$

$$= \sum_{o}^{n} \tau_n\, j^{(n)} J_n(kr) \cos(n\theta)$$

The n = 0 term must be treated separately thus giving rise to the Neumann factor τ_n where $\tau_n = 1$ when $n = 0$

$\tau_n = 2$ when $n > 0$

Similarly

$$E_{refl} = \sum_{o}^{n} \tau_n\, j^{(n)}\, H_n^{(1)}(kr) \cos(n\theta)$$

Therefore equation (A5.28) becomes

$$A_n = \frac{J_n(kr)\ P_n'(r) - kJ_n'(kr)\ P_n(r)}{k\ P_n(r)\ H_n^{(1)\prime}(kr) - P_n'(r) H_n^{(1)}(kr)}\ \tau_n \qquad \text{(A5.30)}$$

substituting this into equation (A5.29)

$$g_{//} = \sum_{o}^{\Lambda} \tau_n \frac{J_n(kr)\, P_n'(r) - kJ_n'(kr)\, P_n(r)}{kP_n(r)\, H_n^{(1)\prime}(kr) - P_n'(r)\, H_n^{(1)}(kr)} \cos(n\theta) \quad \text{--(A5.31)}$$

similarly

$$g_{\perp} = \sum_{o}^{\Lambda} \tau_n \frac{k\, J_n'(kr)\, T_n(r) - J_n(kr) T_n'(r)}{k\, H_n^{(1)\prime}(kr)\, T_n(r) - H_n^{(1)}(kr) T_n'(r)} \cos(n\theta) \quad \text{--(A5.32)}$$

The solution of equations (A5.23), (A5.25), (A5.31) and (A5.32) result in the reflection coefficients for parallel and transverse polarisation of the electric vector.

REFERENCES

Air Force Cambridge Research Laboratories Geophysics Space Data Bulletin, 1971, Special Repts. #126, 8, 48 (Carrigan A.L., Ed.).

Baggaley W.J., 1970, Mon. Not. Roy. Astron. Soc., 147, 231.

Billam E.R. and Browne I.C., 1956, Proc. Phys. Soc. B69, 98.

Blackett P.M.S. and Lovell A.C.B., 1941, Proc. Roy. Soc. A177, 183.

Brysk H. and Buchanan M.L., 1965, Can. J. Phys., 43, 28.

Closs R.L., Clegg J.A. and Kaiser T.R., 1953, Phil. Mag. 44, 313.

Collins J.G., 1969, M.Sc. Thesis, University of Western Ontario, Canada.

Davies K., 1965, "Ionospheric Radio Propagation", Nat. Bur. Stands. Monograph. Ser.

Dohnanyi J.S., 1970, J. Geo. Res., 74, 2531.

Forsyth P.A., Hines C.O. and Vogan E.L., 1955, Can. J. Phys., 33, 600.

Forsyth P.A., Vogan E.L., Hansen D.R. and Hines C.O., 1957, Proc. I.R.E., 45, 1642.

Greenhow J.S. and Hall J.E., 1960, Mon. Not. Roy. Astron. Soc., 121, 183.

_____, 1960, J. Atmos. Terr. Phys. 18, 203.

Herlofson N., 1948, Repts. Prog. in Phys. 11, 444.

_____, 1951, Ark. Fys., 3, 247.

Hey J.S., Parsons S.J. and Stewart G.S., 1947, Mon. Not. Roy. Astron. Soc., 107, 176.

Hey J.S. and Stewart G.S., 1947, Proc. Phys. Soc., 59, 858.

Hines C.O., 1955, Can. J. Phys., 33, 493.

Hines C.O. and Forsyth P.A., 1957, Can. J. Phys. 35, 1033.

Hughes D.W. and Stephenson D.G., 1971, Mon. Not. Roy. Astron. Soc. 155, 1.

Huxley L.G.H., 1952, Aust. J. Sc. Res., A5, 10.

Jacchia L.G., 1963, "The Solar System," Vol. 4, University of Chicago Press, (Middlehurst B.M. and Kuiper G.P. Eds.).

Jackson J.D., 1962, "Classical Electrodynamics", J. Wiley and Sons.

Jones J., 1970, Planet.Space Sci., 18, 1836.

_____, 1968, Can. J. Phys., 46, 1101.

_____, 1969, Can. J. Phys., 47, 1467.

Jones J. and Collins J.G., 1970, Can. J. Phys., 48, 2585.

Jones J. and Kaiser T.R., 1966, Mon. Not. Roy. Astron. Soc. 133, 411.

Jones J. and Read B.A., 1972, Can. J. Phys. 50, 1277.

Kaiser T.R., 1953, Phil. Mag. Supp., 2, 495.

_____, 1960, Mon. Not. Roy. Astron. Soc., 121, 284.

Kaiser T.R. and Closs R.L., 1952, Phil. Mag. 43, 1.

Kaiser T.R. and Greenhow J.S., 1953, Proc. Phys. Soc. B66, 150.

Kaiser T.R., Pickering W.M. and Watkins C.D., 1969, Planet. Space Sci., 17, 519.

Keitel G.H., 1955, Proc. I.R.E., 1481.

Lebedinec V.N. and Portnyagin Yu.I., 1968, Soviet Astr. 11, 700.

Lebedinec V.N. and Sosnova A.K., 1967, "Physics and Dynamics of Meteors," I.A.U. Conference #33, 27.

Lindemann F.A. and Dobson G.B., 1923, Proc. Roy. Soc., 102, 411.

Lovell A.C.B., 1954, "Meteor Astronomy", Clarendon Press.

Lovell A.C.B. and Clegg J.A., 1948, Proc. Phys. Soc., 60, 491.

Lusignan B., 1960, J. Geophys. Res., 65, 3895.

Manning L.A. and Eshelman V.R., 1959, Proc. I.R.E., 47, 186.

McIntosh B.A. and Šimek M., 1969, Can. J. Phys., 47, 7.

McKinley D.W.R., 1961, "Meteor Science and Engineering", McGraw Hill Book Co. Ltd.

Öpik E., 1933, "Atomic collisions and radiation of meteors", Tartu Publications.

Poole L.M.G. and Kaiser T.R., 1967, Planet. Space Sci. 15, 1131.

Plavec M., 1956, "On the evolution of meteor streams" in "Vistas in astronomy", Vol. 2, Pergamon Press.

Scarborough J.B., 1966, "Numerical Mathematical Analysis", The John Hopkins Press.

Shafer J.P. and Goodall W.M., 1932, Proc. I.R.E. 20, 1941.

Šimek M. and McIntosh B.A., 1968, "Physics and Dynamics of Meteors", I.A.U. Conference #33, 362.

Skellet A.M., 1933, Proc. I.R.E., 20, 1932.

Sparrow C.M., 1926, Astrophys. J., 63, 90.

Swihart T.L., 1968, "Astrophysics and Stellar Astronomy", John Wiley and Sons.

Topping J., 1955, "Errors of observation and their treatment", Chapman and Hall Ltd.

Webster A.R., 1963, Ph.D. Thesis, University of Sheffield, England.

Whipple F.L., 1963, "The Solar System", Vol. 4, University of Chicago Press. (Middlehurst B.M. and Kuiper G.P. Eds.).

Wood R.W., 1934, "Physical Optics", Macmillan, New York.

Van Valdenburg M.E., 1954, J. Geophys. Res., 59, 359.

Verniani F., 1966, J. Geophys. Res., 71, 2749.